UCSF
UC San Francisco Electronic Theses and Dissertations

Title
Mechanistic insights into Hsp90 client engagement and remodeling through ATP hydrolysis

Permalink
https://escholarship.org/uc/item/82z0s1ds

Author
Betegon Ramiro, Miguel

Publication Date
2019

Peer reviewed|Thesis/dissertation

eScholarship.org Powered by the California Digital Library
University of California

Mechanistic insights into Hsp90 client engagement and remodeling through ATP hydrolysis

by
Miguel Betegon Ramiro

DISSERTATION
Submitted in partial satisfaction of the requirements for degree of
DOCTOR OF PHILOSOPHY

in

Biophysics

in the

GRADUATE DIVISION
of the
UNIVERSITY OF CALIFORNIA, SAN FRANCISCO

Approved:

DocuSigned by:
David A. Agard
328308DD7E5546A...

David A. Agard
Chair

DocuSigned by:
Carol A. Gross

Carol A. Gross

DocuSigned by:
Jason E. Gestwicki
4909848DBB404E5...

Jason E. Gestwicki

Committee Members

Copyright 2019

by

Miguel Betegon Ramiro

Acknowledgements

I want to thank David Agard for his continued mentorship over the last seven years. His deep thinking and scientific rigor are some of the reasons I switched fields and joined his lab, and some of the traits I've hoped to acquire during these years. I leave with my training in his lab as the scientific standard I will use throughout the rest of my career.

I'm also indebted to Joe DeRisi, with whom I worked for two years before starting grad school, for giving me the opportunity to work on some awesome projects, mentoring me and always treating me, just like David has, as an intellectual peer even though it was far from true.

I want to thank the members of my thesis committee, Carol Gross and Jason Gestwicki, for supporting me throughout my time at UCSF and providing me with scientific and career advice.

My classmates Ted, Zygy, Jordi and Yuan helped me more than they know during my first year, and I'm happy that although we're all scattered around the globe we all stay in touch.

I also want to thank several current and former members of the Agard lab who made the lab great: Elaine Kirschke and Laura Lavery for making me feel welcomed when I joined and for the many exciting scientific conversations, Mariano Tabios for being an excellent person to be around and Daniel Elnatan for mentoring me when I rotated and for the strong scientific collaboration.

I especially want to acknowledge the Friends I've made during my time at UCSF and with whom I've spent a lot of time inside and outside of lab: Klim "Chanchito" Verba, Andrew Lyon and my dear friend Rose Citron. I will miss you.

My parents, Miguel and Charo, my sisters Maria and Beatriz and my niece Emma, even though I don't see them enough, were a very important presence during my PhD.

Lastly, I want to thank Leah, the best person in the world and to whom this thesis is dedicated.

Mechanistic insights into Hsp90 client engagement and remodeling through ATP hydrolysis

By

Miguel Betegon Ramiro

Abstract

The molecular chaperone Hsp90 interacts with around 10% of the proteome, facilitating folding and regulating the biological function of its clients. Decades of work have led to a general understanding of the ATP-driven conformational cycle of Hsp90 and its role in client regulation, however the molecular details of this mechanism remain unknown. This is due in part to the intrinsic instability of Hsp90 clients, which has until recently hampered in-vitro and structural work, as well as to the difficulty in breaking down Hsp90s ATP-driven cycle into discrete steps that can be observed and measured together with changes in client structure and function. The work described in this thesis addresses two of the main questions that the Hsp90 field faces: 1) How is Hsp90's conformational cycle and ATP hydrolysis used to remodel clients and 2) is there a conserved mechanism of client recognition and engagement that allows Hsp90 to functionally interact with dozens of clients of different size, sequence and structure.

The first chapter of this thesis addresses the first question and builds on work from Laura Lavery and James Partridge which revealed that the closed state of the mitochondrial Hsp90, TRAP1, is structurally asymmetric with one protomer in a 'straight' conformation while the other one adopts a novel 'buckled' conformation.

Starting from this catalytic closed state, we investigate the effect of each ATP hydrolysis event on Hsp90's conformation and how Hsp90 uses these hydrolysis-driven changes to remodel and regulate clients. We show that this asymmetry sets up sequential and deterministic hydrolysis, with the buckled protomer hydrolyzing first followed by a flip of the asymmetry that positions the unhydrolyzed protomer in the hydrolysis-favorable buckled conformation, promoting the second hydrolysis leading to reopening of the chaperone. While this asymmetry has not been observed in eukaryotic Hsp90 homologs, we propose that, despite being homodimers, all Hsp90s work as asymmetric machines, either through a structural asymmetry like in the case of TRAP1 or through formation of asymmetric complexes with clients and co-chaperones in the case of eukaryotic Hsp90s.

The third chapter of this thesis addresses the second question through the determination of the cryoEM structure of the bacterial Hsp90, HtpG, in complex with its client ribosomal protein L2. Though this work is still ongoing, the current cryoEM reconstruction of the apo-HtpG:L2 complex shows that, surprisingly, HtpG is in a GRP94-like conformation. Also striking is the fact that L2 interacts with HtpG in a Cdk4-like fashion, with density observed on both sides of HtpG and connected by a thread of density going through the lumen of HtpG along the same region previously identified for L2 and the model client Δ131Δ binding to HtpG. Additionally, L2 makes further interactions with HtpG different from those observed with Cdk4, notably with the N-terminal domain of HtpG around the lid area.

Overall, this work provides further evidence supporting that the different conformational states of Hsp90 are conserved across homologs but differentially regulated, and supports a conserved mechanism of interaction between Hsp90 and different classes of clients where Hsp90 clamps between domains stabilizing structural and likely short-lived transitions in the client.

Table of contents

Introduction **1**

References 5

Symmetry broken and rebroken during the ATP hydrolysis cycle of the mitochondrial Hsp90 TRAP1 ..... **7**

Contributing authors 7

Preface 7

Abstract 10

Introduction 11

Results 14

Two ATP hydrolysis are required by TRAP1 to progress through its ATPase cycle 14

Crystallographic evidence of sequential and deterministic ATP hydrolysis in TRAP1 21

TRAP1 hydrolyzes ATP in solution in absence of Magnesium 23

Asymmetric water dynamics near ATP γ-Phosphate between protomers. 26

Loss of the γ-Phosphate contact determines MD:CTD conformation in the ATP/ADP state 29

Discussion 34

Mechanism of conformational coupling to sequential ATP hydrolysis 35

A model for Hsp90 client maturation mechanism 38

Acknowledgements 40

Methods and experimental procedures 41

Cloning and Protein Purification 41
Crystallization and data collection 42
Structure determination and refinement 42
FRET sample preparation and experiments 43
SAXS experiments and data processing 44
DEER sample preparation and measurements 44
Production of Phoshate-Binding Protein (PBP) and labeling for phosphate release assay 45
Steady-state ATPase assay and analysis 46
Single-turnover radioactive ATPase assay 47
Molecular dynamics simulation 48
References 50
Regulation of Heat Shock Factor 1 by the hsp90/Hsp70 chaperone system 64
Introduction 64
Methods 74
Protein expression and purification 74
Fluorescence polarization binding assay 75
Negative stain electron microscopy 75
References 77
CryoEM structure of the HtpG, in complex with the ribosomal protein L2 79
Introduction 79
Results 83
Graphene Oxide grids are amenable to imaging HtpG:L2 83

Apo HtpG adopts a GRP94-like conformation when in complex with L2 84
L2 interacts with HtpG in a kinase-like fashion 88
Discussion and future directions 91
Methods 95
Protein expression and purification 95
CryoEM grid preparation and data acquisition 95
CryoEM data processing 96
References 97

List of figures

Introduction

Figure 1. Architecture of the Hsp90 homodimer 2

Figure 2. The ATPase cycle of Hsp90 3

Symmetry broken and rebroken during the ATP hydrolysis cycle of the mitochondrial Hsp90 TRAP1

Figure 1. Both ATPs need to be hydrolyzed for efficient cycling 16

Figure 1-figure supplement 1. Raw fluorescence intensities of FRET data 18

Figure 1-figure supplement 2. Steady-state ATPase assays of cysteine-free hTRAP1 and heterodimeric hTRAP1 (+/+ and +/R402A) at 30˚C 19

Figure 2. Kinetic crystallography indicates that the buckled arm hydrolyzes ATP first 22

Figure 3. Without Mg^{2+} hTRAP1 adopts the closed state and slowly hydrolyzes ATP in solution 24

Figure 3-figure supplement 1. ATP-induced dimer closure in absence of Mg^{2+} by FRET in human and zebrafish TRAP1 25

Figure 4. Microsecond all-atom molecular dynamics simulations of zTrap1 reveal asymmetric water dynamics near the ATP γ-phosphate 27

Figure 4-figure supplement 1 Microsecond all-atom molecular dynamics simulations of zTrap1 reveal asymmetric water dynamics near the ATP γ-phosphate at 360 K. 28

Figure 5. The asymmetry is flipped in the ATP/ADP state as revealed by DEER on hemi-hydrolyzed (ATP/ADP) heterodimers 31

Figure 5-figure supplement 1. Interatomic distance distribution, P(r), from SAXS experiments of heterodimeric +/R402A human TRAP1 32
Figure 5-figure supplement 2. Crystal packing interactions for the heterodimeric (+/R417A) zTRAP1 fused to the SpyCatcher-Tag domains 33
Figure 6. Revised model of the TRAP1 ATPase cycle showing the obligatory sequential hydrolysis and conformational switching 37

Regulation of Heat Shock Factor 1 by the hsp90/Hsp70 chaperone system

Figure 1. Architecture of human HSF1 and yeast HSF1 65
Figure 2. Models of hHSF1 inhibition and activation 66
Figure 3. Trimerization of HSF1 and effect of Hsp90 67
Figure 4. Purification of WT hHSF1 from literature 70
Figure 5. Purification of 6His WT hHSF1 70
Figure 6. Successful purification of WT hHSF1 72
Figure 7. hHSF1 trimer with HSE DNA binding curve 73
Figure 8. Negative stain electron microscopy of trimeric hHSF1 74

CryoEM structure of the HtpG in complex with the ribosomal protein L2

Figure 1. Hsp90 in complex with CDK4 and the cochaperone CDC37 80
Figure 2. Structures of L2 and HtpG 82
Figure 3. HtpG:L2 on graphene oxide grids 84
Figure 4. CryoEM map of apo-HtpG:L2 85
Figure 5. HtpG is in a GRP94-like conformation 86

Figure 6. Homology model of HtpG based on GRP94 fit into the cryoEM map 87

Figure 7. The density unaccounted by HtpG fits the globular domain of L2 89

Figure 8. Current model of the apo-HtpG:L2 complex 90

Figure 9. L2 interacts with HtpG at previously mapped regions 91

Figure 10. Model of the region of L2 through the lumen of HtpG 92

Figure 11. apo-HtpG:L2 on GO-NH2 grids 94

List of tables

Symmetry broken and rebroken during the ATP hydrolysis cycle of the mitochondrial Hsp90 TRAP1

Supplementary table 1A. Data collection and refinement statistics 63

Regulation of Heat Shock Factor 1 by the hsp90/Hsp70 chaperone system

Table 1. HSF1 purification schemes from literature..... 69

Chapter I

Introduction

The concept of protein homeostasis is central to life as a broad cellular process composed of many pathways that control protein biogenesis, trafficking, protein state and function, and protein degradation throughout the cell: during biogenesis, proteins must fold into their native states while avoiding aggregation, following which they need to be trafficked to the appropriate destination in the cell and perform their function. During the course of their lifetime, proteins are monitored to ensure their proper foldedness, and are, if necessary, degraded.

Given this, it's easy to imagine that protein homeostasis is an essential and very complex and dynamic process where the state of the proteome must be constantly monitored and regulated to maintain adequate cellular function in response to ever-changing internal and external conditions and stresses.

A class of proteins, termed Heat Shock Proteins (HSPs), play a central role in protein homeostasis. While their function was initially identified in the context of heat stress, HSPs help maintain proper protein homeostasis under any type of cellular stresses as well as during what we can consider normal conditions. Most of the HSPs function as chaperones, that is they prevent other proteins from aggregating during initial folding or stress conditions, usually through binding to exposed hydrophobic regions.

One of its members is Heat shock protein 90 (Hsp90), a highly conserved molecular chaperone. Like most chaperones, it promotes initial folding by preventing aggregation, but it is unique in that it also interacts with its substrates after initial folding, helping them perform their activities by interacting with them in a functional manner throughout their lifetime. Hsp90

interacts with a large part of the proteome (~10% in yeast), with large numbers of clients depending on it beyond initial folding for their function, as is the case for 60% of kinases or many of the nuclear receptors. Hsp90 is therefore at the center of protein homeostasis.

In the cell, Hsp90 exists as a homodimer where each monomer is composed of three domains: an N-terminal domain that binds and hydrolyzes ATP, a middle domain and a C-terminal domain that contains the dimerization interface that forms the homodimer and is responsible, together with the middle domain, for client binding (Genest et al, 2013, Street et al., 2014) (Figure 1).

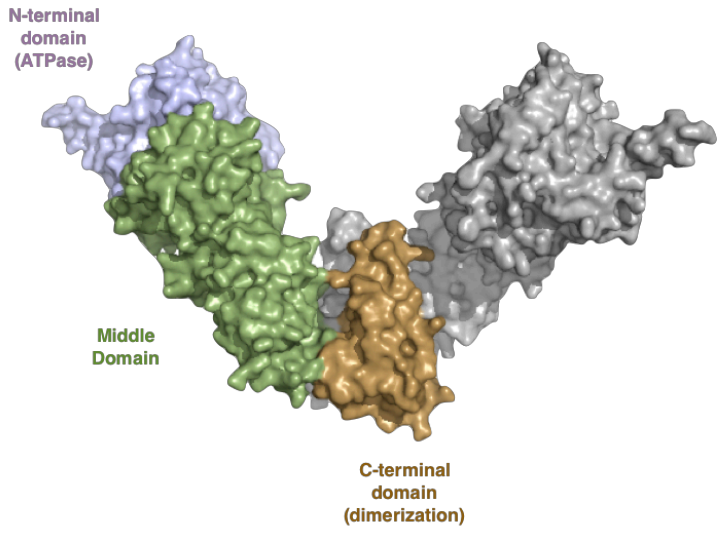

Figure 1. Architecture of the Hsp90 homodimer
One protomer in grey, the other in color showing the three domains of each protomer: N-terminal domain in light purple, the middle domain in green and C-terminal domain in orange.

A number of structures from our lab and others (Shiau et al, 2006, Ali et al., 2006, Krukenberg et al, 2008) have shown that the conformational state of Hsp90 is nucleotide dependent: in the apo state, Hsp90 is in a V-shaped open and flexible state. Binding of nucleotide stabilizes a closed catalytic state where the N-terminal domains rotate and dimerize, promoting

ATP hydrolysis. Upon hydrolysis, Hsp90 reopens, going back to the apo state through a transient and compact ADP/ADP state (Figure 2). At the onset of my PhD, one of the main questions in the Hsp90 field was how the energy from 2 ATPs and the conformational cycle of Hsp90 relate to client remodeling. Specifically, since we know that after both hydrolyses the cycle resets, what is the role of the first hydrolysis and what are its consequences for Hsp90 and its clients? The first chapter of this thesis directly addresses this question.

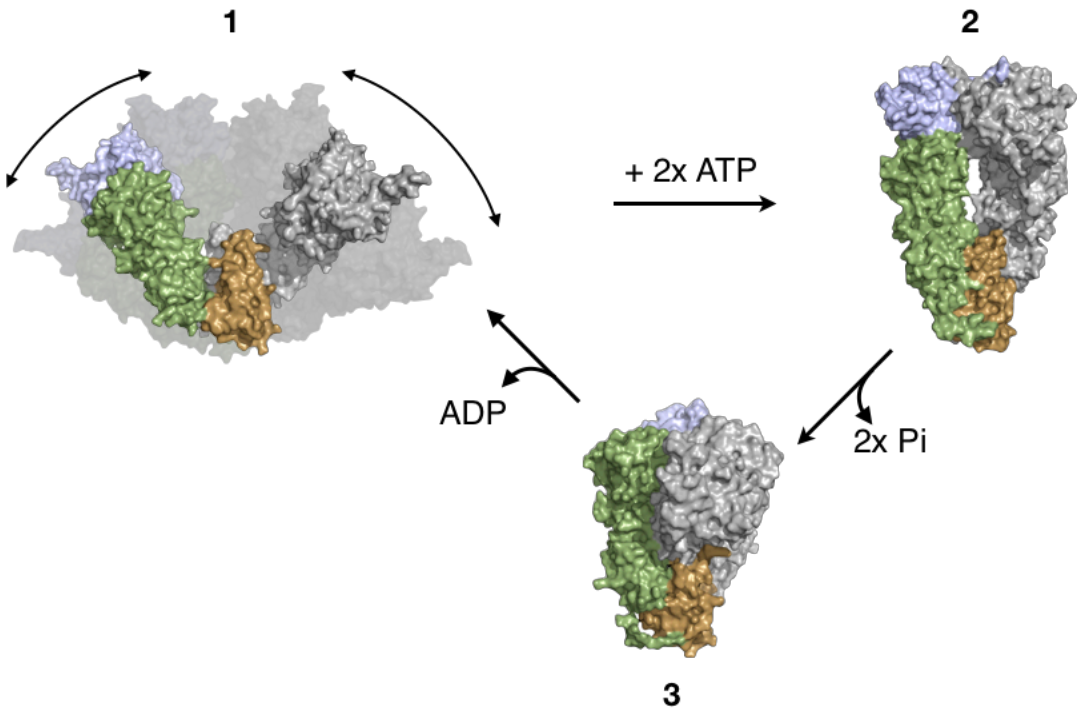

Figure 2. The ATPase cycle of Hsp90
1) The open and flexible apo state. **2**) The ATP/ATP catalytic closed state. **3**) The transient and compact ADP/ADP state.

The other main question in the field was how a single protein can engage with so many different substrates of varying sequence, structure and size. One of the answers to this question is that Hsp90 does not usually work alone. Instead, it functions with other chaperones such as Hsp70 and, in the case of eukaryotic Hsp90s, also with a number of cochaperones that provide

specificity by recruiting specific classes of clients, such as Cdc37 in the case of kinases, or regulate Hsp90's activity, such as the cochaperones Aha1 or p23. In prokaryotes, no Hsp90 cochaperones have been identified and none of the eukaryotic ones that have been tested interact with these Hsp90 homologs (Sung et al., 2016). This is also the case for TRAP1, the mitochondrial Hsp90, which not surprisingly has closer sequence homology to prokaryotic Hsp90s than to the eukaryotic ones. This lack of interaction and regulation by cochaperones implies that whatever function and regulation is encoded in cochaperones is likely encoded in Hsp90 alone for prokaryotic Hsp90 and TRAP1. The overarching theme of this thesis, as hopefully the work herein presented together with the existing literature will show, is that all Hsp90s perform similar functions but have evolved to do it in slightly different ways, and we need to compare and understand these differences to fully understand Hsp90.

References

Ali, M. M. U., Roe, S. M., Vaughan, C. K., Meyer, P., Panaretou, B., Piper, P. W., et al. (2006). Crystal structure of an Hsp90-nucleotide-p23/Sba1 closed chaperone complex. *Nature*, *440*(7087), 1013–1017. http://doi.org/10.1038/nature04716

Genest, O., Reidy, M., Street, T. O., Hoskins, J. R., Camberg, J. L., Agard, D. A., et al. (2013). Uncovering a Region of Heat Shock Protein 90 Important for Client Binding in E. coli and Chaperone Function in Yeast. *Molecular Cell*, *49*(3), 464–473. http://doi.org/10.1016/j.molcel.2012.11.017

Krukenberg, K. A., Förster, F., Rice, L. M., Sali, A., & Agard, D. A. (2008). Multiple conformations of E. coli Hsp90 in solution: insights into the conformational dynamics of Hsp90. *Structure*, *16*(5), 755–765. http://doi.org/10.1016/j.str.2008.01.021

Shiau, A. K., Harris, S. F., Southworth, D. R., & Agard, D. A. (2006). Structural Analysis of E. coli hsp90 reveals dramatic nucleotide-dependent conformational rearrangements., *127*(2), 329–340. http://doi.org/10.1016/j.cell.2006.09.027

Street, T. O., Zeng, X., Pellarin, R., Bonomi, M., Sali, A., Kelly, M. J. S., et al. (2014). Elucidating the Mechanism of Substrate Recognition by the Bacterial Hsp90 Molecular Chaperone. *Sciencedirect.com*. http://doi.org/10.1016/j.jmb.2014.04.001

Sung, N., Lee, J., Kim, J.-H., Chang, C., Joachimiak, A., Lee, S., & Tsai, F. T. F. (2016). Mitochondrial Hsp90 is a ligand-activated molecular chaperone coupling ATP binding to dimer closure through a coiled-coil intermediate. *Proceedings of the National Academy of Sciences*, *113*(11), 201516167–2957. http://doi.org/10.1073/pnas.1516167113

Chapter II

Symmetry broken and rebroken during the ATP hydrolysis cycle of the mitochondrial Hsp90 TRAP1

Contributing authors

Daniel Elnatan[†,1,2], Miguel Betegon[†,1,3], Yanxin Liu[1], Theresa Ramelot[4], Michael A. Kennedy[4], David A. Agard[1]

[1] Howard Hughes Medical Institute and Department of Biochemistry and Biophysics. University of California, San Francisco, CA, USA

[2] Tetrad Graduate program. University of California, San Francisco, CA, USA

[3] Biophysics Graduate program. University of California, San Francisco, CA, USA

[4] Department of Chemistry and Biochemistry, Miami University Oxford, OH, USA

[†] These authors contributed equally

Preface

The bulk of this chapter appears as Elnatan and Betegon *et al.* published in eLife (2017).

The results presented in this chapter follow from work published by former members of the Agard lab, Laura Lavery and James Partridge (Lavery *et al.* 2014, Molecular Cell) and are the fruit of a strong collaboration with now former graduate student Daniel Elnatan and co-author of the manuscript.

As a dynamic molecular machine, the nucleotide-driven conformational states of Hsp90 have long been studied and different structures of various homologs in different nucleotide states have depicted the broad conformational cycle described in chapter I. It is however unclear how that cycle, and in particular the two ATP hydrolysis events, are used by Hsp90 to regulate the activity of its client proteins. While this cycle likely applies to all Hsp90s, in eukaryotes there exists another level of complexity stemming from the regulation of these states and ATP hydrolysis by various cochaperone proteins. In prokaryotes, no Hsp90 cochaperones have been identified and none of the eukaryotic ones that have been tested interact with these Hsp90 homologs. This is also the case for TRAP1, the mitochondrial Hsp90, which not surprisingly has closer sequence homology to prokaryotic Hsp90s than to the eukaryotic ones. This lack of interaction and regulation by cochaperones implies that whatever function and regulation is conserved between both sets of Hsp90s is likely encoded in Hsp90 alone for prokaryotes and TRAP1.

Using TRAP1 as their system, Laura and JP obtained a crystal structure of the ATP/ATP catalytic closed state in the presence of various non-hydrolyzable nucleotides. Unlike previous structures of closed Hsp90 which had two-fold symmetry as expected from a homodimer, TRAP1 presents a structural asymmetry where one protomers in the previously observed conformation but the other one buckles out at the CTD-MD interface, a region that has also been mapped to interact with client proteins (REF). If TRAP1 were to transition from this asymmetric state to the fully symmetric state observed in all other homologs, the client binding interface would change with the potential of effecting changes on the client. As we know that after both ATPs are hydrolyzed Hsp90 reopens, if such a change should occur, this symmetric state would most likely exist as an intermediate and transient state between the ATP/ATP closed asymmetric

state and the open state. In other words, are the ATP hydrolysis events in TRAP1 sequential and does the first one drive a change to a closed symmetric conformation? Furthermore, does the asymmetry set up an order of hydrolysis events where one of the protomer conformations is more favorable to hydrolysis than the other? This are the questions that Daniel Elnatan set to answer during his PhD and were eventually answered by integrating his and my work.

There were several substantial technical difficulties that needed to be overcome to test these hypotheses:

The first one is that to probe an asymmetric system we need an asymmetric Hsp90, that is we need to be able to create heterodimers where we can selectively perturb one of the monomers. Daniel solved this issue by creating obligate heterodimers using the SpyTag/SpyCatcher system that covalently binds Hsp90 monomers, allowing us to combine wildtype Hsp90 with mutants that prevent ATP binding or abolish ATP hydrolysis.

The second one is that to investigate how Hsp90 proceeds after reaching the closed catalytic state we need to be able to move have a population synchronized to that closed state that is also capable of moving forward in the cycle. Accumulating a population of closed TRAP1 is easily achieved using non-hydrolyzable ATP analogs, but these molecules are stuck in the closed state and are not useful for our purposes. The answer to this came from the observation that in the absence of magnesium to catalyze hydrolysis, TRAP1 will accumulate in the closed state in the presence of ATP, and that addition of magnesium will trigger hydrolysis (figures 1E and 1F in this chapter).

The last one is that if TRAP1 does indeed undergo sequential and deterministic ATP hydrolysis and a conformational change occurs after the first one, we need to be able to observe where the first hydrolysis occurs before any conformational changes happen. While trying to

crystalize the ATP/ATP closed state of TRAP1 in the absence of Mg to better understand the determinants of hydrolysis on TRAP1, I obtained a crystal structure from a 3-day old crystal which at first glance appeared to be identical to the previous structures but in fact showed that the ATP of the buckled protomer had hydrolyzed. This serendipitous observation opened the door to answering the first question, which had until now remained impossible to study, as we could now observe hydrolysis occur in crystals of different ages with crystal packing preventing TRAP1 from progressing through its conformational cycle. This, together with Daniel's work on characterizing the asymmetric state of the hemi-hydrolyzed state using his covalent heterodimers in DEER experiments, provided a final and unexpected model (Figure 6 of this chapter) where TRAP1 does not reach a symmetric state after the first hydrolysis and instead the asymmetry is now transferred to the other protomer with the protomers being in the mirrored conformations from the initial ATP/ATP state.

Abstract

Hsp90 is a homodimeric ATP-dependent molecular chaperone that remodels its substrate "client" proteins, facilitating their folding and activating them for biological function. Despite decades of research, the mechanism connecting ATP hydrolysis and chaperone function remains elusive. Particularly puzzling has been the apparent lack of cooperativity in hydrolysis of the ATP in each protomer. A crystal structure of the mitochondrial Hsp90, TRAP1, revealed that the catalytically active state is closed in a highly-strained asymmetric conformation. This asymmetry, unobserved in other Hsp90 homologs, is due to buckling of one of the protomers and is most pronounced at the broadly conserved client-binding region. Here, we show that rather than being cooperative or independent, ATP hydrolysis on the two protomers is sequential and

deterministic. Moreover, dimer asymmetry sets up differential hydrolysis rates for each protomer, such that the buckled conformation favors ATP hydrolysis. Remarkably, after the first hydrolysis, the dimer undergoes a flip in the asymmetry while remaining in a closed state for the second hydrolysis. From these results, we propose a model where direct coupling of ATP hydrolysis and conformational flipping rearranges client-binding sites, providing a paradigm of how energy from ATP hydrolysis can be used for client remodeling.

Introduction

Heat shock protein 90 (Hsp90) is a highly conserved ATP-dependent molecular chaperone. Though originally identified and named as part of the heat shock response, Hsp90's many important roles in the general stress response, regulation of protein function, disease and evolution are now appreciated. Hsp90 physically interacts with ~10% of the proteome (Zhao et al., 2005), highlighting its ability to recognize a broad range of substrate "client" proteins, having diverse functions, sequences, structures, and sizes. Although Hsp90 can function as a canonical chaperone and promote protein folding by suppressing aggregation (Krukenberg et al., 2009; Wiech et al., 1992), it is unique in that it also plays an active role in regulating the activities of a large subset of the proteome, including many proteins involved in signal transduction such as kinases and hormone receptors, thus supporting normal cellular functions. This essential function of Hsp90 is intimately tied to its ATPase activity and mutations that either enhance or suppress this activity compromise cell viability (Nathan and Lindquist, 1995; Panaretou et al., 1998). Conversely, deregulation of cellular Hsp90 levels helps support uncontrolled growth in many human cancers making Hsp90 an important pharmacological target (Whitesell and Lindquist, 2005).

Hsp90 is a V-shaped homodimer, with each protomer consisting of three major domains: a C-terminal dimerization domain (CTD); a middle domain (MD), which has been linked to client binding; and an N-terminal ATPase domain (NTD). The Hsp90 NTD and the upper part of the MD confer membership to the GHKL (DNA Gyrase, Hsp90, Histidine Kinases, MutL mismatch repair protein) family of ATP-powered molecular machines.

In the apo state, Hsp90 is highly dynamic and can sample a range of conformations from a highly extended to a more compact state, potentially accommodating interactions with a diverse set of client structures and sizes (Krukenberg et al., 2008). Large conformational changes are also coupled to nucleotide binding: ATP binding stabilizes a closed state where both NTDs are dimerized, forming the catalytically active state, whereas ADP binding favors a transiently formed compact state (Shiau et al., 2006). Such structural studies have suggested an ATPase cycle of closure, hydrolysis and reopening.

Most higher eukaryotic cells possess four Hsp90 homologs: two cytosolic isoforms, one of which is constitutively expressed while the other is induced by heat shock and stress (Hsp90β and Hsp90α, respectively), one localized to the endoplasmic reticulum (Grp94) and one localized to the mitochondria (TRAP1). Despite some sequence divergence and a few insertions/deletions decorating the globular domains, the structures of all Hsp90 homologs remain conserved, suggesting a fundamental mechanism that adapted to different cellular environments. Indeed, a survey of conformational states in bacterial, yeast, and human Hsp90 revealed species-specific tuning of conformational equilibria and ATPase rates (Southworth and Agard, 2008). In general, reaching the NTD-dimerized closed state is rate limiting for ATP hydrolysis. In the case of TRAP1, the formation of this closed state is further regulated by a temperature-sensitive kinetic barrier imparted by an extra N-terminal extension (Partridge et al., 2014). For eukaryotic

cytosolic Hsp90s, binding of co-chaperones can stabilize particular conformational states and modulate ATPase activity (Eckl et al., 2013; Retzlaff et al., 2010; Southworth and Agard, 2011).

Despite the wealth of information regarding Hsp90 dynamics, little is known about how the energy of ATP hydrolysis is coupled to client protein remodeling. The current model focuses attention on the ATP-induced large conformational change going from a wide-open V-shape to the NTD-dimerized closed state, whereas conversion to the compact ADP state would displace the bound client, followed by reopening to reset the chaperone. However, given that these conformational states are roughly isoenergetic and that ATP binding only marginally stabilizes the closed state (Mickler et al., 2009; Southworth and Agard, 2008), this model does not provide a clear connection between utilization of energy from ATP hydrolysis and client remodeling.

A recent crystal structure of AMPPNP-bound zebrafish TRAP1 (zTRAP1) in a closed state (Lavery et al., 2014) revealed a novel conformational asymmetry between the protomers, most pronounced at the MD:CTD interfaces where one has 2.5-fold more buried surface area than the other (400 $Å^2$ vs. 1000 $Å^2$). One of the protomer arms is buckled while the other remains straight, nearly identical to the previously observed conformation in p23-bound yeast Hsp90 (yHsp90) closed state (Ali et al., 2006). Notably, the previously determined client-binding site (Genest et al., 2013; Street et al., 2012) located at the MD:CTD interface is maximally affected by the protomer asymmetry.

Using TRAP1 as a model system for Hsp90, here we investigate how ATP hydrolysis is coupled to its conformational asymmetry and propose a model connecting it to client remodeling. We examine whether ATP hydrolysis in TRAP1 is sequential, what the order of hydrolysis events is, and how the asymmetry is coupled to the nucleotide states along the ATPase cycle. By covalently linking TRAP1 monomers, we created homogeneous populations of obligate

heterodimers having one hydrolysis-dead protomer, and determined that TRAP1 must undergo ATP hydrolysis in both protomers to efficiently progress through the cycle. Crystal structures of WT TRAP1 closed with ATP in the absence of Mg^{2+} showed that the buckled protomer hydrolyzes ATP more rapidly than the straight one. Microsecond-long molecular dynamics simulations reveal differences in water dynamics within the nucleotide binding pocket of each protomer, highlighting distinct environments surrounding the ATP that may establish differences in hydrolysis rates. Pulsed electron paramagnetic resonance (EPR) distance measurements using dipolar electron-electron resonance (DEER) methods revealed that, in solution, a TRAP1 mutant mimicking the hemi-hydrolyzed (ATP/ADP) state adopts a uniform conformation distinct from the stochastic mixture seen in WT. In this heterodimer, the protomer containing ATP is buckled while the protomer containing the ADP-mimicking mutation is straight. Integrating this data, we propose a revised model of the TRAP1 ATP-driven cycle where the two hydrolysis events are sequential and deterministic, with the buckled protomer being most competent for ATPase hydrolysis, followed by a flip in the MD:CTD asymmetry to position the opposite protomer in the buckled conformation, promoting hydrolysis of the second ATP and allowing TRAP1 to proceed through the cycle.

Results

Two ATP hydrolysis are required by TRAP1 to progress through its ATPase cycle

Previous studies on various Hsp90s show that their ATPase activities follow simple, non-cooperative kinetics despite having two ATP binding sites (Dollins et al., 2007; Frey et al., 2007; McLaughlin et al., 2002; Richter et al., 2008). Consistent with these observations, the activity of

the wildtype ATPase domain is unaffected by whether its partner carries a mutation that does not bind ATP or one that does not hydrolyze ATP (Cunningham et al., 2008; Richter, 2001). Such heterodimeric studies are possible because Hsp90 dimers dynamically exchange within minutes (Hessling et al., 2009; Richter, 2001). Simply mixing wildtype and mutant proteins creates a mixture of dimer species (wildtype + heterodimer + mutant) at equilibrium. Using this approach, we looked at human TRAP1 (hTRAP1) ATPase activity mixing wildtype and a point mutant (E115A) that impairs ATP hydrolysis, but not ATP binding (Panaretou et al., 1998) at different ratios. In contrast to previous studies, the activities of these TRAP1 mixtures are lower than what is expected if the two ATPase domains were to act independently (Figure 1A), suggesting TRAP1 requires that both bound ATPs to be hydrolyzed in its ATPase cycle. Since these experiments were done under steady-state conditions, the decreased activity of heterodimers can be due to either an impaired ability to form the closed state or an impaired ability to exit the closed state, thus changing the rate-limiting step.

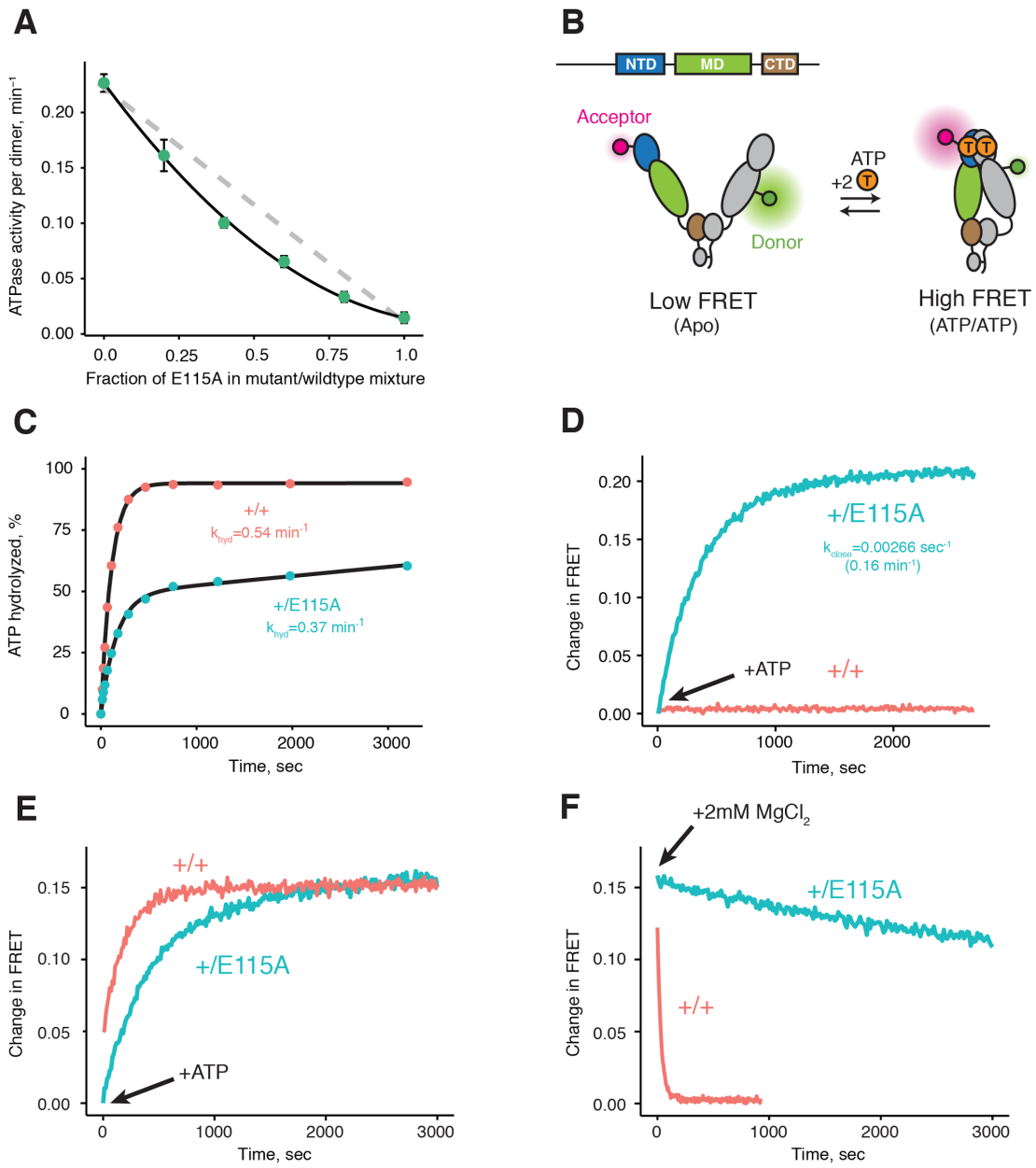

Figure 1. Both ATPs need to be hydrolyzed for efficient cycling
A) Steady-state ATPase assay with constant dimer concentration and varying ratios of wildtype and catalytically-dead E115A mutant show that ATP hydrolysis by each protomer is not independent. Each point and error bar are one standard deviation and averaged from triplicate experiments. Black line is a fit to a binomial distribution of wildtype:mutant:heterodimer, solved for only the heterodimeric activity. The gray dashed line shows the expected activity for independent ATP hydrolysis. **B**) Covalently linked heterodimers for the FRET assay with fluorescent labels on the NTD and MD (E140C, K413C respectively). **C**) Single-turnover ATPase kinetics of wildtype (+/+, red) and heterodimeric, hemi-hydrolyzing (+/E115A, blue), show activity of the remaining site is not compromised. Black curves are exponential fits with an

additional linear term to account for a slow steady-state activity in the +/E115A. **D**) FRET assay looking at build up of closed state (high FRET) in the +/E115A heterodimer (+/E115A, blue) and wildtype (+/+, red) in presence of $MgCl_2$ to allow ATP turnover. The +/E115A data were fit to an exponential with the indicated rate, k_{close}. **E**) FRET assay showing closed state build up in both +/+ (red) and +/E115A (blue) heterodimers after addition of 2 mM ATP in absence of $MgCl_2$. **F**) Addition of excess $MgCl_2$ triggers efficient dimer reopening, as measured by FRET, in +/+ (red) but not +/E115A (blue) heterodimers in reactions pre-incubated with ATP without Mg^{2+}.

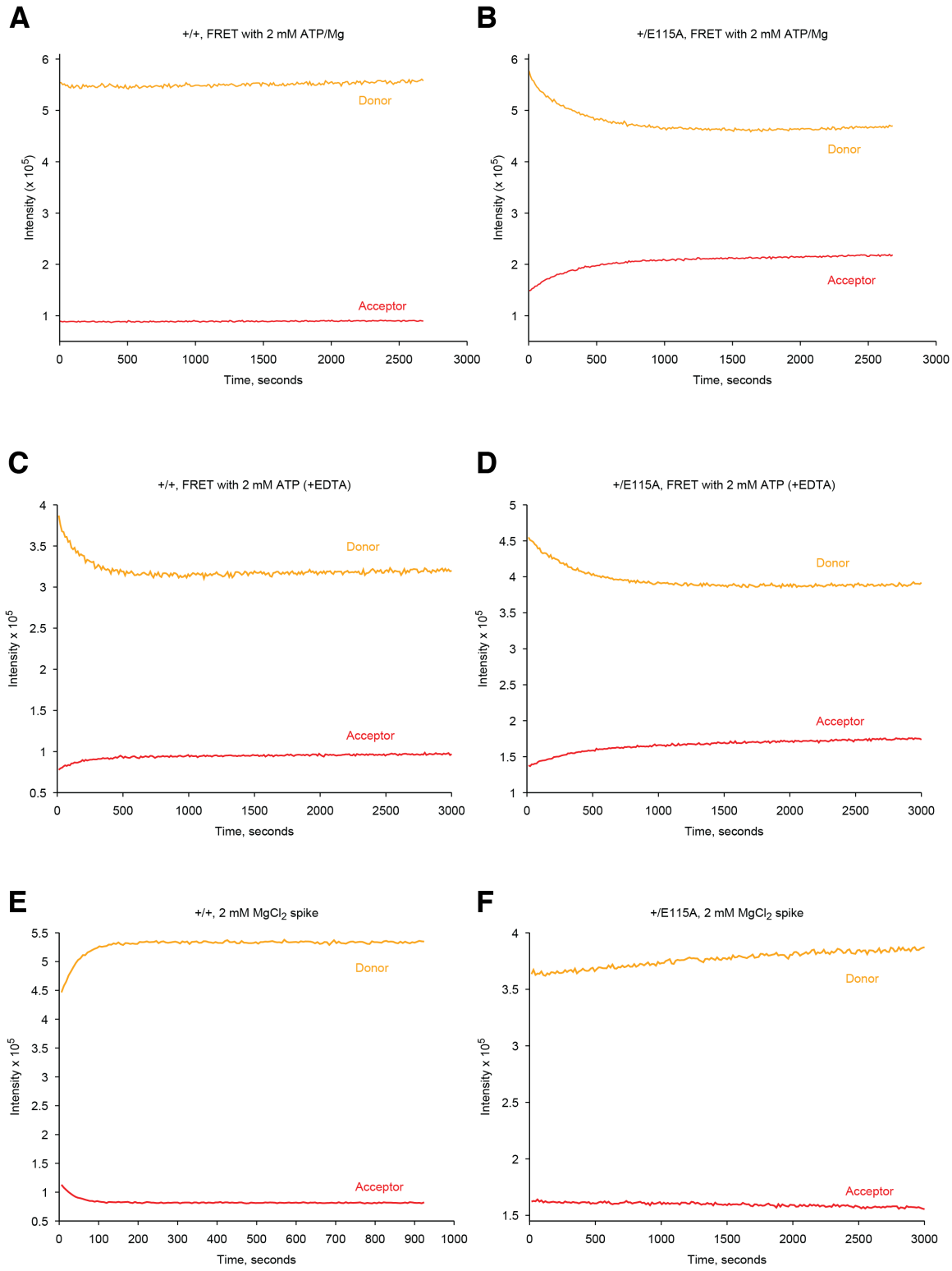

Figure 1-figure supplement 1. Raw fluorescence intensities of FRET data
Donor intensities are colored orange and acceptor intensities are colored red. **A-B)** Raw fluorescence intensities of wildtype (+/+, A) and hemi-hydrolyzing heterodimer (+/E115A, B) in presence of ATP/Mg added at t=0 seconds from Figure 1D. **C-D**) Raw fluorescence intensities of

+/+ (C) and +/E115A (D) showing dimer closure after addition of ATP at t=0 seconds in absence of MgCl2 (with EDTA added) in Figure 1E. **E-F**) Raw fluorescence intensities of +/+ (E) and +/E115A (F) showing dimer reopening after addition of 2 mM of MgCl2 at t=0 seconds.

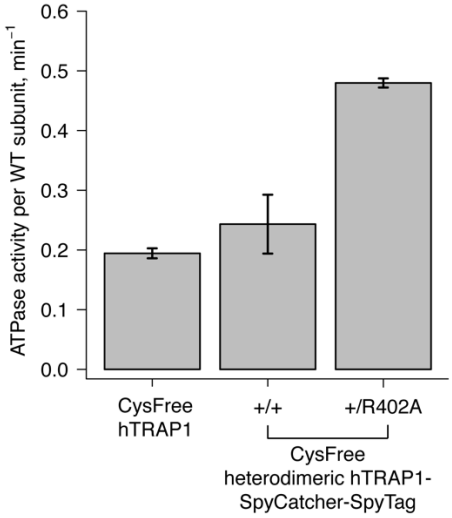

Figure 1-figure supplement 2. Steady-state ATPase assays of cysteine-free hTRAP1 and heterodimeric hTRAP1 (+/+ and +/R402A) at 30˚C
Each bar and error bar are one standard deviation and averaged from triplicate experiments. ATPase activities displayed are normalized per wildtype subunit.

To distinguish between these models, one can form heterodimers by mixing and use FRET to directly probe the conformation of the dimer (Hessling et al., 2009). However, a significant drawback is that the resulting mixture of dimer species complicates further biochemical or especially structural analyses. To allow precise targeting of protomer-specific mutations and produce a homogeneous population of heterodimers without dimer exchange, a covalently bound heterodimeric hTRAP1 was engineered using SpyCatcher/SpyTag (Zakeri et al., 2012) appended after the CTD dimerization domain. Similar to our previous studies (Partridge et al., 2014), we can efficiently monitor TRAP1 closure by attaching FRET probes to cysteines engineered into the NTD (E140C) and MD (K413C) of a cysteine-free chaperone

(Figure 1B). Using the covalent heterodimers, the E115A mutation was introduced to one of the protomers. Appropriate functionality was confirmed by observing that only half of the bound ATP was hydrolyzed under single-turnover conditions (Figure 1C). Since dimer closure is required to hydrolyze ATP, this rules out the model where the heterodimer cannot form the closed state. Furthermore, it suggests that the impaired steady-state ATPase of the dimer may be due to an inability to exit the closed state. If true, this would lead to a build up of the closed state under multiple-turnover conditions that can be monitored by FRET (high FRET), whereas constant turnover of the wildtype enzyme would maintain a low FRET signal. Indeed, this is just what is observed upon addition of 2 mM ATP/$MgCl_2$ to either wildtype or +/E115A TRAP1 (Figure 1D). The buildup rate of the heterodimer (0.16 min^{-1}) is comparable to the steady-state ATP turnover rate of the cysteine-free wildtype (0.19 min^{-1}, Figure 1-figure supplement 2), indicating that having only one active ATP site does not affect the kinetics of forming the closed state. Since the closure rate of the +/E115A construct is not affected and dimer closure precedes ATP hydrolysis, the reduced steady-state ATPase rate must be due to a slower process that happens after the dimer is closed.

To directly test the ability of the hemi-hydrolyzed dimer to exit the closed state, a FRET experiment was designed to look at the kinetics of dimer opening after ATP hydrolysis starting from a synchronized closed state population. This is possible because TRAP1 accumulates the closed state upon addition of ATP in absence of Mg^{2+} (Figure 1E), whereupon hydrolysis can be initiated by addition of excess $MgCl_2$ (Partridge et al., 2014). If hydrolysis of both bound ATPs is required to reset TRAP1 back to an open state, then the hemi-hydrolyzing mutant should have an impaired re-opening rate after $MgCl_2$ is added. Indeed, a very slow re-opening rate is observed for the +/E115A heterodimers whereas the wildtype protein rapidly returns to low FRET baseline

(Figure 1F). These observations strongly support a model where two ATP hydrolyses are required for TRAP1 to progress efficiently through its ATPase cycle.

Crystallographic evidence of sequential and deterministic ATP hydrolysis in TRAP1

The observed accumulation of TRAP1 closed state upon addition of ATP in the absence of Mg^{2+} appears to be specific to the mitochondrial homolog, as bacterial Hsp90 (bHsp90) and yHsp90 don't exhibit this behavior and remain in the open state (data not shown). To characterize this unique state and, through it, gain insight into the TRAP1 ATPase cycle, we crystallized zebrafish TRAP1 (zTRAP1) closed with ATP in the absence of Mg^{2+} with an excess of EDTA. An initial crystal, collected 3 days after setting crystal trays, diffracted to 2.5 Å and was solved using molecular replacement with the previously published TRAP1 structure closed with AMPPNP (Lavery et al., 2014) (PDB:4IPE). The refined model showed no major conformational differences with any of the previously published full-length TRAP1 structures closed with non-hydrolyzable nucleotides (Figure 2A). The same pronounced asymmetry (one straight protomer and one buckled protomer) was clearly observed. However, differences exist in the ATP binding pocket: as expected, the Mg^{2+} electron density previously observed contacting the nucleotide phosphates is missing and, surprisingly, while the straight protomer contained a mostly intact ATP, the buckled protomer had only weak density for the γ-phosphate (Figure 2B, Day 3). This clearly indicated that the buckled protomer preferentially hydrolyzes ATP, but does not inform on whether hydrolysis occurred before or after crystallization.

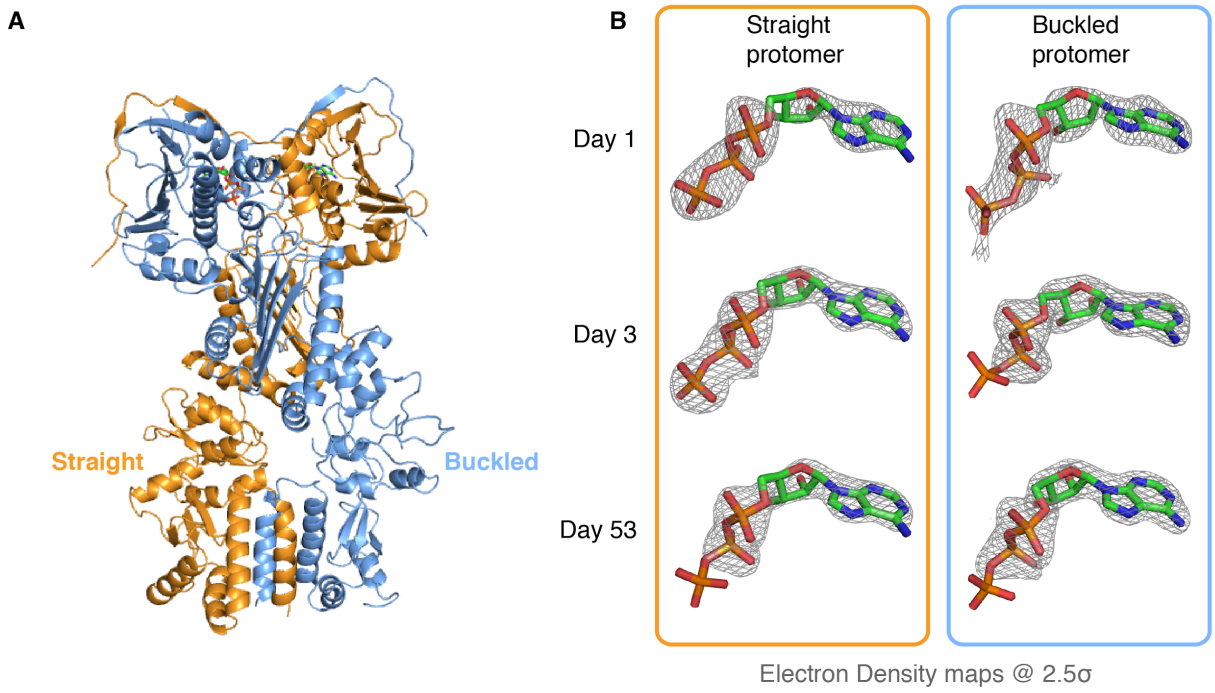

Figure 2. Kinetic crystallography indicates that the buckled arm hydrolyzes ATP first
A) 2.3 Å crystal structure of zTRAP1 closed with ATP obtained from a 3-day old crystal showing minimal conformational changes without Mg^{2+}. Buckled protomer is in blue and Straight protomer is in orange. **B**) ATP electron density maps for the buckled and straight protomers from crystals of different ages showing the evolution of in-crystal hydrolysis.

To differentiate between these possibilities, we took advantage of the fact that our crystals grow overnight, allowing collection and freezing of crystals every 24 hours for a time-resolved experiment. After screening crystals from multiple time points for diffraction quality, two additional datasets were collected (1-day and 53-day old crystals), solved and refined through the same methods to resolutions of 3.5 Å and 2.2 Å respectively. Similar to the three-day old crystal, no significant conformational differences were observed and no Mg^{2+} ion density was present in the ATP binding pocket. However, electron densities for the ATP molecules showed a monotonic progression from an ATP-ATP structure (one day old crystal) through an ATP-ADP intermediate (3-day old crystal) to an ADP-ADP structure (53-day old crystal) (Figure

2B), clearly demonstrating that hydrolysis is occurring in the crystal. This result leads to a model in which TRAP1 hydrolysis events are sequential and deterministic, with the buckled protomer conformation being catalytically favorable and hydrolyzing first. At least in the context of the crystal lattice, no major conformational rearrangements of the symmetry are linked to the first ATP hydrolysis.

TRAP1 hydrolyzes ATP in solution in absence of Magnesium

The fortuitous crystallographic observation of two different ATP hydrolysis rates in the closed state indicates that TRAP1 has the capacity for ATP hydrolysis in the absence of Mg^{2+}, albeit slowly. To exclude the possibility that this was somehow unique to the crystal, we needed an extremely sensitive solution assay that could detect TRAP1 ATPase activity in the absence of Mg^{2+} – a level that could be near the rate of spontaneous ATP hydrolysis. A sensitive fluorescent phosphate sensor (Brune et al., 2002) was chosen for a simple kinetic assay as done by McLaughlin et al. with human Hsp90 (hHsp90). While ideally this would be done using zTRAP1 to match the crystallography, its much weaker K_m would require an order of magnitude higher ATP concentration to trap the closed state than the human homolog (Figure 3A). This would be problematic as it introduces a high free phosphate background from ATP alone. Instead, human TRAP1 was used to detect ATP hydrolysis in solution with 500 μM of ATP in the presence of excess EDTA. At this ATP concentration, there is no significant amount of apo state by size exclusion chromatography (Figure 3B) and the ATP titration by FRET estimates at least 80% closed state (Figure 3A).

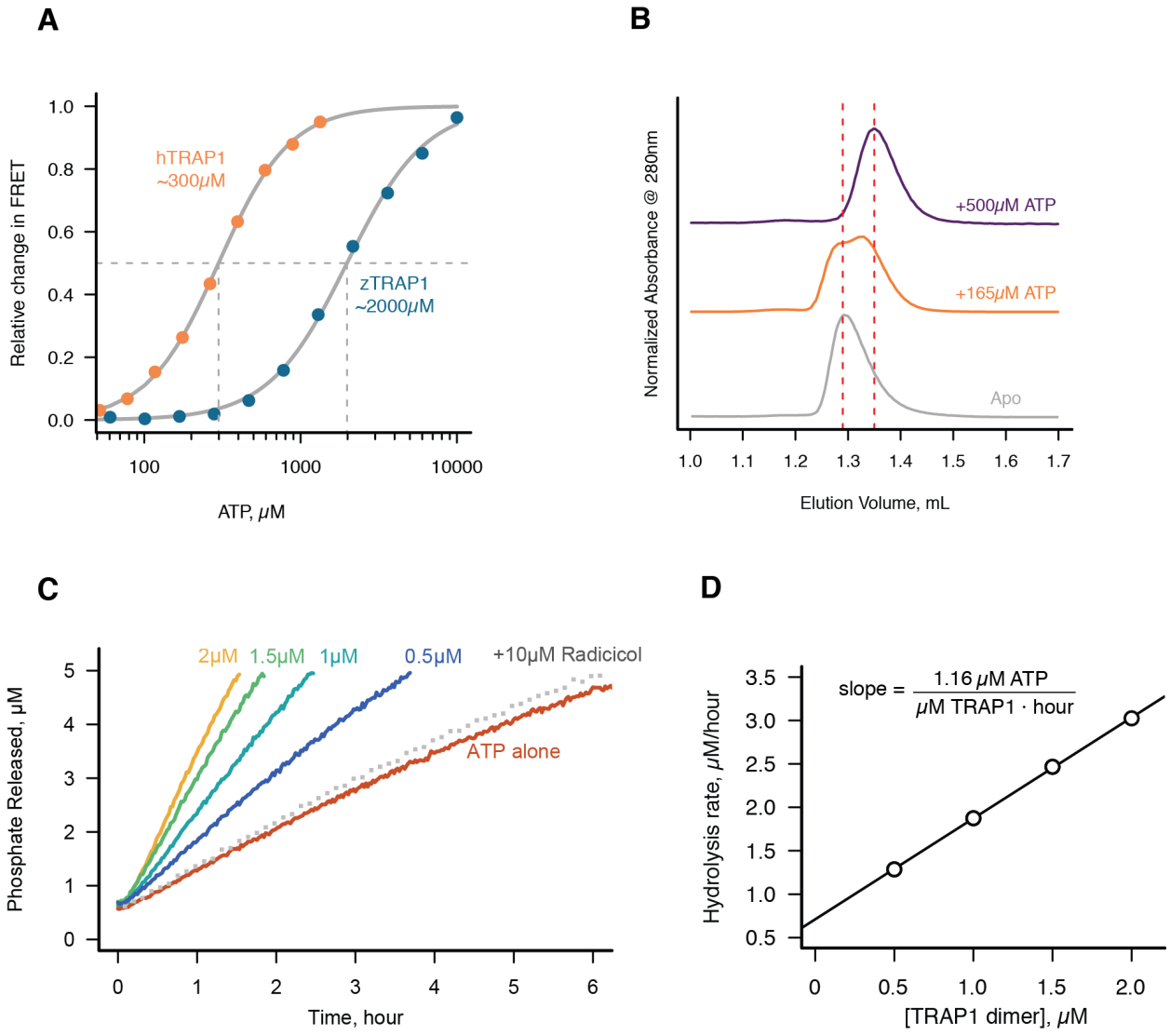

Figure 3. Without Mg^{2+} hTRAP1 adopts the closed state and slowly hydrolyzes ATP in solution

A) Equilibrium titration of closure in response to ATP in presence of excess EDTA hTRAP1 (orange) and zTRAP1 (dark blue) using FRET. The indicated half-max concentrations are obtained from fits to the Hill equation (gray lines). **B**) Size-exclusion chromatography of cysteine-free TRAP1 under apo (gray), and after 1.5-hour incubation at 30˚C with 165 μM ATP (partial closure, orange), and 500 μM ATP (full closure, purple). Red dashed lines are guides for apo and closed state peak positions. **C**) Ultra sensitive assay of ATP hydrolysis using fluorescent phosphate-release assay with PBP-MDCC with ATP alone (red) and varying dimer concentrations of cysteine-free TRAP1, and 2 μM TRAP1 + 10 μM radicicol (gray dotted line). **D**) Initial rates from phosphate-release kinetics plotted against TRAP1 dimer concentration confirming that the rate above baseline is TRAP1 dependent. The ATPase hydrolysis rate per TRAP1 dimer is 1.16 μM ATP· μM $TRAP1^{-1}$ · $hour^{-1}$.

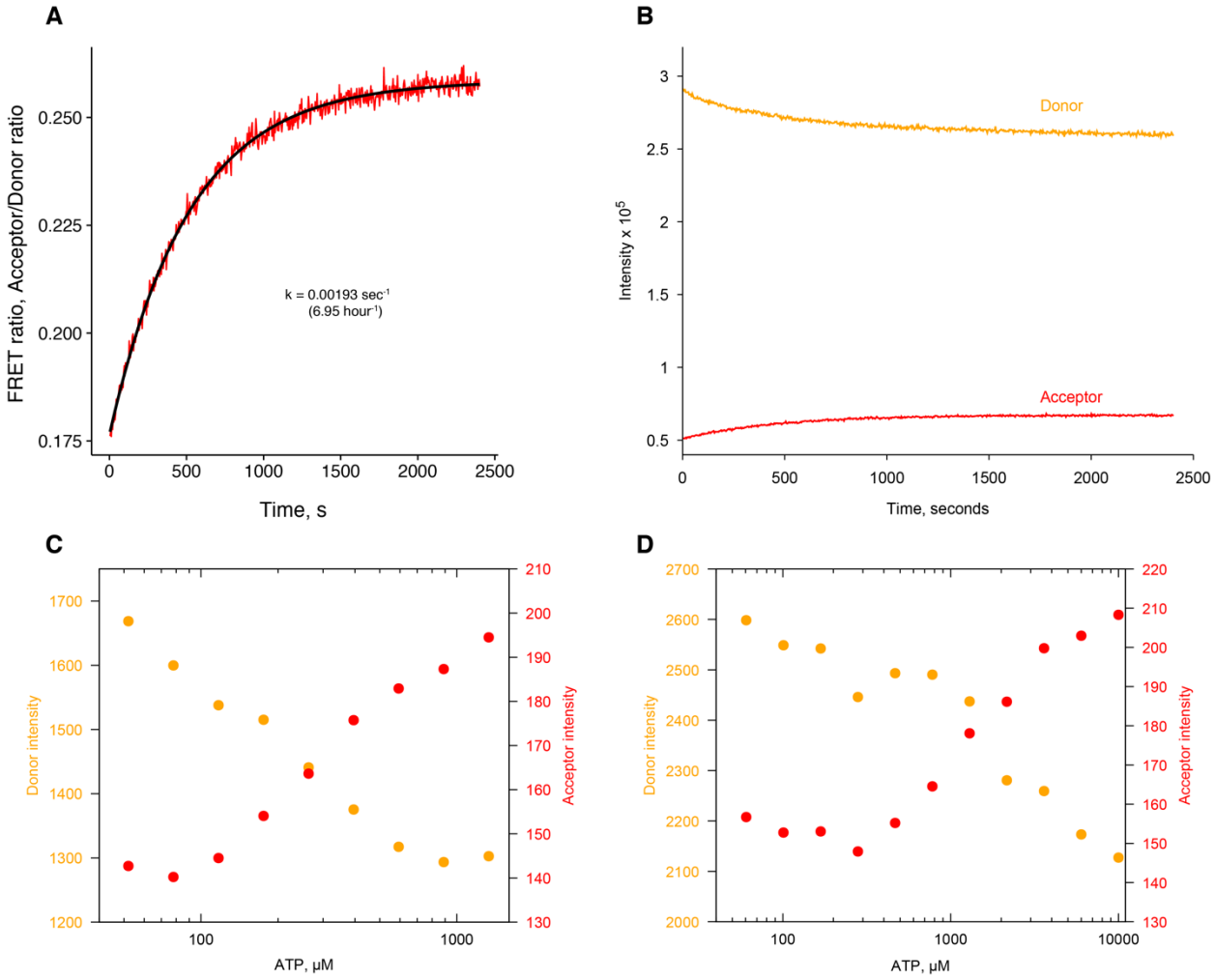

Figure 3-figure supplement 1. ATP-induced dimer closure in absence of Mg^{2+} by FRET in human and zebrafish TRAP1

A) hTRAP1 dimer closure as seen by FRET after addition of 500 µM ATP at 30˚C. Closure rate is much faster than hydrolysis rate in absence of Mg^{2+}. Black line is the fit to an exponential function with the given rate constant. **B**) Raw donor (orange) and acceptor (red) fluorescence intensities of FRET data in A. **C**) Raw donor (orange) and acceptor (red) intensities of ATP titration to human TRAP1 from Figure 3A. **D**) Raw donor (orange) and acceptor (red) intensities of ATP titration to zebrafish TRAP1.

Under this condition, a low but significant ATPase activity is detected in solution (Figure 3C). This ATPase is specific to TRAP1, since the rate of hydrolysis scales with TRAP1 concentration (Figure 3D), and it can be inhibited by the addition of Radicicol (Figure 3C), a

potent ATPase inhibitor for Hsp90 (Leskovar et al., 2008). From this experiment, the spontaneous and TRAP1-catalyzed (Mg^{2+}-free) ATP hydrolysis rates are 0.00155 and 0.5808 per hour (per active site), respectively. Spontaneous hydrolysis would take 62 days whereas the protein-catalyzed hydrolysis would take 4 hours to hydrolyze 90% of the initial ATP concentration. Although we do not have time points between 1, 3, and 53 days for the crystallography, within an order of magnitude, the solution rates roughly correspond to what we see in the crystal. After three days, ATP is fully hydrolyzed by the buckled protomer while ATP remains intact in the straight protomer. Under the same experimental conditions, the rate of dimer closure is an order of magnitude faster (6.95 per hour) than the observed hydrolysis rates (Figure 3-figure supplement 1). Since dimer closure is no longer the slowest step in hydrolysis, it's likely that in absence of Mg^{2+}, hydrolysis of the first ATP by the buckled protomer is now the rate-limiting step.

Asymmetric water dynamics near ATP γ-Phosphate between protomers.

To further explore the structural origins of the differential rates of ATP hydrolysis by the two protomers, we performed microsecond all-atom molecular dynamics simulations based on the crystal structure of the asymmetric zTrap1 dimer (PDB ID: 4IYN). We focused on dynamics as no significant differences in the coordinates of the two active sites were observed in the crystal structures. As part of the straight ATP binding pocket lid was disordered in the crystal structure, the ATP lid regions of both protomers were modeled to be identical and ordered. The ATP analog ADP-AlF_4 in the crystal structure was replaced with ATP in the presence of Mg^{2+}. The simulations were carried out with explicit water at two different temperatures (310 K and 360 K). The high temperature was used to enhance the conformational sampling.

The structures are intact throughout the simulations at both temperatures and exhibit a high degree of flexibility at the microsecond time scale. To investigate a possible mechanism of how the differential ATP hydrolysis is established, we focused on the environment surrounding the ATP. We monitored the numbers of water molecules within a 5 Å radius of the ATP β- and γ-phosphate along the trajectories, sampled every 3 ns.

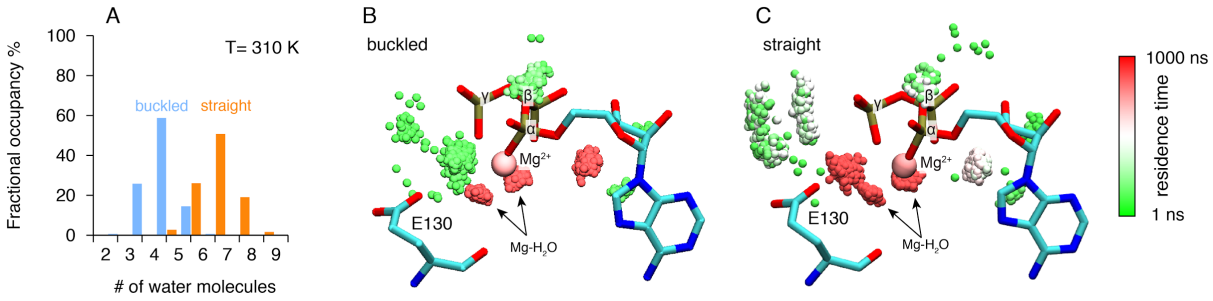

Figure 4. Microsecond all-atom molecular dynamics simulations of zTrap1 reveal asymmetric water dynamics near the ATP γ-phosphate
A) Histogram of water molecules counted near the ATP β- and γ-phosphates (< 5 Å) throughout the simulation (each frame is 3 ns) in the buckled protomer (blue) and the straight protomer (orange) at T = 310 K. **B)** and **C)** Fractional residence time of each individual water molecule in the ATP binding pocket for the buckled and straight protomers at T = 310 K, showing significant differences in solvation near the E130. Only the oxygen of water molecules near the ATP β- and γ-phosphates (< 5 Å) are shown. Points are accumulated from all frames along the trajectory after aligning the system based on the ATP. Black arrows point to the persistent magnesium-coordinated water molecules, Mg-H_2O, which are conserved for the two conformers. Water molecules were colored based on their residence time as indicated by the color bar.

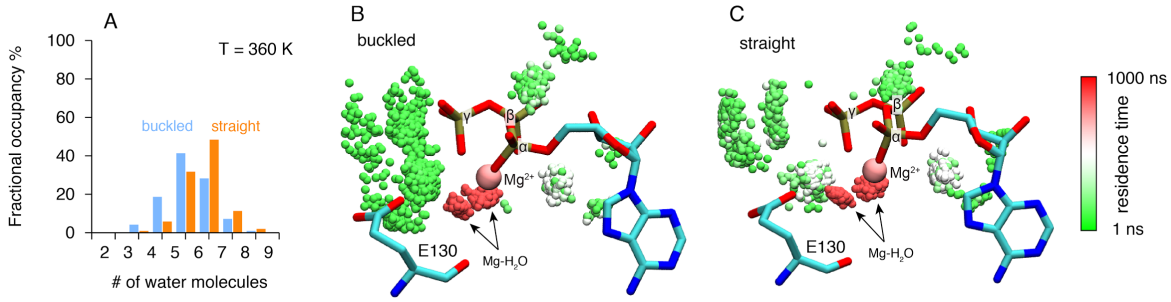

Figure 4-figure supplement 1. Microsecond all-atom molecular dynamics simulations of zTrap1 reveal asymmetric water dynamics near the ATP γ-phosphate at 360 K.
A) Fractional occupancy of water molecules near the ATP β- and γ-phosphate (< 5 Å) within each 3 ns window in the buckled protomer A (blue) and the straight protomer B (orange). **B)** and **C)** Dwell time of each individual water molecule in ATP binding pocket for buckled protomer and straight at T = 360 K. The figures were rendered by showing the water molecules (only oxygen for clarity) near the ATP β- and γ-phosphate (< 5 Å) of all frames along the trajectory after aligning the system based on ATP. Black arrows point to magnesium-coordinated water molecules, Mg-H_2O. The water molecules were colored based on how long they stay in the vicinity of the ATP.

On average, the ATP γ-phosphate in the buckled protomer has fewer water molecules in proximity than the one in the straight protomer (Figure 4A). At higher temperature, the same trend is maintained despite a larger overlap between the distributions (Figure 4-figure supplement 1A). This was unexpected given that both of the nucleotide binding pockets appear to be essentially identical. The average RMSD between the N-terminal domain of the two protomers is 1.74 Å. The different water dynamics likely arises from differential dynamics of the two protomers.

In addition to the different water occupancy, the most striking difference between protomers observed in the simulations are the water dynamics near the two ATP β- and γ-phosphates. Excluding the Mg^{2+} coordination waters (Figure 4B,C), most of the waters spend only a few nanoseconds (Figure 4B, green) in the buckled protomer. In contrast, in the straight protomer, there are longer-lived waters positioned between E130 and the γ-phosphate (Figure

4C, red vs 4B, green) and also more waters positioned above E130 (Figure 4C, white). This trend is also observed at high temperature (Figure 4-figure supplement 1B,C). While the precise mechanism is still unclear, this asymmetry in water occupancy and dynamics between two protomers likely correlates with the observed preferential hydrolysis of the buckled protomer ATP observed in the time-resolved X-ray crystallography.

Loss of the γ-Phosphate contact determines MD:CTD conformation in the ATP/ADP state

ATP analogs have been successfully used to capture pre- and post-hydrolysis transition intermediate conformational states of several ATPases providing insights into their mechanisms (Chen et al., 2007; Fisher et al., 2002; Wittinghofer, 1997). In contrast, previous TRAP1 experiments with these analogs resulted in similar asymmetric structures with no obvious conformational differences. In our time-resolved crystallography experiments, the solved structures remain in essentially the same conformation despite having gone through a full conversion from two ATPs to two ADPs. Because crystallographic packing likely prevents any significant conformational changes that might occur after the first ATP hydrolysis, DEER (Pannier et al., 2011) was again the optimal choice for directly probing the solution MD:CTD conformation of hTRAP1 in the hemi-hydrolyzed (ATP/ADP) state. The challenge is then to capture a stable ATP/ADP hybrid state.

To generate an ADP-state in only one protomer, we make use of the observation that the MD-Arg (R402 in hTRAP1), the only residue in Hsp90 that contacts the γ-phosphate, acts as an ATP sensor (Cunningham et al., 2012) and mutating this residue would effectively mimic the ADP state. Using the SpyCatcher/SpyTag heterodimer, we introduced a point mutant (R402A) to break the γ-phosphate contact in only one protomer. This heterodimeric construct (+/R402A) can

form the closed state upon incubation with the ATP analog ADP-BeF (Figure 5-figure supplement 1) and has minimally perturbed (2-fold increase) ATPase activity (Figure 1-figure supplement 2). A cysteine-free version of this heterodimer was used for site-directed spin labeling at the MD (K439C) and CTD (D684C). These positions optimally report on unique MD:CTD distances within each protomer. By measuring the distance between these probes via DEER, one can distinguish between a buckled or straight conformation of the labeled protomer in the closed state (Lavery et al., 2014). As expected for the wild type heterodimer, two peaks were observed centered at about 22Å and 41Å with roughly equal proportions (Figure 5A). This is close to the 50:50 probability of a protomer randomly adopting either conformation in an asymmetric closed state. Although the observed distances do not exactly match the corresponding values from the crystal structures, they are well within measurement uncertainties when the maleimide linker (~8 Å) and broad distribution of distances are taken into account. Placing this spin-label pair on a protomer carrying the R402A mutation (+/R402A *cis*) or across from that mutant protomer (+/R402A *trans*) can independently report on both MD:CTD conformations of the hemi-hydrolyzed dimer in the closed state.

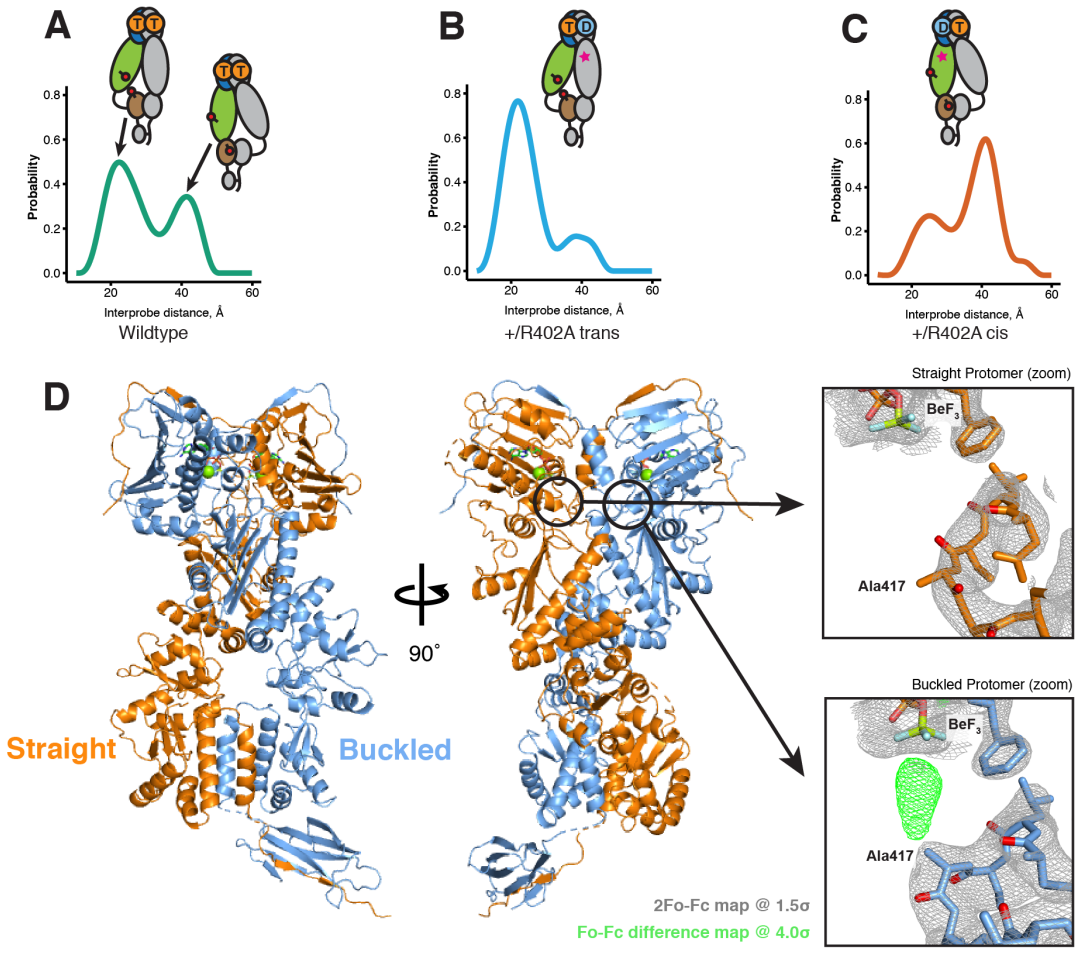

Figure 5. The asymmetry is flipped in the ATP/ADP state as revealed by DEER on hemi-hydrolyzed (ATP/ADP) heterodimers

The cartoons depict hTRAP1 heterodimers (one protomer colored by domains and the other in gray; NTD, blue; MD, green; CTD, brown) with spin-labels (red circles) and the relevant nucleotide state (D or T, for ADP or ATP respectively) as well as the R402A mutation (ADP state mimic; magenta star). The SpyCatcher-SpyTag is shown attached to the CTD tails. **A**) +/+ heterodimers (green line) partition roughly equally between the buckled (left, 22 Å) and straight (right, 41 Å) conformations. **B**) Spin-labels on the opposite (*trans*) protomer of +/R402A heterodimers (blue line) show that nearly all molecules are buckled on the ATP arm. **C**) +/R402A heterodimers (orange line) carrying spin-labels on the same (*cis*) protomer as the R402A mutation, showing that the protomer prefers the straight conformation. **D**) Crystal structure of +/R417A heterodimeric zTrap1 with the SpyCatcher-SpyTag fusion in the asymmetric closed state showing buckled (blue) and straight (orange) protomers. The dashed line indicates disordered residues. Insets show that the γ-phosphate sensing R417 is only present on the buckled arm. Phases come from a model having Ala on both protomers. 2Fo-Fc density (gray mesh) and Fo-Fc difference map (green mesh) around the position of the asymmetric

R417A mutation. Strong positive density (green mesh) on the difference map is observed only at the buckled protomer.

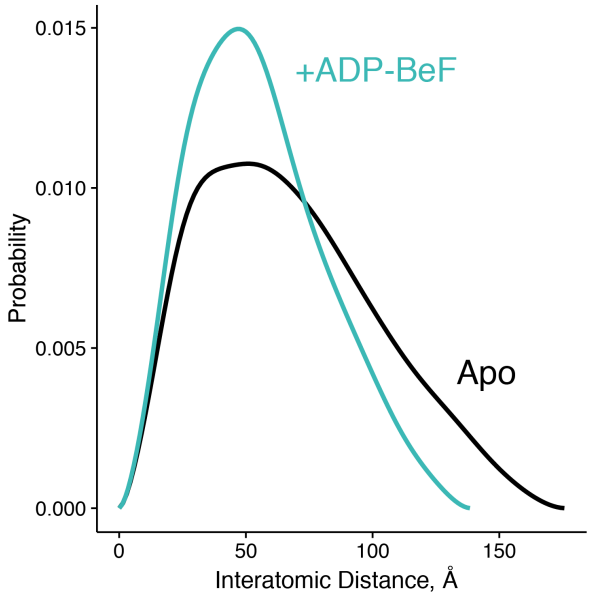

Figure 5-figure supplement 1. Interatomic distance distribution, P(r), from SAXS experiments of heterodimeric +/R402A human TRAP1
The heterodimer is fully capable of closing, shown as overall reduction in the width and maximum dimension of the P(r) distribution upon incubation with an ATP analog (ADP-BeF, teal). The black curve is the P(r) of the apo dimer.

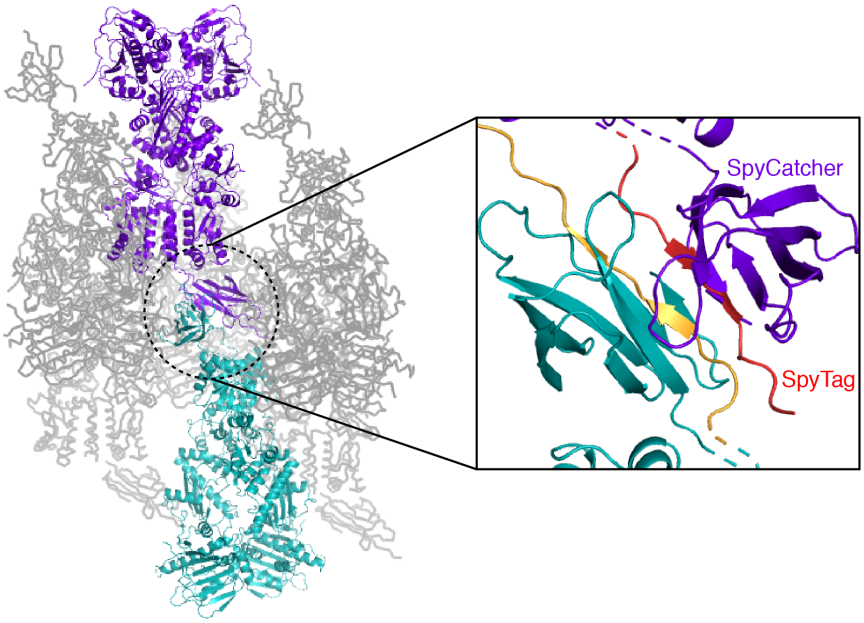

Figure 5-figure supplement 2. Crystal packing interactions for the heterodimeric (+/R417A) zTRAP1 fused to the SpyCatcher-Tag domains
A pair of symmetry mates is colored purple and teal whose SpyCatcher-Tag domains pack against each other (black inset, a close-up of the dotted circle). The SpyCatcher and SpyTag belonging to one dimer are colored purple and red, respectively. The corresponding SpyCatcher-SpyTag symmetry mate is colored teal and yellow, respectively.

If TRAP1 adopts a symmetric closed state after losing one γ-phosphate contact, a single distance should be observed irrespective of spin-label placement in the hemi-hydrolyzed state. Instead, two different distances were observed depending on the placement of the spin-labels with respect to the R402A mutation. Protomers with an intact γ-phosphate contact adopt mostly a 22 Å MD:CTD distance - consistent with the buckled conformation (Figure 5B), whereas spin-labeled protomers lacking the γ-phosphate contact exhibit a major peak at 41 Å - consistent with the straight conformation (Figure 5C). Our interpretation that these distances faithfully report on

the MD:CTD conformations rely on assumptions that the spin-labels, the R417A mutation, or the SpyCatcher fusion did not introduce unintended perturbations.

To address this concern, we crystallized an equivalent heterodimeric construct of zTRAP1 (+/R417A in zebrafish sequence numbering) in the presence of ADP-BeF. The heterodimeric crystal diffracted to 3.2 Å and was solved with molecular replacement using the published model of ADP-BeF-bound zTRAP1 (Lavery et al., 2014) (PDB:4J0B) and a SpyCatcher-SpyTag complex(L. Li et al., 2014) (PDB:4MLS). As predicted from the DEER results, the heterodimer adopts an essentially identical asymmetric closed state (Figure 5D), and the C-terminal-fused SpyCatcher-SpyTag complex packs against its symmetry mate in the opposing dimer (Figure 5-figure supplement 2). The structure shows that the R417A mutation does not perturb the overall closed state. To avoid model bias, the dataset was refined starting with alanines replacing arginines at positions 417 on both protomers. The Fo-Fc difference map (Figure 5D, insets) show strong positive density for the arginine only on the buckled protomer (ATP state), while the R417A mutation is on the straight protomer (ADP state). This is completely consistent with the interprobe distances measured in the DEER experiments correctly representing the buckled and straight protomer conformations. Altogether, this demonstrates that the loss of the γ-phosphate contact within the closed dimer is a strong determinant of the corresponding protomer conformation. Thus, the first ATP hydrolysis directly alters dimer asymmetry upon phosphate release.

Discussion

Previous equilibrium Hsp90 structural studies have provided a picture of a dynamic molecular machine whose conformational ensemble, well described by rigid-body motions of its

globular domains, is differentially tuned, but not exclusively determined by nucleotide binding. While ATP-binding has a clear role in stabilizing the NTD-dimerized closed state — depicted clearly by closed states of yHsp90 (Ali et al., 2006), zTRAP1 (Lavery et al., 2014), and hHsp90 (Verba et al., 2016) — the role of ATP hydrolysis in Hsp90's conformational cycle remains unclear. In this study, we present evidence for a sequential, deterministic hydrolysis of the two ATPs within the mitochondrial Hsp90 (TRAP1) dimer. Each step of hydrolysis drives conformational changes at the client binding site located at the juncture between the middle and C-terminal domains. We discuss below how this provides a new framework for understanding the mechanism of ATP-dependent client remodeling by Hsp90.

Mechanism of conformational coupling to sequential ATP hydrolysis

Earlier TRAP1 studies had shown how the strain of closing results in a markedly asymmetric (straight:buckled) two-ATP (ATP/ATP) closed state both in the crystal and in solution (Lavery et al., 2014). Unlike the stochastic picture that emerged from equilibrium structural studies (Krukenberg et al., 2008; Mickler et al., 2009; Southworth and Agard, 2008) here we show that hydrolysis of both ATPs is required for efficient reopening. Thus, once closed, kinetic rather than thermodynamic processes govern progression through the conformational cycle. Given this observation, we focused on whether the order of ATP hydrolysis depends upon the asymmetry and on what happens after the first ATP is hydrolyzed.

To facilitate this work, covalent heterodimers were efficiently created using C-terminal fusions with SpyCatcher and SpyTag (Zakeri et al., 2012). Also critical was the ability to close TRAP1 with ATP but in the absence of Mg^{2+}, allowing the normally rate-limiting closure step to be bypassed, thereby synchronizing all molecules in a closed ATP/ATP state. The fortuitous

ability of the Mg^{2+}-free closed state to be crystallized with ATP, allowed the slow hydrolysis process to be examined crystallographically using crystals of different ages – revealing that the buckled protomer hydrolyzes ATP first while the straight protomer is still bound to an intact ATP. Concerned that the slow hydrolysis seen in the crystal could be an artifact of packing effects on the ATP lid, quantitative kinetics using a highly sensitive assay for phosphate release confirmed that in the absence of Mg^{2+}, ATP hydrolysis does occur slowly in solution.

What happens structurally after the first ATP is hydrolyzed? Unfortunately, beyond small perturbations, the crystal lattice blocks significant conformational rearrangements, even after weeks when both ATPs have been hydrolyzed. To resolve this, we used DEER measurements on heterodimers engineered to mimic the mixed ADP:ATP state in solution. In the ATP:ATP state, the labeled protomers adopt roughly an equal mixture of the two conformers, due to the random buckling on transition to the highly strained closed state. By contrast, after the first ATP hydrolysis, essentially all the molecules are in a defined state with the ADP protomer being straight and the ATP protomer buckled.

Combined, these results indicate that hydrolysis of the first ATP must alter the conformational asymmetry in all molecules such that the ADP containing protomer straightens while the remaining ATP protomer adopts the buckled, catalytically favorable conformation. Including our observation that reopening only efficiently occurs from the ADP:ADP state leads to the proposed conformational cycle revealing how ATP hydrolysis can potentially perform work to remodel a bound client protein (Figure 6).

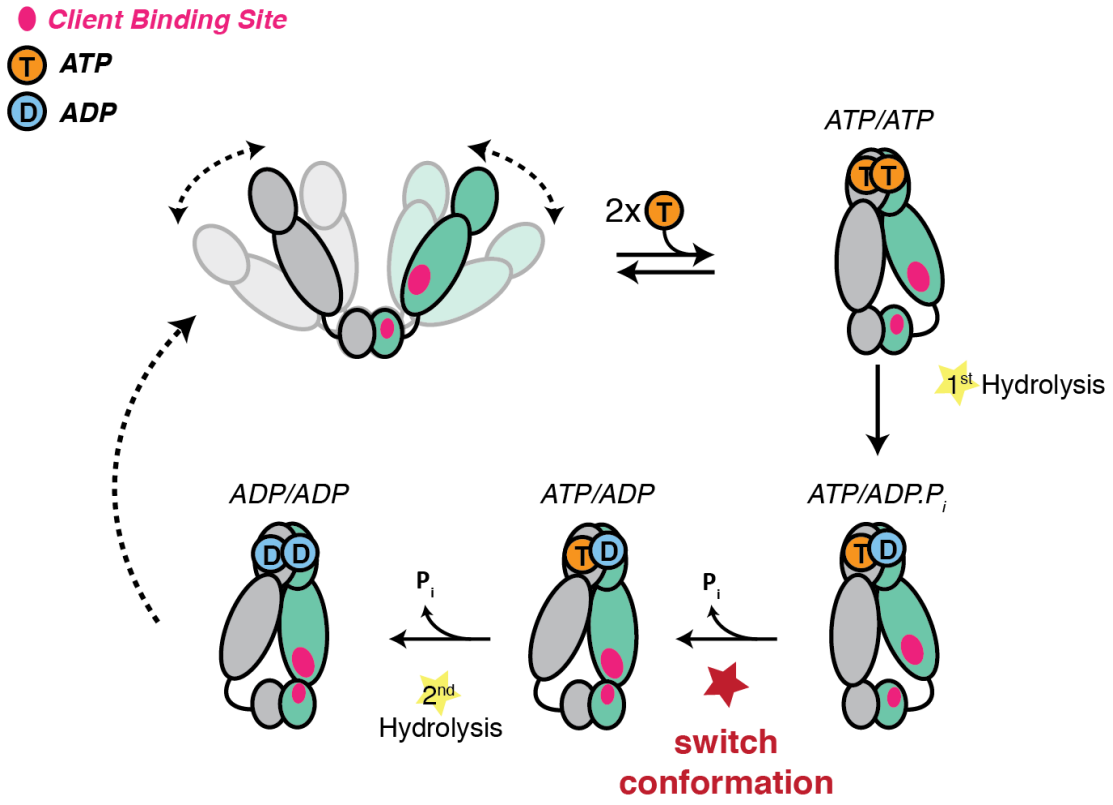

Figure 6. Revised model of the TRAP1 ATPase cycle showing the obligatory sequential hydrolysis and conformational switching
The protomers are colored teal and gray. The dynamic apo state (upper left) binds two ATPs, which stabilize a strained asymmetric NTD-dimerized closed state. Within this closed state, ATP is hydrolyzed first by the buckled protomer. Release of Pi likely drives the observed conformational switch of the straight protomer (ATP) to a buckled conformation, while the previously buckled protomer (now ADP), straightens. Concomitant with the flip, the client binding sites (magenta ellipses) are rearranged, to facilitate client remodeling. Now in a buckled conformation, the second ATP is set up to be hydrolyzed. Finally, the ADP/ADP dimer re-opens releasing nucleotides, resetting the TRAP1 to the apo state.

(i) Binding ATP leads to stabilization of a strained, high-energy closed state (Lavery et al., 2014; Partridge et al., 2014). (ii) The buckled protomer preferentially hydrolyzes ATP, transiently producing a buckled ADP state. (iii) The asymmetry flips so that the ATP protomer is now buckled, setting it up for hydrolysis. (iv) The second ATP is hydrolyzed, leading to reopening, fully relieving strain. While this work was done with the mitochondrial Hsp90

ortholog, the proposed sequential hydrolysis mechanism also explain the lack of ATPase cooperativity observed in other Hsp90s (Frey et al., 2007; Richter et al., 2008).

A model for Hsp90 client maturation mechanism

Although Hsp90 has been studied for over 30 years and its importance in many key cellular processes established, the mechanism by which it matures a large set of diverse clients remains uncertain. This is partly due to Hsp90 preferentially interacting with intrinsically unstable proteins, which has hampered in vitro studies of the chaperone in the context of these clients. In the absence of client proteins, Hsp90 cycles between a wide-open V-shaped apo state and a more compact closed state. In principle, rearrangements of hydrophobic residues accompanying the large conformational change (open-to-closed) could be used to remodel client protein, leading to a molecular "clamp" model (Prodromou et al., 2000). However, we note that constricting the large open-to-close transition, as done by forcing constitutive dimerization of the NTDs, has no major adverse effect on cell growth and only modestly impairs client activation (Pullen and Bolon, 2011). This observation, plus the marginal impact of ATP binding in driving dimer closure, the typically quite weak ATP affinity, and the fact that the open and closed states are roughly isoenergetic, implies that the open-to-close transition is unlikely to be the ATP-driven mechanism for client remodeling by Hsp90.

The conformational changes directly linked to ATP-hydrolysis, especially at client-interacting residues, seem better suited for such a mechanism. Studies on HtpG with the model client Δ131Δ (Street et al., 2011) as well as the very recently determined atomic structure of the human Hsp90:Cdc37:Cdk4 kinase complex (Verba et al., 2016), have begun to map critical determinants of client binding residues at the juncture of the Middle and C-terminal domains. As

noted by Lavery et al, this coincides with the region of maximal asymmetry in TRAP1 (Lavery et al., 2014). Our observation of a hydrolysis-driven conformational switch in which ATP hydrolysis directly promotes a rearrangement of the client binding region provides a mechanism for actively inducing conformational changes in the client. Equally important is that flipping of the entire TRAP1 population allows clients preferentially bound to either protomer, depending on their size, conformation or other characteristics, to be remodeled via rearrangement of their binding interface. Thus, the first hydrolysis would be used for client remodeling while the second one would be used to reset the ATP-dependent cycle of TRAP1. Notably, there is some evidence that such a sequential ATP hydrolysis mechanism may be shared among other GHKL ATPases. Yeast topoisomerase II, an enzyme which unlinks double-stranded DNA catenanes, hydrolyzes two ATP sequentially (Harkins et al., 1998), and the first ATP hydrolysis appears to be used to facilitate DNA transport in decatenation (Baird et al., 2001). Whether this asymmetric mechanism is conserved throughout all GHKL family members remains to be seen.

A critical feature of our model is the presence of functional asymmetry within the Hsp90 homodimer. Such asymmetry can either be intrinsic to Hsp90 or induced by interactions with other components. Indeed, emerging evidence suggests that functional complexes are preferentially asymmetric (Ebong et al., 2011; Kirschke et al., 2014; J. Li et al., 2011; Verba et al., 2016). For the eukaryotic cytosolic enzymes, this asymmetry can be provided by the numerous Hsp90-specific cochaperones or asymmetric post-translational modifications (Mollapour et al., 2014). By contrast, TRAP1 and its bacterial homologs have no known cochaperones. The results and data presented here suggest that, in the case of the mitochondrial and bacterial chaperones, this necessary functional asymmetry may be an intrinsic property encoded by the structural asymmetry of the closed state.

Acknowledgements

We thank members of the Agard Lab for helpful discussions. We especially thank John Bruning for collecting diffraction data on heterodimeric zTRAP1 crystals. We also thank Nariman Naber and Roger Cooke for help with CW EPR measurements. We thank Jarett Wilcoxen at the UC Davis CalEPR center for help with DEER measurements. Support for this work was provided by the NIH Protein Structure Initiative–Biology Grant U01 GM098254 (to D.A.A.), U54-GM094597 to (M.A.K. and G.T. Montelione), the Howard Hughes Medical Institute (to D.A.A.), and an HHMI Helen Hay Whitney Foundation Postdoctoral Fellowship (to Y.L.). Molecular dynamics simulation was performed using computational resources from the Extreme Science and Engineering Discovery Environment (XSEDE), which is supported by NSF grant ACI-1053575, and the Anton supercomputer at the Pittsburgh Supercomputing Center (PSC) supported by NIH grant R01GM116961. The Anton supercomputer at PSC was generously made available by D.E. Shaw Research.

We also thank James Holton, George Meigs, and staff at Advanced Light Source (ALS) beamline 8.3.1 for help with data collection. Beamline 8.3.1 at the ALS is operated by the University of California Office of the President, Multicampus Research Programs and Initiatives grant MR-15-328599 and Program for Breakthrough Biomedical Research, which is partially funded by the Sandler Foundation.

Methods and experimental procedures

Cloning and Protein Purification

The constructs for Human and Zebrafish TRAP1 were the same as previously used (Lavery et al., 2014). Covalent Heterodimeric constructs were made by fusing SpyCatcher and SpyTag (Zakeri et al., 2012) domain via an 8-a.a Gly-Ser (GGSGSGSG) linker at the C-terminus of TRAP1. The SpyCatcher domain was obtained from the pDEST14 plasmid obtained via AddGene. The construct used for heterodimeric zebrafish TRAP1 crystallography (+/R417A) has modified linker lengths appended to its C-terminus to account for the offset in starting amino acid residues between SpyCatcher and SpyTag. The SpyCatcher fusion has only a 2 a.a. (GS) linker and the SpyTag fusion has a 6 a.a. (GGSGSS) linker. Proteins were expressed in E. coli BL21(DE3)-RIL. Cells were grown in TB media at 37˚C to OD_{600} of ~0.8 and then induced with 0.5 mM IPTG for 8-12 hours at 16˚C. Proteins were purified by Nickel-affinity chromatography, anion exchange (MonoQ 10/100GL, GE) and gel filtration (S200 16/60, GE).

Heterodimeric constructs were expressed separately and then combined in roughly stoichiometric amounts after imidazole elution and incubated overnight at 4˚C while dialyzing into a low-salt buffer (10 mM Tris pH 8.0, 1 mM DTT). The heterodimers are separated via anion exchange with KCl gradient from 5 mM to 250 mM in 14 column volumes. Heterodimeric peaks were pooled and then incubated with TEV protease overnight at 4˚C to cleave the N-terminal His-tag. Finally, proteins were further purified by gel filtration before they were snap frozen with liquid N_2.

Crystallization and data collection

Wildtype zTRAP1 protein at 5 mg/mL in 50 mM HEPES pH 7.5, 50 mM KCl and 1 mM TCEP was incubated with 10 mM ATP and 10 mM EDTA for one hour at RT to allow TRAP1 closure before setting 2 µL hanging drops by mixing 1:1 with crystallization condition consisting of 0.2 M Na/K tartrate, 19% (v/v) PEG3350 and 36 mM hexammine cobalt. Heterodimeric (+/R417A) zTRAP1 was incubated with 10 mM ADP-BeF/$MgCl_2$ for 1 hour at 30˚C to allow dimer closure. After incubation, samples were spun at 16,000xg for 10 minutes and transferred to new tubes. The crystals were grown in 0.19 M potassium acetate with varying PEG3350 (20-22%) and benzamidine hydrochloride (5-25 mM) as an additive. For each well condition, three protein concentrations: 0.5, 1, and 1.5 mg/mL were used to set 2 µl (1:1 protein to condition) hanging drops per concentration. All diffraction data were collected at beamline 8.3.1 at the Advanced Light Source in Berkeley, CA (at 1.116 Å wavelength and 91.4K).

Structure determination and refinement

Wildtype zTRAP1 datasets were indexed using iMosflm 7.2 (Battye et al., 2011), and solved using molecular replacement (Phenix 1.10 - Phaser-MR) with PDB:4IPE and refined with phenix.refine (Adams et al., 2010) and manual refinement in Coot 0.8.3. Ramachandran statistics for the refined zTRAP1 1-day structure are 94.6% favored, 5% allowed, 0.3% outlier. Ramachandran statistics for the refined zTRAP1 3-day structure are 95.4% favored, 3.5% allowed, 1.1% outlier. Ramachandran statistics for the refined zTRAP1 53-day structure are 94.8% favored, 4.3% allowed, 0.9% outlier.

Heterodimeric (+/R417A) zTRAP1 dataset was indexed using XDS (KabschIUCr, 2010) and initially solved by molecular replacement with PDB:4J0B using using Phaser (simple

interface) via CCP4i2-alpha interface (Winn et al., 2011). Then a sequential search with the SpyCatcher-SpyTag complex (PDB:4MLS (L. Li et al., 2014)) is performed while keeping the previous solution fixed. Refinements of the heterodimeric zTRAP1 were done with Refmac5 (Murshudov et al., 1997) using TLS groups and jelly-body restraints. Ramachandran statistics for the refined zTRAP1 +/R417A structure are 94% favored, 4.2% allowed, 1.7% outlier. Data and refinement statistics for all crystals are summarized in Supplementary file 1A.

FRET sample preparation and experiments

Two cysteines were introduced to the cysteine-free heterodimeric hTRAP1 constructs: one at the NTD at Glu140 (E140C) and another on the MD at Lys413 (K413C). Analogous constructs for the zebrafish TRAP1 was created by introducing point mutants G151C and K428C. Purified proteins were labeled with an equal mixture of Alexa Fluor 555 and Alexa Fluor 647 maleimide (ThermoFisher) at 2X molar excess to cysteines and incubated overnight at 4˚C. Unreacted dyes were then quenched with addition of 5 mM β-MeOH and removed using HiTrap desalting column (2x5 mL). For FRET experiments, 0.5 μM of labeled heterodimers were used. Measurements were obtained using a Horiba Jobin Yvon FluoroMax 4 spectrofluorometer equipped with a chilling/heating water bath. Samples were excited at 532 nm and emission wavelengths were collected at 567 nm and 668 nm for donor and acceptor fluorescence, respectively. Relative FRET efficiencies are calculated by taking the ratio of acceptor to donor fluorescence intensity. The change in FRET is the change of this ratio relative to timepoint 0.

SAXS experiments and data processing

Protein samples were buffer exchanged via size-exclusion chromatography using S200 10/300 GL (GE Healthcare Life Sciences) prior to the experiment. 6 mg/mL of heterodimeric hTRAP1 (+/R402A) was incubated at 30˚C for 3 hours with 1 mM ADP-BeF in reaction buffer (20 mM potassium phosphate pH7.0, 50 mM KCl, 2 mM MgCl2, 1 mM DTT). After incubation, samples were spun down at 16,000xg for 10 minutes and transferred to a new tube. Each experiment was collected with a total of 90-minute exposure (15 sec x 360 frames) using an in-house (Anton Paar SAXSESS mc^2) SAXS instrument. Fitting of scattering intensity was done using a custom-written software written in Python2.7 and Fortran (Elnatan, 2017). The software applies smearing correction accounting for slit-collimated geometry of the X-ray beam, and it uses a Bayesian algorithm to choose an optimal D_{max} and smoothness of the P(r)(Hansen, 2000). The software also estimates protein molecular mass from an invariant, Q_r (Rambo and Tainer, 2013).

DEER sample preparation and measurements

Cysteine-free variants of heterodimeric hTrap1 were used for site-directed spin-labeling with maleimide spin-labels (4-maleimido-TEMPO, Sigma-Aldrich) after introduction of cysteines at positions K439 and D684. Prior to labeling, proteins were incubated with 5 mM DTT for 15 minutes at 4˚C, and DTT was then removed using a HiTrap desalting column (2x5 mL) equilibrated with N_2-purged labeling buffer (20 mM HEPES pH7.5, 100 mM KCl). Spin labels were incorporated by immediate addition of 3-fold molar excess spin-label and incubated at 4˚C overnight. Unreacted probes were removed using HiTrap Desalting (2x5 mL) columns equilibrated with DEER reaction buffer (20 mM potassium phosphate pH 7.0, 50 mM KCl, 2

mM $MgCl_2$). Separation of free-labels and extent of labeling was assessed by continuous wave (CW) EPR using a Bruker EMX EPR spectrometer (9.83 GHz). Labeled proteins were then buffer exchanged via a 30 kDa MWCO concentrator into the same buffer made in D_2O. Spin-labeled hTrap1 (~140 μM dimer) was incubated with 1 mM ADP + 2 mM BeF mix (2 mM $BeCl_2$ + 10 mM KF) in presence of 2 mM $MgCl_2$ for 1 hour at 30˚C. Glycerol-d_8 (Sigma-Aldrich) was then added to a final ~30% (v/v) before snap freezing 10 ul samples in 1.1 mm ID quartz capillary tubes in liquid N_2. Four-pulse DEER data collection and analysis was done as previously described(Lavery et al., 2014). Data analysis was done with DeerAnalysis 2013 (http://www.epr.ethz.ch/software.html) in MATLAB to determine distance distributions as previously described (Lavery et al., 2014).

Production of Phoshate-Binding Protein (PBP) and labeling for phosphate release assay

Phosphate release was assayed using Phosphate Binding Protein (PBP) labeled with MDCC (abcam, ab145370) according to Brune et al. with modifications in the protein purification and labeling. The PhoS gene was cloned from BL21 E. coli genomic DNA, and DeoD (E. Coli purine nucleoside phosphorylase, ecPNPase) and DeoB (E. coli phosphodeoxyribomutase, ecPDRM) were synthesized using the BioXP3200 platform (SGI DNA) and cloned into pet28a expression vectors with an N-terminal 6xHis tag. Ala197Cys point mutation in PhoS was introduced for site-specific labeling. All of the purification and labeling used plastic containers instead of glass to minimize phosphate contamination, which reduces labeling efficiency. Proteins were purified via Ni^{2+}-affinity chromatography, and eluted with 400 mM Imidazole, and then run through HiTrap Desalting column equilibrated with 20 mM HEPES pH 7.5, 50 mM KCl. Proteins were then flash-frozen in liquid N_2. For labeling, PhoS.A197C (at

~200 μM) was incubated with 1 μM PNPase, 0.5 μM PDRM, 50 μM $MnCl_2$, 50 μM α-D-glucose-1,6-bisphosphate and 0.5 mM 7-methylguanosine (Sigma-Aldrich) to mop-up contaminating phosphate. MDCC dissolved in DMSO was then added stepwise and gently mixed by inverting the tube, totaling up to 2X-molar excess of cysteines. The labeling reaction takes place at room temperature in the dark for 1 hour. Excess dyes were removed by loading the labeling reaction onto a HisTrap (5 mL) column and protein was eluted with a gradient of 20 mM to 500 mM imidazole. Labeled proteins were dialyzed into 20 mM HEPES pH 7.5, 50 mM KCl and concentrated up to ~300 μM before freezing in aliquots.

For the phosphate release assay, a standard curve of free phosphate was prepared with 10 μM PBP-MDCC and varying concentrations of potassium phosphate. Fluorescence measurements were taken in the SpectraMax M5 platereader with SoftMax Pro software for data acquisition. Samples were excited at 375 nm and emission was recorded at 467 nm with 'Low' sensitivity setting. Only fluorescence counts below the detector linearity was used for analysis (<20000 RFU).

Steady-state ATPase assay and analysis

Steady-state ATPase activity was measured using enzyme-coupled NADH absorbance assay with 1 mM phosphoenol-pyruvate (PEP), 0.18 mM NADH, 30 U/mL of both pyruvate kinase and lactate dehydrogenase. Kinetic absorbance measurements were carried out in Molecular Devices SpectraMax M5, at wavelengths 340 nm for NADH and 420 nm for background. Slopes were obtained from linear fits within linear regimes of each trace. Each reaction volume is 70 μL and a pathlength calibration is applied to convert absorbance to molar concentrations. For heterodimeric mixing experiment with TRAP1, wildtype and mutant proteins

were mixed with different ratios while keeping total protein concentration constant. Each mixture was incubated at 30˚C for 1.5 hour to allow for dimer exchange. The final reaction has 2 μM dimer in ATPase reaction buffer (20 mM HEPES pH 7.5, 100 mM KCl, 5 mM $MgCl_2$). The total ATPase activity is fitted according to a binomial distribution of dimer species:

$$V_{total} = V_{wildtype} \cdot f_{wildtype}^2 + V_{mutant} \cdot f_{mutant}^2 + V_{heterodimer} \cdot f_{mutant} \cdot f_{wildtype}$$

Where V denotes ATPase activity, f denotes the corresponding fractional population of wildtype and mutant. Since protein concentration is constant in all experiments, $f_{wildtype} = 1 - f_{mutant}$. Heterodimeric protein activity is simply the average of $V_{wildtype}$ and V_{mutant} if assuming independence between activities.

Single-turnover radioactive ATPase assay

For radioactive atpase assays, reactions are initiated with addition of trace amounts [γ-^{32}P]ATP (Perkin Elmer, 10 μCi/μL EasyTide Lead) mixed with cold ATP totalling up to ~300 μM. The final radioactivity per 30 μL reaction is 0.1 μCi/μL. The ratio of TRAP1 dimer to ATP concentration is kept at 0.5:1, with slight protein excess at concentrations well above the K_m for ATP to ensure single-turnover condition. Time points were taken by chemically quenching 1.5 μL aliquots with an equal volume of 40 mM Tris pH 8.0, 100 mM EDTA, 2% SDS and 2.5 mg/mL proteinase K. Aliquots (1 μl) of quenched reactions were spotted at 1 cm from the bottom of a PEI Cellulose F TLC plate (Millipore), and 6% formic acid, 0.5 M LiCl was used as mobile phase. The radioactive phosphate migrates about ~0.8 of plate length from the origin. Radioactive signal was quantified via exposing the plates to a storage phosphor screen (Amersham) for ~1 minute, and plate images were scanned with Typhoon FLA 9000. Image quantification was done in ImageJ (Wayne Rasband, NIH. https://imagej.nih.gov/ij/).

Molecular dynamics simulation

MD simulations were performed in explicit solvent using the TIP3P water model (Jorgensen et al., 1983) and the CHARMM22 force field with CMAP corrections for protein and ions (Mackerell, 2004; MacKerell et al., 1998; Mackerell et al., 2004). The initial protein structure was modeling based on the crystal structure of zebrafish Trap1 (PDB ID: 4IYN) (Lavery et al., 2014) and subsequently solvated in a cubic water box at 150mM NaCl salinity, neutralized with extra ions employing VMD (Humphrey et al., 1996). All simulations were carried out with periodic boundary conditions in a constant particle number, temperature, and pressure ensemble (NPT). The initial energy minimization and equilibration were carried out on general purpose supercomputers using NAMD 2.10 (Phillips et al., 2005). The system to be simulated was first subjected to 10000 steps of conjugate gradient minimization and equilibrated for 2 ns with harmonic restraints applied to all the heavy atoms of the protein. The simulation was then continued for 10 ns without restraints at a constant pressure of 1 bar using Nosé–Hoover Langevin piston barostat and at a constant temperature (310 K or 360 K) maintained using Langevin dynamics with a damping constant of 1.0 ps^{-1}. Multiple time stepping was employed with an integration time step of 2.0 fs, short-range forces being evaluated every time step and long-range electrostatics evaluated every three time steps. Cutoff for short-range nonbonded interactions was 10.0 Å; long-range electrostatics was calculated using the particle-mesh Ewald method (Darden et al., 1993). All bonds involving hydrogen in the protein were constrained using RATTLE (Andersen, 1983), while the geometries of water molecules were maintained using SETTLE (Miyamoto and Kollman, 1992). The resulting equilibrated structure was employed as the initial state for production simulations, carried out on the special purpose supercomputer Anton (Shaw et al., 2008; 2009) for ~1.1 μs, where constant temperature (310 K

or 360 K) and constant pressure (P = 1 bar) were maintained. Multiple time stepping was employed, with an integration time step of 2.0 fs. Short-range forces were evaluated every time step and long-range electrostatics every three time steps. Cutoff for the short-range nonbonded interactions was 9.5 Å; long-range electrostatics was calculated using the k-Gaussian Split Ewald method (Shan et al., 2005) with a 64 × 64 × 64 grid. All bonds involving hydrogen atoms were constrained using SHAKE (Ryckaert et al., 1977).

References

Adams, P.D., Afonine, P.V., Bunkóczi, G., Chen, V.B., Davis, I.W., Echols, N., Headd, J.J., Hung, L.-W., Kapral, G.J., Grosse-Kunstleve, R.W., McCoy, A.J., Moriarty, N.W., Oeffner, R., Read, R.J., Richardson, D.C., Richardson, J.S., Terwilliger, T.C., Zwart, P.H., 2010. PHENIX: a comprehensive Python-based system for macromolecular structure solution. Acta Crystallogr. D Biol. Crystallogr. 66, 213–221. doi:10.1107/S0907444909052925

Ali, M.M.U., Roe, S.M., Vaughan, C.K., Meyer, P., Panaretou, B., Piper, P.W., Prodromou, C., Pearl, L.H., 2006. Crystal structure of an Hsp90-nucleotide-p23/Sba1 closed chaperone complex. Nature 440, 1013–1017. doi:10.1038/nature04716

Andersen, H.C., 1983. Rattle: A "velocity" version of the shake algorithm for molecular dynamics calculations. Journal of Computational Physics 52, 24–34. doi:10.1016/0021-9991(83)90014-1

Baird, C.L., Gordon, M.S., Andrenyak, D.M., Marecek, J.F., Lindsley, J.E., 2001. The ATPase reaction cycle of yeast DNA topoisomerase II. Slow rates of ATP resynthesis and P(i) release. J. Biol. Chem. 276, 27893–27898. doi:10.1074/jbc.M102544200

Battye, T.G.G., Kontogiannis, L., Johnson, O., Powell, H.R., Leslie, A.G.W., 2011. iMOSFLM: a new graphical interface for diffraction-image processing with MOSFLM. Acta Crystallogr. D Biol. Crystallogr. 67, 271–281. doi:10.1107/S0907444910048675

Brune, M., Hunter, J.L., Corrie, J.E.T., Webb, M.R., 2002. Direct, Real-Time Measurement of Rapid Inorganic Phosphate Release Using a Novel Fluorescent Probe and Its Application to Actomyosin Subfragment 1 ATPase. Biochemistry 33, 8262–8271. doi:10.1021/bi00193a013

Chen, B., Doucleff, M., Wemmer, D.E., De Carlo, S., Huang, H.H., Nogales, E., Hoover, T.R., Kondrashkina, E., Guo, L., Nixon, B.T., 2007. ATP Ground- and Transition States of Bacterial Enhancer Binding AAA+ ATPases Support Complex Formation with Their Target Protein, σ54. Structure 15, 429–440. doi:10.1016/j.str.2007.02.007

Cunningham, C.N., Krukenberg, K.A., Agard, D.A., 2008. Intra- and Intermonomer Interactions Are Required to Synergistically Facilitate ATP Hydrolysis in Hsp90. Journal of Biological Chemistry 283, 21170–21178. doi:10.1074/jbc.M800046200

Cunningham, C.N., Southworth, D.R., Krukenberg, K.A., Agard, D.A., 2012. The conserved arginine 380 of Hsp90 is not a catalytic residue, but stabilizes the closed conformation required for ATP hydrolysis. Protein Sci. 21, 1162–1171. doi:10.1002/pro.2103

Darden, T., York, D., Pedersen, L., 1993. Particle mesh Ewald: An N·log(N) method for Ewald sums in large systems. The Journal of Chemical Physics 98, 10089–10092. doi:10.1063/1.464397

Dollins, D.E., Warren, J.J., Immormino, R.M., Gewirth, D.T., 2007. Structures of GRP94-nucleotide complexes reveal mechanistic differences between the hsp90 chaperones. Molecular Cell 28, 41–56. doi:10.1016/j.molcel.2007.08.024

Ebong, I.-O., Morgner, N., Zhou, M., Saraiva, M.A., Daturpalli, S., Jackson, S.E., Robinson, C.V., 2011. Heterogeneity and dynamics in the assembly of the heat shock protein 90 chaperone complexes. PNAS 108, 17939–17944. doi:10.1073/pnas.1106261108

Eckl, J.M., Rutz, D.A., Haslbeck, V., Zierer, B.K., Reinstein, J., Richter, K., 2013. Cdc37 (Cell Division Cycle 37) Restricts Hsp90 (Heat Shock Protein 90) Motility by Interaction with N-terminal and Middle Domain Binding Sites. J. Biol. Chem. 288, 16032–16042. doi:10.1074/jbc.M112.439257

Elnatan, D., 2017. UCSFsaxs. GitHub. https://github.com/delnatan/UCSFSaxs. 1a7d705

Fisher, A.J., Smith, C.A., Thoden, J., Smith, R., Sutoh, K., Holden, H.M., Rayment, I., 2002. X-ray Structures of the Myosin Motor Domain of Dictyostelium discoideum Complexed with MgADP.cntdot.BeFx and MgADP.cntdot.AlF4. Biochemistry 34, 8960–8972. doi:10.1021/bi00028a004

Frey, S., Leskovar, A., Reinstein, J., Buchner, J., 2007. The ATPase cycle of the endoplasmic chaperone Grp94. J. Biol. Chem. 282, 35612–35620. doi:10.1074/jbc.M704647200

Genest, O., Reidy, M., Street, T.O., Hoskins, J.R., Camberg, J.L., Agard, D.A., Masison, D.C., Wickner, S., 2013. Uncovering a Region of Heat Shock Protein 90 Important for Client Binding in E. coli and Chaperone Function in Yeast. Molecular Cell 49, 464–473. doi:10.1016/j.molcel.2012.11.017

Hansen, S., 2000. Bayesian estimation of hyperparameters for indirect Fourier transformation in small-angle scattering. J Appl Crystallogr. doi:10.1107/S0021889800012930

Harkins, T.T., Lewis, T.J., Lindsley, J.E., 1998. Pre-steady-state analysis of ATP hydrolysis by Saccharomyces cerevisiae DNA topoisomerase II. 2. Kinetic mechanism for the sequential hydrolysis of two ATP. Biochemistry 37, 7299–7312. doi:10.1021/bi9729108

Hessling, M., Richter, K., Buchner, J., 2009. Dissection of the ATP-induced conformational cycle of the molecular chaperone Hsp90. Nature Structural & Molecular Biology 16, 287–293. doi:10.1038/nsmb.1565

Humphrey, W., Dalke, A., Schulten, K., 1996. VMD: Visual molecular dynamics. Journal of Molecular Graphics 14, 33–38. doi:10.1016/0263-7855(96)00018-5

Jorgensen, W.L., Chandrasekhar, J., Madura, J.D., Impey, R.W., Klein, M.L., 1983. Comparison of simple potential functions for simulating liquid water. The Journal of Chemical Physics 79, 926–935. doi:10.1063/1.445869

Kabsch, W., IUCr, 2010. XDS. Acta Crystallogr. D Biol. Crystallogr. 66, 125–132. doi:10.1107/S0907444909047337

Kirschke, E., Goswami, D., Southworth, D., Griffin, P.R., Agard, D.A., 2014. Glucocorticoid Receptor Function Regulated by Coordinated Action of the Hsp90 and Hsp70 Chaperone Cycles. Cell 157, 1685–1697. doi:10.1016/j.cell.2014.04.038

Krukenberg, K.A., Förster, F., Rice, L.M., Sali, A., Agard, D.A., 2008. Multiple conformations of E. coli Hsp90 in solution: insights into the conformational dynamics of Hsp90. Structure 16, 755–765. doi:10.1016/j.str.2008.01.021

Krukenberg, K.A., Southworth, D.R., Street, T.O., Agard, D.A., 2009. pH-dependent conformational changes in bacterial Hsp90 reveal a Grp94-like conformation at pH 6 that is highly active in suppression of citrate synthase aggregation. Journal of Molecular Biology 390, 278–291. doi:10.1016/j.jmb.2009.04.080

Lavery, L.A., Partridge, J.R., Ramelot, T.A., Elnatan, D., Kennedy, M.A., Agard, D.A., 2014. Structural asymmetry in the closed state of mitochondrial Hsp90 (TRAP1) supports a two-step ATP hydrolysis mechanism. Molecular Cell 53, 330–343. doi:10.1016/j.molcel.2013.12.023

Leskovar, A., Wegele, H., Werbeck, N.D., Buchner, J., Reinstein, J., 2008. The ATPase cycle of the mitochondrial Hsp90 analog Trap1. J. Biol. Chem. 283, 11677–11688. doi:10.1074/jbc.M709516200

Li, J., Richter, K., Buchner, J., 2011. Mixed Hsp90-cochaperone complexes are important for the progression of the reaction cycle. Nat Struct Mol Biol 18, 61–66. doi:10.1038/nsmb.1965

Li, L., Fierer, J.O., Rapoport, T.A., Howarth, M., 2014. Structural analysis and optimization of the covalent association between SpyCatcher and a peptide Tag. Journal of Molecular Biology 426, 309–317. doi:10.1016/j.jmb.2013.10.021

Mackerell, A.D., 2004. Empirical force fields for biological macromolecules: overview and issues. J Comput Chem 25, 1584–1604. doi:10.1002/jcc.20082

MacKerell, A.D., Bashford, D., Bellott, M., Dunbrack, R.L., Evanseck, J.D., Field, M.J., Fischer, S., Gao, J., Guo, H., Ha, S., Joseph-McCarthy, D., Kuchnir, L., Kuczera, K., Lau, F.T., Mattos, C., Michnick, S., Ngo, T., Nguyen, D.T., Prodhom, B., Reiher, W.E., Roux, B., Schlenkrich, M., Smith, J.C., Stote, R., Straub, J., Watanabe, M., Wiórkiewicz-Kuczera, J., Yin, D., Karplus, M., 1998. All-atom empirical potential for molecular modeling and dynamics studies of proteins. J Phys Chem B 102, 3586–3616. doi:10.1021/jp973084f

Mackerell, A.D., Feig, M., Brooks, C.L., 2004. Improved treatment of the protein backbone in empirical force fields. J. Am. Chem. Soc. 126, 698–699. doi:10.1021/ja036959e

McLaughlin, S.H., Smith, H.W., Jackson, S.E., 2002. Stimulation of the weak ATPase activity of human hsp90 by a client protein. Journal of Molecular Biology 315, 787–798. doi:10.1006/jmbi.2001.5245

Mickler, M., Hessling, M., Ratzke, C., Buchner, J., Hugel, T., 2009. The large conformational changes of Hsp90 are only weakly coupled to ATP hydrolysis. Nat Struct Mol Biol 16, 281–286. doi:10.1038/nsmb.1557

Miyamoto, S., Kollman, P.A., 1992. Settle: An analytical version of the SHAKE and RATTLE algorithm for rigid water models. J Comput Chem 13, 952–962.

Mollapour, M., Bourboulia, D., Beebe, K., Woodford, M.R., Polier, S., Hoang, A., Chelluri, R., Li, Y., Guo, A., Lee, M.-J., Fotooh-Abadi, E., Khan, S., Prince, T., Miyajima, N., Yoshida, S., Tsutsumi, S., Xu, W., Panaretou, B., Stetler-Stevenson, W.G., Bratslavsky, G., Trepel, J.B., Prodromou, C., Neckers, L., 2014. Asymmetric Hsp90 N Domain SUMOylation Recruits Aha1 and ATP-Competitive Inhibitors. Molecular Cell 53, 317–329. doi:10.1016/j.molcel.2013.12.007

Murshudov, G.N., Vagin, A.A., Dodson, E.J., IUCr, 1997. Refinement of Macromolecular Structures by the Maximum-Likelihood Method. Acta Crystallogr. D Biol. Crystallogr. 53, 240–255. doi:10.1107/S0907444996012255

Nathan, D.F., Lindquist, S., 1995. Mutational analysis of Hsp90 function: interactions with a steroid receptor and a protein kinase. Mol. Cell. Biol. 15, 3917–3925.

Panaretou, B., Prodromou, C., Roe, S.M., O'Brien, R., Ladbury, J.E., Piper, P.W., Pearl, L.H., 1998. ATP binding and hydrolysis are essential to the function of the Hsp90 molecular chaperone in vivo. EMBO J. 17, 4829–4836. doi:10.1093/emboj/17.16.4829

Pannier, M., Veit, S., Godt, A., Jeschke, G., Spiess, H.W., 2011. Dead-time free measurement of dipole–dipole interactions between electron spins. Journal of Magnetic Resonance 213, 316–325. doi:10.1016/j.jmr.2011.08.035

Partridge, J.R., Lavery, L.A., Elnatan, D., Naber, N., Cooke, R., Agard, D.A., 2014. A novel N-terminal extension in mitochondrial TRAP1 serves as a thermal regulator of chaperone activity. eLife Sciences 3. doi:10.7554/eLife.03487

Phillips, J.C., Braun, R., Wang, W., Gumbart, J., Tajkhorshid, E., Villa, E., Chipot, C., Skeel, R.D., Kalé, L., Schulten, K., 2005. Scalable molecular dynamics with NAMD. J Comput Chem 26, 1781–1802. doi:10.1002/jcc.20289

Prodromou, C., Panaretou, B., Chohan, S., Siligardi, G., O'Brien, R., Ladbury, J.E., Roe, S.M., Piper, P.W., Pearl, L.H., 2000. The ATPase cycle of Hsp90 drives a molecular "clamp" via transient dimerization of the N-terminal domains. EMBO J. 19, 4383–4392. doi:10.1093/emboj/19.16.4383

Pullen, L., Bolon, D.N., 2011. Enforced N-domain proximity stimulates Hsp90 ATPase activity and is compatible with function in vivo. Journal of Biological Chemistry 286, 11091–11098. doi:10.1074/jbc.M111.223131

Retzlaff, M., Hagn, F., Mitschke, L., Hessling, M., Gugel, F., Kessler, H., Richter, K., Buchner, J., 2010. Asymmetric Activation of the Hsp90 Dimer by Its Cochaperone Aha1. Molecular Cell 37, 344–354. doi:10.1016/j.molcel.2010.01.006

Richter, K., 2001. Coordinated ATP Hydrolysis by the Hsp90 Dimer. Journal of Biological Chemistry 276, 33689–33696. doi:10.1074/jbc.M103832200

Richter, K., Soroka, J., Skalniak, L., Leskovar, A., Hessling, M., Reinstein, J., Buchner, J., 2008. Conserved conformational changes in the ATPase cycle of human Hsp90. J. Biol. Chem. 283, 17757–17765. doi:10.1074/jbc.M800540200

Ryckaert, J.-P., Ciccotti, G., Berendsen, H.J.C., 1977. Numerical integration of the cartesian equations of motion of a system with constraints: molecular dynamics of n-alkanes. Journal of Computational Physics 23, 327–341. doi:10.1016/0021-9991(77)90098-5

Shan, Y., Klepeis, J.L., Eastwood, M.P., Dror, R.O., Shaw, D.E., 2005. Gaussian split Ewald: A fast Ewald mesh method for molecular simulation. The Journal of Chemical Physics 122, 54101. doi:10.1063/1.1839571

Shaw, D.E., Deneroff, M.M., Dror, R.O., Kuskin, J.S., Larson, R.H., Salmon, J.K., Young, C., Batson, B., Bowers, K.J., Chao, J.C., Eastwood, M.P., Gagliardo, J., Grossman, J.P., Ho, C.R., Ierardi, D.J., Kolossváry, I., Klepeis, J.L., Layman, T., McLeavey, C., Moraes, M.A., Mueller, R., Priest, E.C., Shan, Y., Spengler, J., Theobald, M., Towles, B., Wang, S.C., 2008. Anton, a special-purpose machine for molecular dynamics simulation. Communications of the ACM 51, 91–97. doi:10.1145/1364782.1364802

Shaw, D.E., Dror, R.O., Salmon, J.K., Grossman, J.P., 2009. Proceedings of the conference on high performance computing networking, storage and analysis.

Shiau, A.K., Harris, S.F., Southworth, D.R., Agard, D.A., 2006. Structural Analysis of E. coli hsp90 reveals dramatic nucleotide-dependent conformational rearrangements. Cell 127, 329–340. doi:10.1016/j.cell.2006.09.027

Southworth, D.R., Agard, D.A., 2011. Client-loading conformation of the Hsp90 molecular chaperone revealed in the cryo-EM structure of the human Hsp90:Hop complex. Molecular Cell 42, 771–781. doi:10.1016/j.molcel.2011.04.023

Southworth, D.R., Agard, D.A., 2008. Species-Dependent Ensembles of Conserved Conformational States Define the Hsp90 Chaperone ATPase Cycle. Molecular Cell 32, 631–640. doi:10.1016/j.molcel.2008.10.024

Street, T.O., Lavery, L.A., Agard, D.A., 2011. Substrate Binding Drives Large-Scale Conformational Changes in the Hsp90 Molecular Chaperone. Molecular Cell 42, 96–105. doi:10.1016/j.molcel.2011.01.029

Street, T.O., Lavery, L.A., Verba, K.A., Lee, C.-T., Mayer, M.P., Agard, D.A., 2012. Cross-Monomer Substrate Contacts Reposition the Hsp90 N-Terminal Domain and Prime the Chaperone Activity. Journal of Molecular Biology 415, 3–15. doi:10.1016/j.jmb.2011.10.038

Verba, K.A., Wang, R.Y.-R., Arakawa, A., Liu, Y., Shirouzu, M., Yokoyama, S., Agard, D.A., 2016. Atomic structure of Hsp90-Cdc37-Cdk4 reveals that Hsp90 traps and stabilizes an unfolded kinase. Science 352, 1542–1547. doi:10.1126/science.aaf5023

Whitesell, L., Lindquist, S.L., 2005. HSP90 and the chaperoning of cancer. Nature Reviews Cancer 5, 761–772. doi:10.1038/nrc1716

Wiech, H., Buchner, J., Zimmermann, R., Jakob, U., 1992. Hsp90 chaperones protein folding in vitro. Nature 358, 169–170. doi:10.1038/358169a0

Winn, M.D., Ballard, C.C., Cowtan, K.D., Dodson, E.J., Emsley, P., Evans, P.R., Keegan, R.M., Krissinel, E.B., Leslie, A.G.W., McCoy, A., McNicholas, S.J., Murshudov, G.N., Pannu, N.S., Potterton, E.A., Powell, H.R., Read, R.J., Vagin, A., Wilson, K.S., 2011. Overview of the CCP4 suite and current developments. Acta Crystallogr. D Biol. Crystallogr. 67, 235–242. doi:10.1107/S0907444910045749

Wittinghofer, A., 1997. Signaling mechanistics: Aluminum fluoride for molecule of the year. Current Biology 7, R682–R685. doi:10.1016/S0960-9822(06)00355-1

Zakeri, B., Fierer, J.O., Celik, E., Chittock, E.C., Schwarz-Linek, U., Moy, V.T., Howarth, M., 2012. Peptide tag forming a rapid covalent bond to a protein, through engineering a bacterial adhesin. PNAS 109, E690–7. doi:10.1073/pnas.1115485109

Zhao, R., Davey, M., Hsu, Y.-C., Kaplanek, P., Tong, A., Parsons, A.B., Krogan, N., Cagney, G., Mai, D., Greenblatt, J., Boone, C., Emili, A., Houry, W.A., 2005. Navigating the chaperone network: an integrative map of physical and genetic interactions mediated by the hsp90 chaperone. Cell 120, 715–727. doi:10.1016/j.cell.2004.12.024

Supplementary table 1A. Data collection and refinement statistics (molecular replacement)

	zTRAP1 +/R417A	WT zTRAP1 Day 1	WT zTRAP1 Day 3	WT zTRAP1 Day 53
Data collection				
Space group	C 1 2 1	C 1 2 1	C 1 2 1	C 1 2 1
Cell dimensions				
a, *b*, *c* (Å)	180.086, 95.711, 126.558	175.881, 96.9902, 124.961,	178.49, 97.181, 125.904	178.491, 96.82, 125.78
α, β, γ (°)	90.0, 134.592, 90.0	90, 134.568, 90	90, 134.641, 90	90, 134.18, 90
Resolution (Å)	49.0 - 3.20	44.52 - 2.3	42.67 - 2.14	40.54 - 1.99
R_{sym} or R_{merge}	0.146	0.516	0.043	0.055
I / σI	9.1 (1.0)	2.2 (0.29)	11 (0.76)	7.8 (0.29)
Completeness (%)	83.03	93.4	99.5	99.6
Redundancy	2.5	1.8	1.9	1.9
Refinement				
Resolution (Å)	49.0 -3.20	39.67 - 3.5	39.89 - 2.5	39.97 - 2.2
No. reflections	21134 (2095)	18821 (1856)	98531 (9720)	77629 (7714)
R_{work} / R_{free}	0.213 / 0.257	0.1977 / 0.2558	0.1804 / 0.2377	0.1885 / 0.2365
No. atoms				
Protein	10383	9592	9597	9570
Ligand/ion	66	62	66	62
Water	-			
B-factors				
Protein	87.70	72.29	68.56	66.32
Ligand/ion	59.90	72.36	45.99	69.99
Water	-	62.38	52.91	55.34
R.m.s. deviations				
Bond lengths (Å)	0.0122	0.003	0.008	0.007
Bond angles (°)	1.4721	0.604	1.01	0.96

*Each dataset was collected from a single crystal.
*Values in parentheses are for highest-resolution shell.

Chapter III

Regulation of Heat Shock Factor 1 by the hsp90/Hsp70 chaperone system

Introduction

A largely unnoticed paper published in 1962 (Ritossa et al, 1962) described the appearance of a set of puffs on the salivary gland chromosomes of *Drosophila busckii* that had been subjected to heat or chemical stress. Twelve years after it was found that the presence of these heat-induced puffs was accompanied by synthesis of a small number of new proteins (Tissiéres, Mitchell, & Tracy, 1974). These proteins turned out to be what we now know as chaperones, and together constitute the bulk of the Heat Shock Response (HSR), an adaptive mechanism that has evolved in eukaryotes to maintain protein homeostasis under heat or other kinds of stress.

Heat shock factors are a transcription factors that regulate the expression of proteins in the HSR including heat shock proteins such as Hsp70 and Hsp90.

While they are highly conserved across higher eukaryotes, there are significant domain differences between these and their yeast homolog (yHSF1), in particular the lack of an auto-inhibiting domain in yHSF1 that results in constitutive trimerization and nuclear localization (Figure 1).

In humans there exist 4 HSF homologs, HSF 1 through 4, with human HSF1 (hHSF1) being the primary heat shock factor driving the HSR. hHSF1 exists as a 57kDa monomer in its inactive state and upon cellular stress trimerizes exposing a nuclear localization signal and localizing to the nucleus where it binds Heat Shock Elements (HSEs), DNA elements that

contain three copies of the GAA motif recognized by each monomer, in alternating strands such that the HSE contains the sequence …GAA…TTC…GAA… or small variations of it. In vitro, this interaction has an affinity of around 12nM. Once HSF1 is bound to the HSE it recruits the transcription machinery to initiate mRNA synthesis for the target gene.

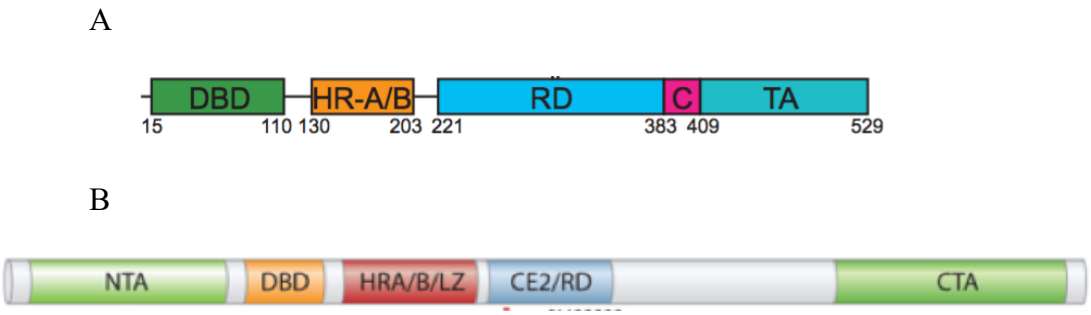

Figure 1. Architecture of human HSF1 and yeast HSF1
A) Human HSF1 contains an N-terminal DNA-Binding Domain (DBD), a Hydrophobic region (HR-A/B) that serves as the trimerization interface to form the active trimer, a regulatory domain (RD) that contains multiple phosphorylation sites that impart target specificity, a second hydrophobic region (HR-C) that binds the HR-A/B region in the self-inhibited monomeric state, and a C-terminal transcriptional activation domain that recruits the transcriptional machinery to drive expression of target genes. **B)** Yeast HSF1 contains an additional N-terminal transcription activation domain (TA) and lacks the hydrophobic region C present in human HSF1.

There are at least two models for HSF1 monomeric inactive state: in the first one, HSF1 is kept monomeric through a self-inhibiting interaction between the HR-C and the trimerization interface HR-A/B. In the second model, Hsp90 binds to HSF1 keeping it monomeric. In the first model, heat stress would dissociate the two HRs relieving the self-inhibition and allowing trimerization (Figure 2A). In the second model, heat or other proteotoxic stresses that increase the amount of partially unfolded protein in the cell that needs chaperoning would displace HSF1 from Hsp90, freeing it and allowing it to trimerize (Figure 2B). Neither model seems, however, satisfactory: self-inhibition alone seems to discard stresses other than heat stress. Hsp90

inhibition and competition by unfolded proteins also seems unlikely as Hsp70 and other chaperones are more likely to take part in addressing the burden of buffering unfolded proteins. More importantly, both models imply a simple mechanism that doesn't allow for fine regulation of the HSR.

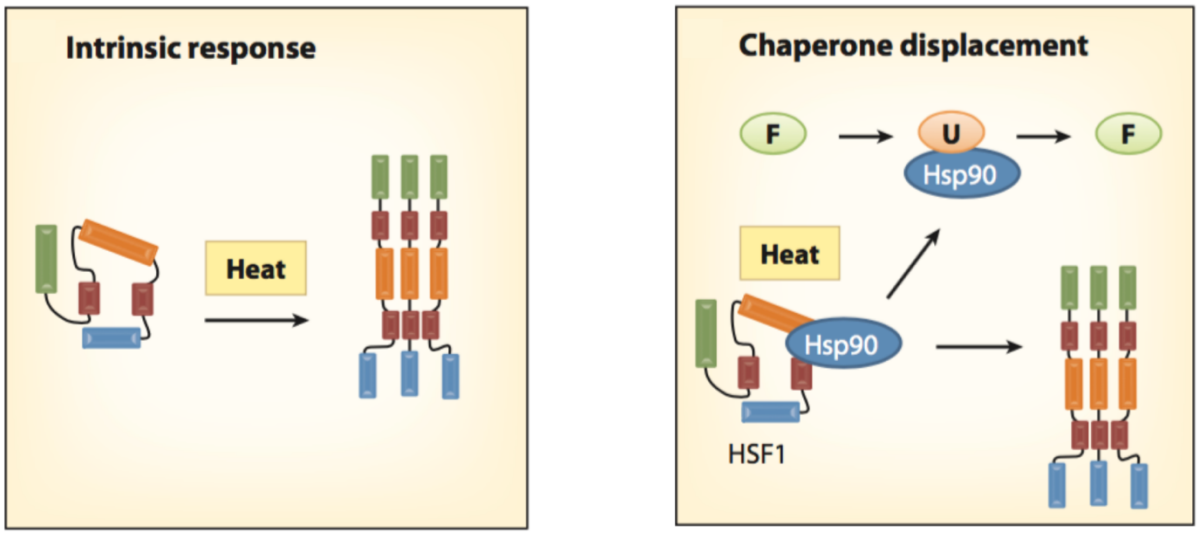

Figure 2. Models of hHSF1 inhibition and activation
A) In the intrinsic response model, HSF1 is maintained in the inactive monomeric conformation through interaction between the trimerization interface (HR-A/B) and HR-C region. Heat stress disrupts this interaction leading to trimerization. **B)** In the chaperone displacement model, HSF1 is kept monomeric through interaction with Hsp90. Proteotoxic stress causes proteins to unfold and require chaperoning, displacing HSF1 from Hsp90 (figure from (Anckar & Sistonen, 2011)).

Despite having known that Hsp90 interacts with HSF1 for decades, it wasn't until a 2017 paper (Hentze et al, 2016) was published that we obtained the first insights into the mechanistic details of HSF1 regulation by using, for the first time in HSF1's literature, quantitative in-vitro methods to probe HSF1 activity and the effect of Hsp90 on its conversion from inactive monomer to active trimer. Using hydrogen-deuterium exchange (HDX) mass spectrometry they first show that hHSF1 is indeed self-inhibited through the HR-A/B – HR-C interaction: with increasing temperatures, the HR-C region shows increased HDX, consistent with it dissociating

from HR-A/B and being instead free in solution. Concomitantly, the HR-A/B region shows decreased HDX as trimerization through that interface occludes it from solvent (Figure 3A).

They then investigate the effect of Hsp90 by looking at HSF1 binding to DNA containing an HSE at different temperatures and in the presence and absence of Hsp90. In this key experiment they show that Hsp90 is not just sequestering monomeric HSF1. HSF1 alone binds HSE in a temperature-dependent fashion, although in quite a switch-like behavior across a short temperature range. In the presence of Hsp90, the range of temperatures at which HSF1 binds DNA is increased, and the mid-point temperature is also decreased from around 38C to 32C (Figure 3B). This indicates that not only does Hsp90 not inhibit HSF1 activity, but it helps it trimerize and bind DNA at lower temperatures and in a more graded way, either by maintaining it in a trimerization favorable monomeric state or by catalyzing trimerization and in a temperature dependent manner.

A

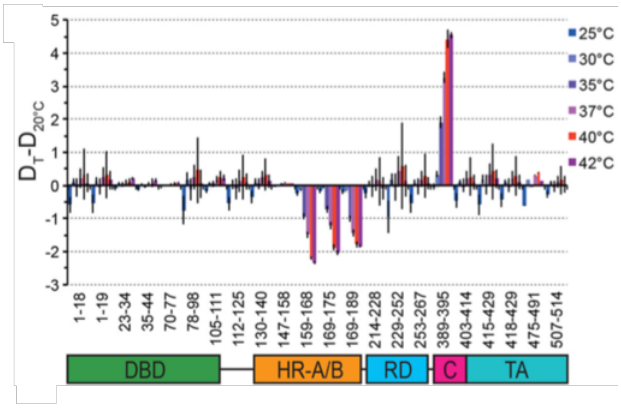

B

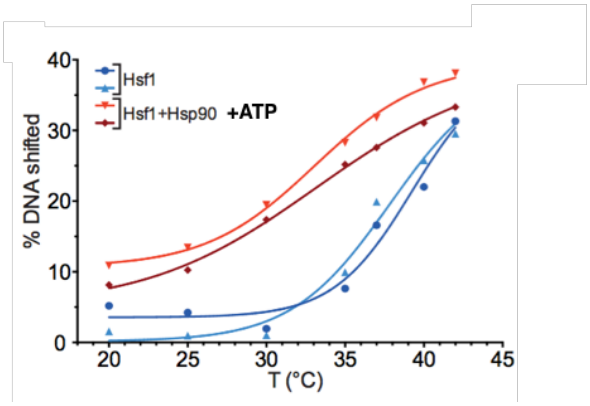

Figure 3. Trimerization of HSF1 and effect of Hsp90
A) In the intrinsic response model, HSF1 is maintained in the inactive monomeric conformation through interaction between the trimerization interface (HR-A/B) and HR-C region. Heat stress disrupts this interaction leading to trimerization. **B)** In the chaperone displacement model, HSF1

is kept monomeric through interaction with Hsp90. Proteotoxic stress causes proteins to unfold and require chaperoning, displacing HSF1 from Hsp90 (figure from Anckar & Sistonen, 2011).

Based on these results and the fact that in this paper and in a second contemporaneous paper (Jaeger et al, 2014) purification of hHSF1 from bacterial expression follows a simple protocol of lysis, nickel affinity and size exclusion to produce monomeric and trimeric fractions, I set out to investigate the role of the Hsp90/Hsp70 chaperone machinery in both HSF1 trimerization and DNA binding as well as DNA release and inactivation. Is HSF1 regulated by Hsp70 and Hsp90 in a similar way to how the glucocorticoid receptor (GR) (Kirschke et al, 2014) is? The HSR occurs within minutes, needs to be regulated so that it's graded and needs to be able to occur again shortly after subsiding if conditions require it, so it's likely not degraded to shut down the HSR and is instead recycled. Furthermore, HSF1 has a half-life of 13-20 hours in the cell (Naidu & Kostova, 2017), suggesting that the same molecule may be reused multiple times rather than just once. Therefore, it's easy to imagine a model where the Hsp90/Hsp70 machinery will play a role in activating and inhibiting it similar as with GR, where Hsp70 inhibits it be releasing ligand (unbinding it from DNA in the case of HSF1) while Hsp90 helps trimerization and binding to HSEs. This system would also yield complexes for cryoEM with different chaperones and in various nucleotide states that would bring insight into the structural aspects of HSF1 trimerization and inhibition by Hsp90 as well as into HSp90 mechanism.

The polarization anisotropy binding experiments using labeled DNA described in (Jaeger et al., 2014) seem to provide a robust assay to test these hypotheses, allowing for similar experiments as those performed with GR to be conducted.

Unfortunately, while this project seemed primed for fast scientific progress and, while HSF1 is an important medical target that despite decades of study remains elusive in terms of

mechanism and structure making the project of significant scientific impact, it was ultimately abandoned due to its poorly behaved purification and functional reproducibility. I initially followed the protocols in (Hentze et al., 2016) and (Jaeger et al., 2014), which are quite similar overall:

Table 1. HSF1 purification schemes from literature

Jaeger et al	**Hentze et al**
6His tag	6His tag + SUMO tag
Expresson in BL21(DE3) at 37C to OD_{600} of 0.6	Expression in BL21 rosetta at 37C to OD_{600} of 0.6
Induction at 15C ,1mM IPTG, 2 hours	Induction at 20C, 0.1mM IPTG, 16 hours
Lysis in: 50mM HEPES pH 7.5 300mM NaCl 20mM imidazole	Lysis in: 25mM HEPES pH 7.5 150mM NaCl 10% glycerol 3mM BMe Protease inhibitor tablet
Ni column with ATP wash	Ni column with 1M NaCl wash
No tag cleavage	Ulp1 cleavage 2hr 4C
S400 SEC	S200 SEC
Stored at 10µM in: 25mM HEPES pH 7.5 150mM NaCl	Stored at 10µM in: 25mM HEPES pH 7.4 150mM NaCl 10% glycerol 2mM DTT

Both these protocols should produce two peaks on size exclusion, one for monomeric HSF1 and one for trimeric HSF1 (Figure 4).

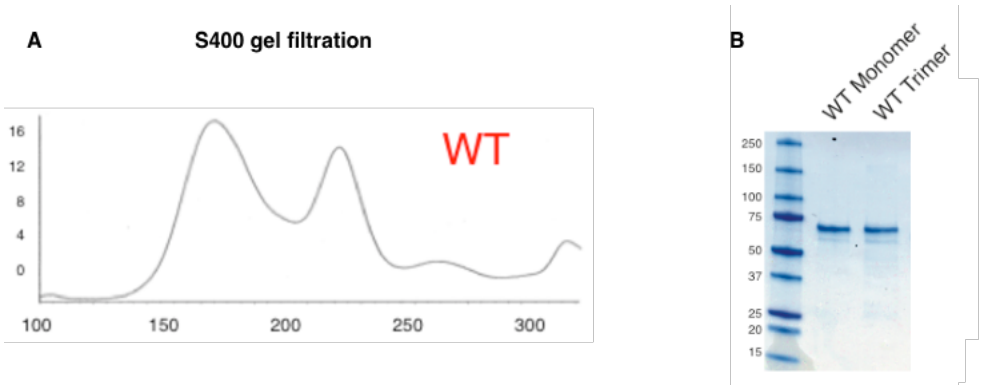

Figure 4. Purification of WT hHSF1 from literature
A) Abs_{280} trace from gel filtration of hHSF1 showing trimeric and monomeric HSF1 peaks. **B**) SDS-PAGE gel of the monomeric and trimeric fractions of hHSF1.

I initially started using a 6His-TEV-hHSF1 construct purified using the protocol from Jaeger et al but, in my hands, this produced very different results. After Ni affinity and SEC, this construct was never pure, showing many contaminants on SDS-PAGE gels with the major bands not matching the molecular weight expected for hHSF1 (Figure 5).

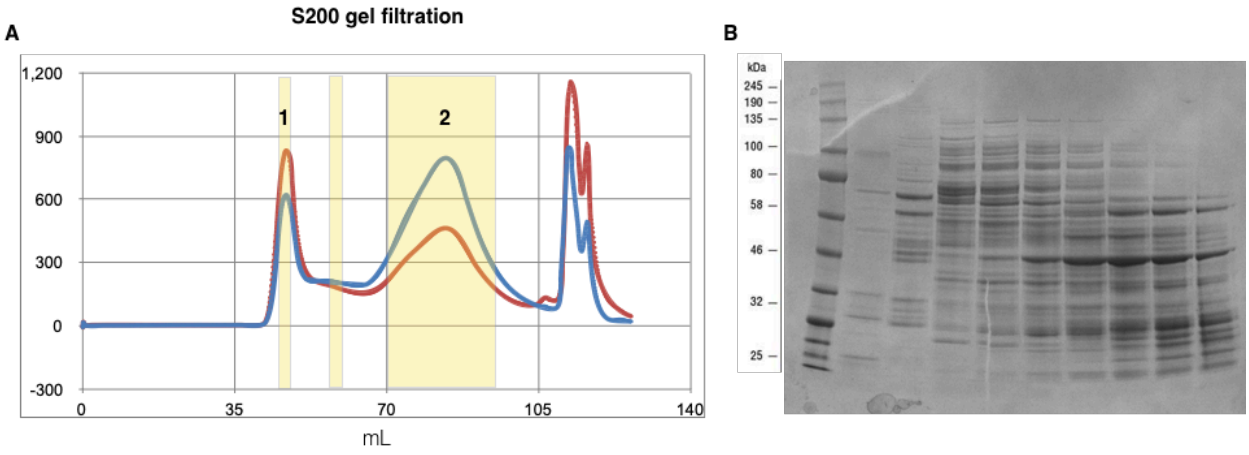

Figure 5. Purification of 6His WT hHSF1
A) Abs280 (blue) and Abs260 (red) traces from gel filtration of hHSF1 showing monomeric and trimeric peaks. **B**) SDS-PAGE gel of the fractions highlighted in yellow in A.

Given these results, I tried many purification schemes:

Induction temperature and length: 16 for 4 hours and overnight, 37 for 3 hours

IPTG concentrations: 0.1mM and 1mM

Cells: Rosetta pLysS, DE3 RIL

Higher salt washes on nickel 0.5M, 1M, 1.5M

EDTA present starting at lysys

Heparin column before size exclusion

Glycerol: 0% and 100%

Constructs: SUMO-hHSF1, WT hHSF1 and hHSF1 1-417

Eventually, the following purification scheme produced pure protein but only of the hHSF1 trimer.

Expression was done in BL21 rosetta cells grown at 37C to OD_{600}=0.6, induced with 0.1mM IPTG at 16C for 3 to 4 hours, lysis in 40mM HEPES pH 7.5, 500mM NaCl, 3mM BMe, 1 Roche protease inhibitor tablet and 5mM EDTA. Clarified lysate was incubated with Roche nickel resin (that can tolerate EDTA) for 20 minutes, washed with 2CV of high salt buffer, washed with 2CV low salt buffer, and finally eluted with 300mM Imidazole-HCl. This elution was run on a GE 5mL heparin column connected to an akta and run with a 10% - 100% gradient of 1M NaCl (Figure 6A). Absorbance at 280 showed two major peaks from the heparin column, with the second one showing bands of the right size on SDS-PAGE (Figure 6B). This second peak was then further purified on an S200 SEC column where the major peak contained what's likely to be mostly pure trimeric hHSF1 (Figure 6C and 6D).

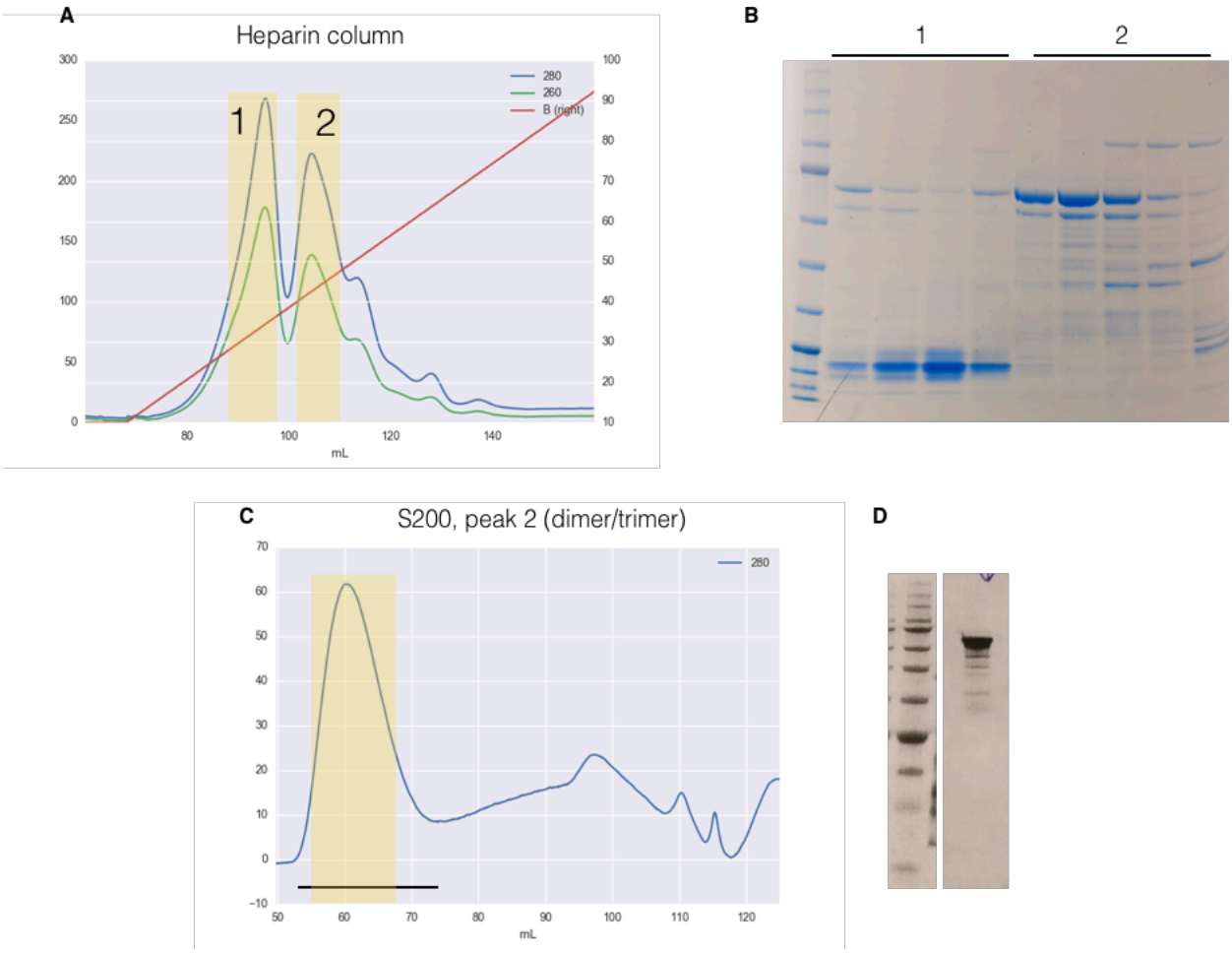

Figure 6. Successful purification of WT hHSF1
A) Elution profile of hHSF1 on heparin column. **B**) SDS-PAGE of peaks 1 and 2 from the heparin column. Only peak 2 contains full-length hHSF1 **C**) Elution profile of peak 2 from heparin on an S200 SEC column. D) SDS-PAGE of the main peak from S200.

This purification did not provide with monomeric hHSF1, the essential state needed to investigate the role of Hsp90 on HSF1 activation through trimerization. While it provides clean trimeric hHSF1 (at low yields), this population cannot be driven back to monomeric hHSF1 through dilution (Hentze et al., 2016) of the trimer. This severely limited the usefulness of the material in the context of the goals of the project. Furthermore, while reproducible in terms of purity, only one purification of 5 attempted following the same protocol yielded functional

hHSF1 trimer in the context of a fluorescence polarization anisotropy assay with labeled HSE DNA. The one time this assay worked (Figure 7) it produced a Kd of ~25nM, in line with the affinities previously reported in literature.

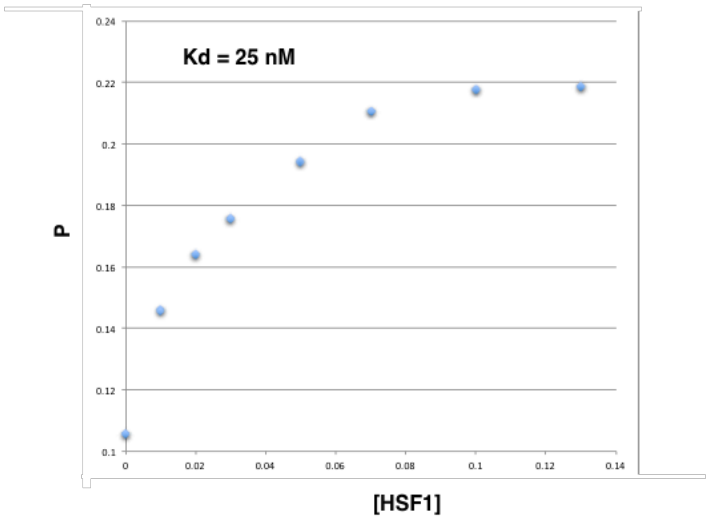

Figure 7. hHSF1 trimer with HSE DNA binding curve
Binding curve generated from a polarization anisotropy assay showing a Kd of 25nM.

Negative stain electron microscopy of the purified hHSF1 trimer from a protein purification that yielded non-functional HSF1 showed discrete but very heterogeneous particles, both in the absence and presence of HSE DNA (Figures 8A and 8B), While it's possible that HSF1, being a transcription factor that's likely to contain disordered regions especially at the C-terminal part, is intrinsically heterogeneous, it suggests that the purified protein is defective, in particular in light of the lack of obvious differences between particles from hHSF1 in the presence of HSE DNA, that should be more stable than those from apo hHSF1.

300nM hHSF1 **300nM hHSF1 + 1μM HSE DNA**

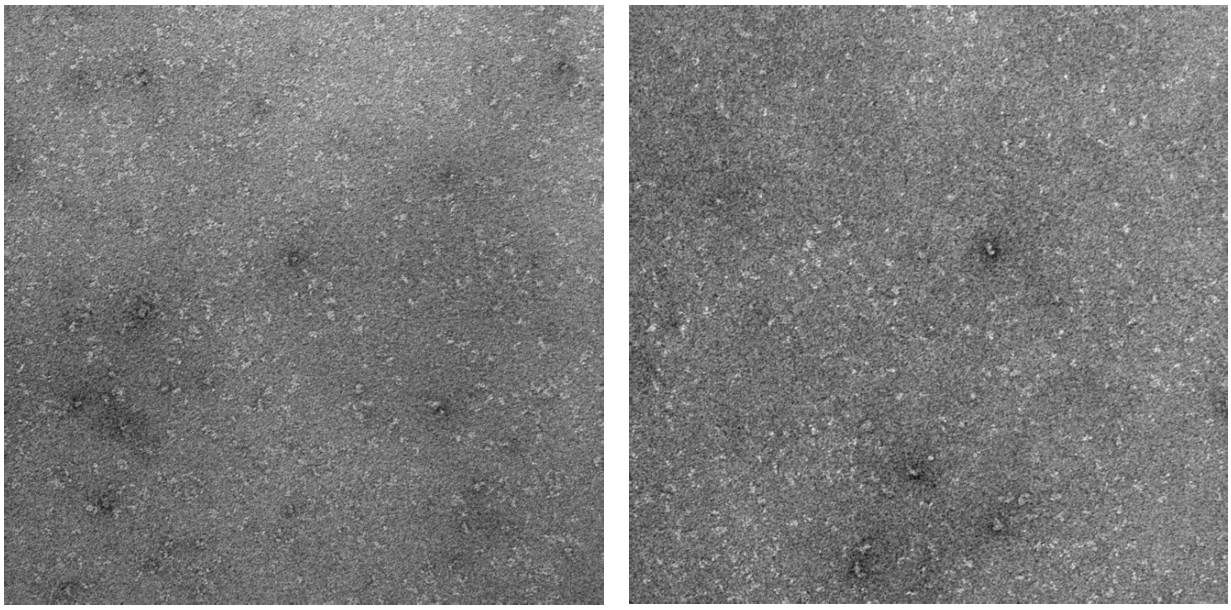

Figure 8. Negative stain electron microscopy of trimeric hHSF1
A) Trimeric HSF1. **B**) Trimeric hHSF1 in the presence of excess HSE DNA

The difficulties I and others have encountered in purifying HSF1, together with another project taking off (see chapter 3) eventually steered my attention away from this project. If this project is continued, it is my recommendation that hHSF1 be expressed in mammalian cells.

Methods

Protein expression and purification

A pET28 vector containing 6His-TEV-WT hHSF1 was transformed into BL21 rosetta cells. A single colony was used to grow 7mL of culture overnight. Cultures were scaled up by adding 10mL of overnight culture to 1L of TB media supplemented with 1x Kanamycin for a total of 6L. Cultures were grown at 37C to OD_{600}=0.6, induced with 0.1mM IPTG at 16C for 3 to 4 hours and lysed in 40mM HEPES pH 7.5, 500mM NaCl, 3mM BMe, 1 Roche protease

inhibitor tablet and 5mM EDTA. Lysate was spun down at 3500G and the supernatant incubated with Roche nickel resin (that can tolerate EDTA) for 20 minutes, washed with 2CV of 40mM HEPES pH 7.5, 1M NaCl and 1mM DTT, washed with 2CV of 40mM HEPES pH 7.5, 100mM NaCl and 1mM DTT, and finally eluted with 40mM HEPES pH 7.5, 100mM NaCl, 1mM DTT and 300mM Imidazole-HCl. The elution was run on a GE 5mL heparin column connected to an akta and run with a 10% - 100% buffer B gradient (Buffer A: 40mM HEPES pH 7.5, 100mM NaCl, 1mM DTT, buffer B: 40mM HEPES pH 7.5, 1M NaCl, 1mM DTT). Absorbance at 280 showed two major peaks from the heparin column, with the second one showing bands of the right size on SDS-PAGE. This second peak was then further purified on an S200 SEC column (40mM HEPES pH 7.5, 150mM NaCl, 1mM DTT) with the major peak pooled, concentrated to 10μM, flash-frozen in LN2 and stored at -80C.

Fluorescence polarization binding assay

Fluorescently labeled HSE (FL-HSE) ssDNA (CCTGGAATATTCCCGAACTGGC) with a 5'Fluorescein was annealed to its unlabeled complementary sequence by heating to 95C and slowly cooling to RT to produce FL-HSE dsDNA. A titration of trimeric hHSF1 was performed by incubating each concentration with 5nM FL-HSE for 5 minutes before taking a reading.

Negative stain electron microscopy

Samples of trimeric hHSF1 (300 μM, in SEC buffer with or without 1μM HSE) were negatively stained with uranyl formate (pH ~6.0) on thin-carbon layered 400-mesh copper grids (Ted Pella) that were glow discharged before sample was applied. Samples were imaged using a

Tecnai T12 Spirit TEM (FEI) operated at 120 keV. Micro- graph images were acquired with ~1.5-μm defocus on a 4k × 4k CCD camera (Gatan) at a magnification of 67,000× with a pixel size of 1.73 Å.

References

Anckar, J., & Sistonen, L. (2011). Regulation of HSF1 function in the heat stress response: implications in aging and disease, *80*(1), 1089–1115. http://doi.org/10.1146/annurev-biochem-060809-095203

Experientia, F. R., 1962. (n.d.). A new puffing pattern induced by temperature shock and DNP in Drosophila. *Springer*

Hentze, N., Le Breton, L., Wiesner, J., Kempf, G., & Mayer, M. P. (2016). Molecular mechanism of thermosensory function of human heat shock transcription factor Hsf1. *eLife*, *5*, 1153. http://doi.org/10.7554/eLife.11576

Jaeger, A. M., Makley, L. N., Gestwicki, J. E., & Thiele, D. J. (2014). Genomic Heat Shock Element Sequences Drive Cooperative Human Heat Shock Factor 1 DNA Binding and Selectivity. *The Journal of Biological Chemistry*, *289*(44), jbc.M114.591578–30469. http://doi.org/10.1074/jbc.M114.591578

Kirschke, E., Goswami, D., Southworth, D., Griffin, P. R., & Agard, D. A. (2014). Glucocorticoid receptor function regulated by coordinated action of the Hsp90 and Hsp70 chaperone cycles. *Cell*, *157*(7), 1685–1697. http://doi.org/10.1016/j.cell.2014.04.038

Naidu, S. D., & Kostova, A. T. D. (2017). Regulation of the mammalian heat shock factor 1. *The FEBS Journal*, *284*(11), 1606–1627. http://doi.org/10.1111/febs.13999@10.1002/(ISSN)1742-4658(CAT)StateoftheArtReviews(VI)SoAReviews

Tissiéres, A., Mitchell, H. K., & Tracy, U. M. (1974). Protein synthesis in salivary glands of Drosophila melanogaster: Relation to chromosome puffs. *Journal of Molecular Biology*, *84*(3), 389–398. http://doi.org/10.1016/0022-2836(74)90447-1

Chapter IV

CryoEM structure of the HtpG in complex with the ribosomal protein L2

Introduction

Until recently, structural work on Hsp90 has been limited to crystallography, severely limiting work with Hsp90-client complexes due to the intrinsic instability of Hsp90 clients that is adverse to crystal formation. Recent advances in the field of cryoEM, mainly through the introduction of direct electron detectors and the development of better algorithms, now allow us to structurally investigate these complexes despite their heterogeneity and small molecular size.

This is exemplified by the recent cryoEM structure by now former graduate of the Agard lab, Kliment Verba, of the human cytosolic Hsp90 in complex with the kinase CDK4 and the kinase-specific cochaperone CDC37 (Verba et al., 2016). For years other groups had tried to obtain a crystal structure of this complex, and it was not until cryoEM could be applied to this complex that a structure emerged.

This structure provided significant insight into how Hsp90 engages clients as well as on the functional role of Hsp90, showing that the traditional view of Hsp90 acting as a client activator, at least in a direct way through interaction with a client, may not be completely accurate. Indeed, in this structure, the kinase is held in an inherently inactive conformation where the two kinase lobes are split apart, each sitting on either side of a closed Hsp90 that clamps around an unfolded strand going through the lumen of the chaperone (Figure 1).

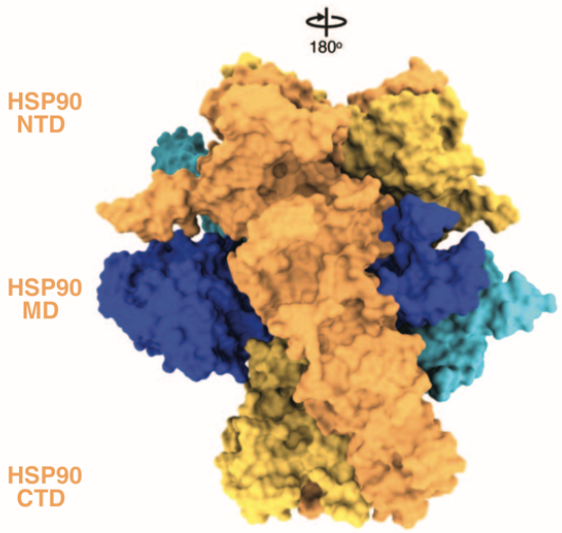

Figure 1. Hsp90 in complex with CDK4 and the cochaperone CDC37
Hsp90 (orange) clamps around an unfolded beta-strand of CDK4 (dark blue) separating the kinase lobes that are now on either side of Hsp90 and connected by an unfolded beta-strand through the lumen of Hsp90 (Verba et al., 2016)

While this structure provides the first complete structural description of Hsp90 in complex with a client, more structures of Hsp90 complexes, ideally with members of other client families, different Hsp90 homologs and different nucleotide states, are needed to establish which aspects of this structure are unique to its components and which are conserved modes of interaction, and to ultimately understand at the molecular level how the ATPase cycle of Hsp90 is used to regulate clients. As Hsp90 interacts with dozens of client proteins it's unlikely that it does so in a different way for each, but there could perhaps be shared modes of interaction within different families of clients such as the kinases or the hormone receptors, or perhaps all clients interact in a similar way, or, perhaps, a combination of both. In order to explore these questions, I set out to obtain a cryoEM structure of the bacterial Hsp90, HtpG, in complex with one of its few known clients, the ribosomal protein L2.

High temperature protein G (HtpG) has high sequence and structural homology to other Hsp90 homologs, in particular, and unexpectedly, to TRAP1. Like it, it doesn't have any known cochaperones, lacks the C-terminal EEVD motif of eukaryotic Hsp90s that mediates interactions with TPR domains of several cochaperones such as HOP and does not functionally interact with any of the eukaryotic cochaperones (Sung et al., 2016). While initially not many clients of HtpG were identified (L2 being one of them), its role in several important bacterial processes such as CRISPR/Cas immunity (Yosef, et al, 2011) has started to emerge. Structurally, its architecture is similar to that of other Hsp90s (Figure 2B) and has a similar nucleotide dependent conformational cycle that is however differently tuned. Indeed, unlike most eukaryotic Hsp90s, HtpG is more sensitive to nucleotide state, accumulating in the closed state in the presence of ATP. This behavior is similar to that of TRAP1, and likely related to their lack of cochaperones that regulate the ATPase activity of Hsp90 in eukaryotic systems. It is also highly sensitive to pH, where at pH 6 it is in a mostly closed conformation whereas at pH 9 it adopts an open and extended conformation. At physiological pH, HtpG exists at equilibrium of these two states (Krukenberg et al, 2009).

Ribosomal protein L2 in an essential bacterial protein that is part of the 50S large ribosomal subunit. It's required for association of the 30S and 50S subunits to form the 70S ribosome as well as for tRNA binding and peptide bond formation. This 273 residue-long and 29.9 kDa protein is composed of an N-terminal tail (first 60 residues), a small beta-rich globular domain and a C-terminal tail (Figure 2A). L2 is a bona-fide HtpG client and as such exhibits all the characteristics of Hsp90 clients: it increases the ATPase activity of HtpG and interacts with the middle and C-terminal domains of the chaperone. In bacteria, HtpG is found associated with

L2 when cells are grown under minimal media and under heat shock at 42C (Motojima-Miyazaki et al, 2010). Under these stress conditions protein biogenesis is likely stopped, and ribosomes can fall apart. In this scenario, HtpG could be buffering a pool of L2, keeping it from aggregating and maintaining it ready to be used to reassemble ribosomes and continue protein synthesis once stress has ceased.

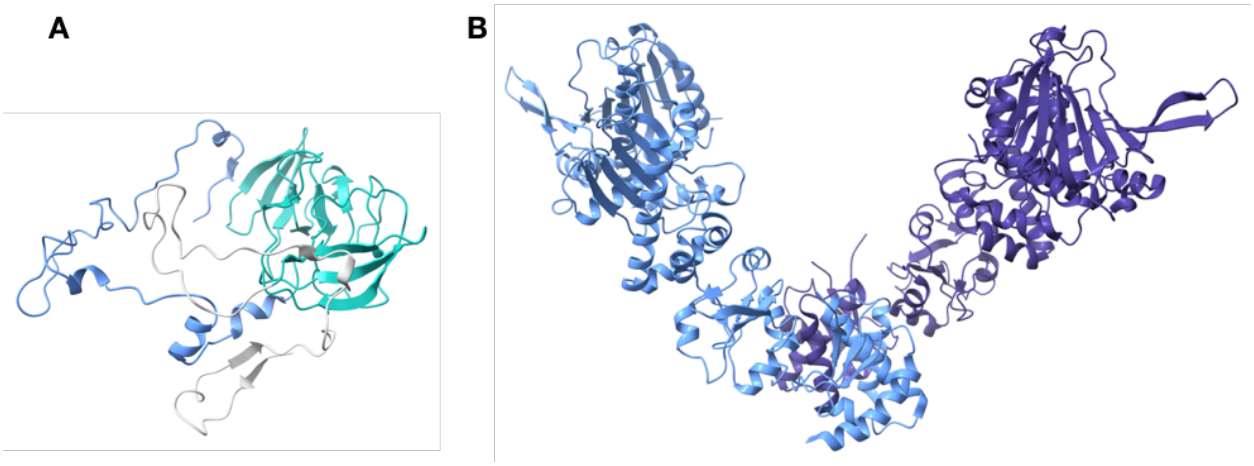

Figure 2. Structures of L2 and HtpG
A) Structure of L2 from a ribosome crystal structure (PDB: 4YBB). L2 is composed of an N-terminal tail (in gray), a small globular domain (in turquoise) and a C-terminal tail (in blue) **B)** Crystal structure og apo-HtpG (PDB: 2IOQ).

Former members of the Agard lab, Daniel Elnatan and Kliment Verba, had previously attempted to apply cryoEM to this complex encouraged by good negative stain EM data. However, despite going to high concentrations, particles of this complex would only be found on thick carbon or the edges of grid holes, making data collection on these grids almost impossible. Given the affinity of the complex for carbon and the fact that a new member of the lab, Feng Wang, had started producing grids covered with sheets of graphene oxide (GO), it seemed that the project would have a good chance of moving forward.

Results

Graphene Oxide grids are amenable to imaging HtpG:L2

As hoped, the complex between HtpG and L2 has high affinity for graphene oxide grids, showing high particle density at 250nM of complex (Figure 3A) that generate 2D classes with recognizable Hsp90 shapes (Figure 3B). 3D ab-initio classification yields classes that are mostly homogeneous in terms of HtpG conformation, with most differences appearing to be mostly in the quality of the 3D class (Figure 3C).

A

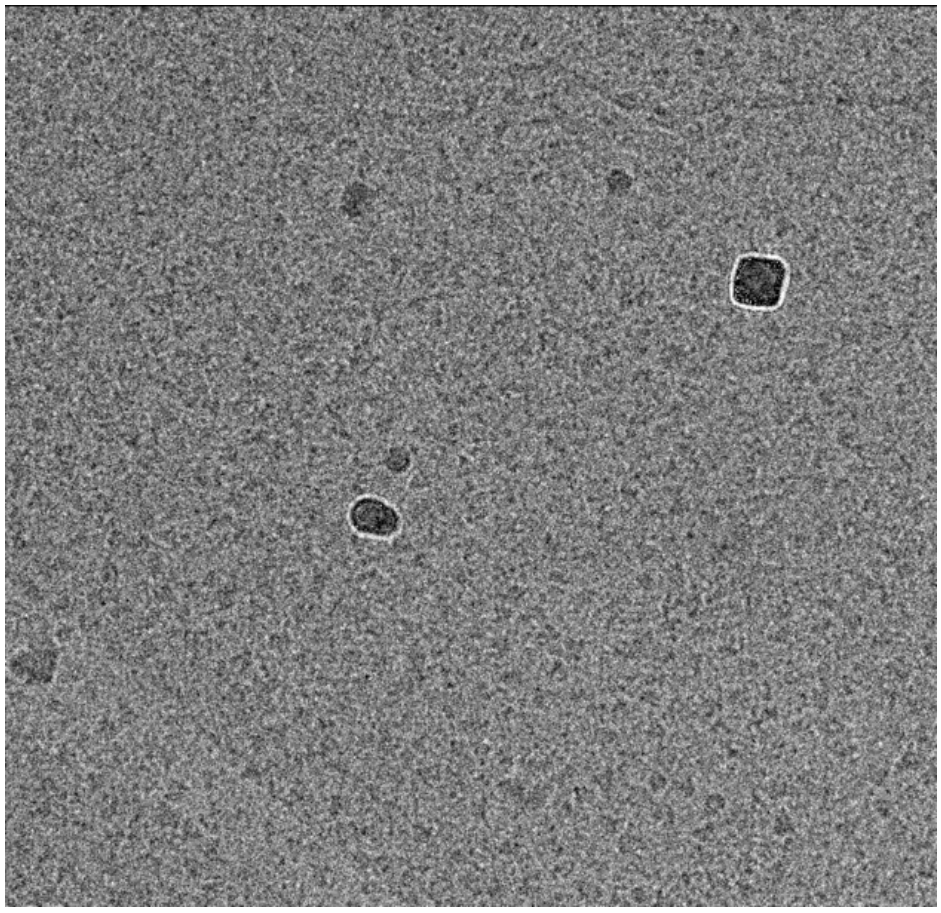

B

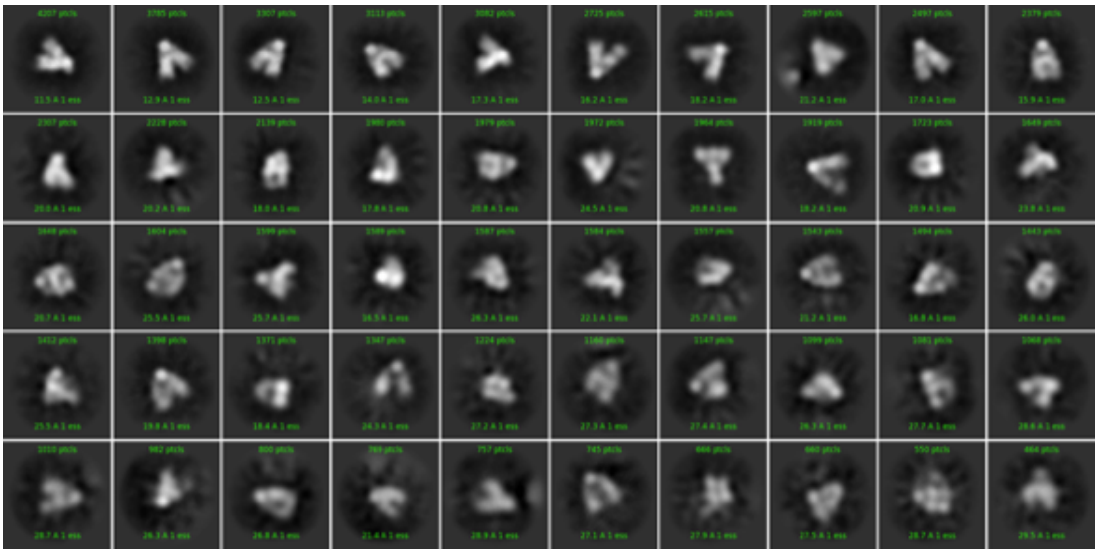

C

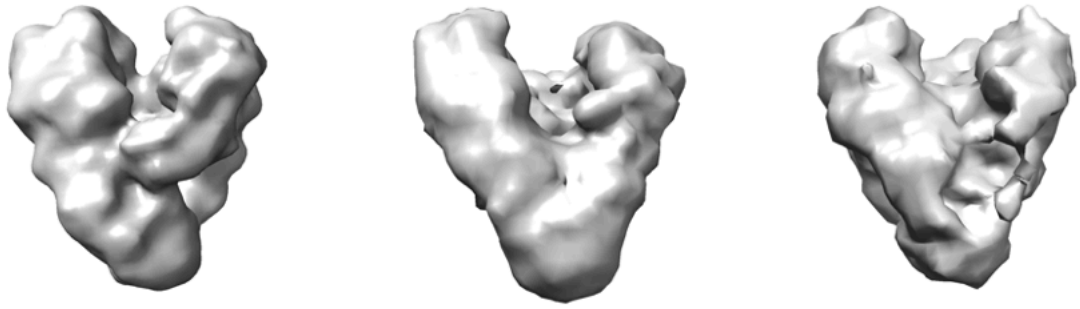

Figure 3. HtpG:L2 on graphene oxide grids
A) Representative micrograph of HtpG:L2 on graphene oxide grids, 250nM complex. **B)** 2D classification. **C)** Ab-initio classes containing 58.4%, 36.2% and 15.3% of particles respectively. The first class was selected for further refinement.

Apo HtpG adopts a GRP94-like conformation when in complex with L2

The current reconstruction shows unambiguous density for HtpG, where the two protomers are easily recognizable (Figures 4A, 4B and 4C). None of the existing structures of HtpG (apo, ADP-bound crystal structures, PDB codes 2IOP and 2IOQ (Shiau, Harris, Southworth, & Agard, 2006) fit in the cryoEM map (Figure 5A). Neither model derived from

SAXS data at pH 6 or pH 9 values fit in the cryoEM density either. Instead, HtpG in complex with L2 is in a single conformation as evidenced by the 2D and 3D classes from all particles (Figures 3B and 3C).

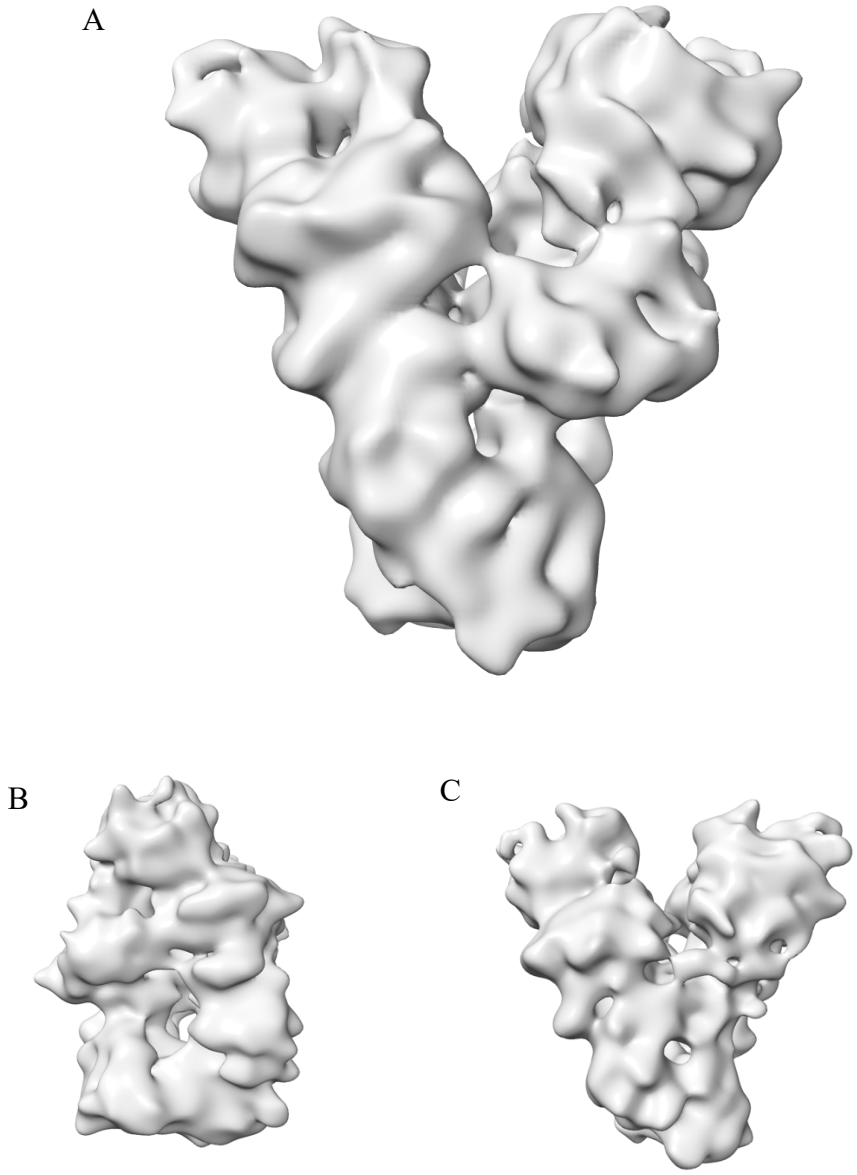

Figure 4. CryoEM map of apo-HtpG:L2
A) 12Å map of HtpG:L2 shows distinct density for both HtpG protomers plus additional density for the client. **B**) Rotated 90° along the vertical axis **C**) Rotated 180° along the vertical axis.

Looking at the conformations from structures of other Hsp90s showed that, unexpectedly, HtpG is in a conformation almost identical to that of GRP94 crystallized in the presence of either AMPPNP or ADP (Dollins et al, 2007) (Figure 5B). both at the protomer level and at the domain level.

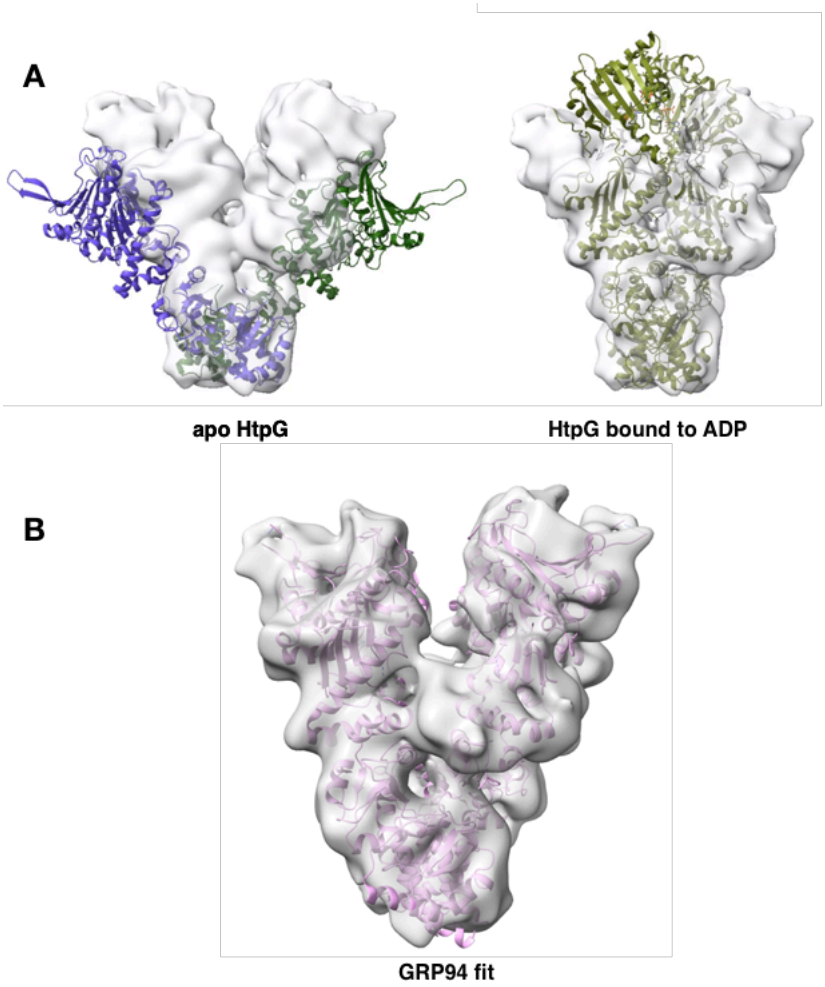

Figure 5. HtpG is in a GRP94-like conformation
A) None of the existing structures of HtpG (apo, ADP-bound crystal structures, PDB codes 2IOP and 2IOQ (Shiau et al., 2006) fit in the cryoEM map. **B**) The crystal structure of GRP94 fits well in the map for HtpG

In particular the N-terminal domains of HtpG are still in the unrotated apo conformation observed in the crystal structure of full length HtpG (Shiau et al., 2006) that is incompatible with N-terminal dimerization required to stabilize the closed state. In fact, the electron density of each

individual protomer fits well the protomer model from the apo HtpG crystal structure. This indicates that the major effect that client binding has on HtpG is partial closure of the protomers.

Given this conformational similarity, I produced a homology model of HtpG based on the crystal structure of GRP94 (PDB: 2O1V) and relaxed the model inside the density using Rosetta (Figure 6).

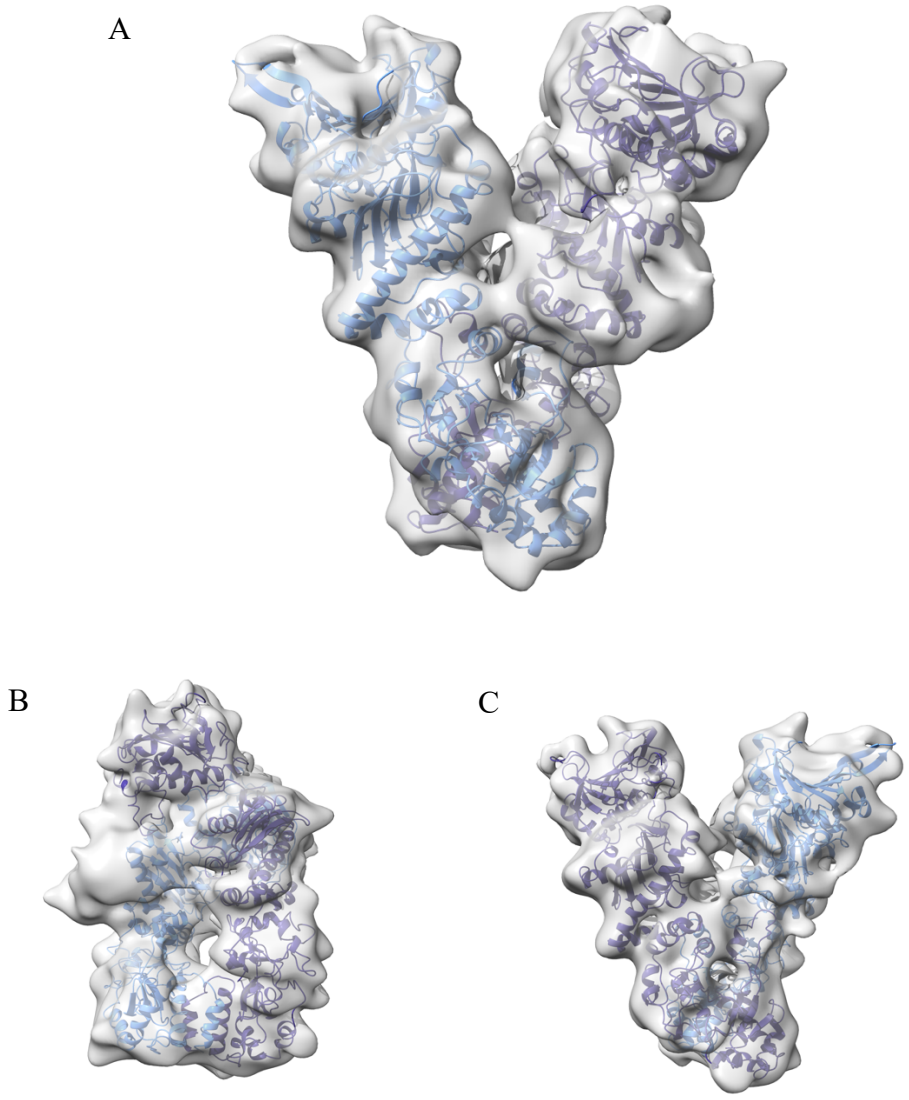

Figure 6. Homology model of HtpG based on GRP94 fit into the cryoEM map
A) Homology model of HtpG based on GRP94 and relaxed in Rosetta. **B**) Rotated 90° along the vertical axis C) Rotated 180° along the vertical axis.

L2 interacts with HtpG in a kinase-like fashion

Subtracting the density accounted for by HtpG reveals the density for L2 (Figures 7A and 7B). Similar to CDK4, L2 shows a globular density on one side of HtpG which extends through the lumen of the chaperone as a tubular density that, at this resolution, could accommodate an unfolded beta-strand or a helix, and comes out to the other side of HtpG to a small portion of density (Figure 7C). Fitting one of the many structures of L2 from ribosomes (PDB: 4YBB) inside this density shows that the globular domain of L2 fits well inside the client's larger globular density on one of the sides of HtpG (Figure 7D). This fit positions the C-terminal tail of L2 so that it extends inside the tubular density that goes through the lumen of HtpG. At this point, the remainder of the C-terminal tail of L2 from the existing structures of L2, which are in the context of ribosomes, diverges from what could fit in the map, but as this tail is mostly devoid of secondary structure it seems reasonable that it would continue and exit the lumen of HtpG on the other side, making some contacts on that side of HtpG where the smaller globular density is observed, and the remaining portion would be disordered (Figure 7D).

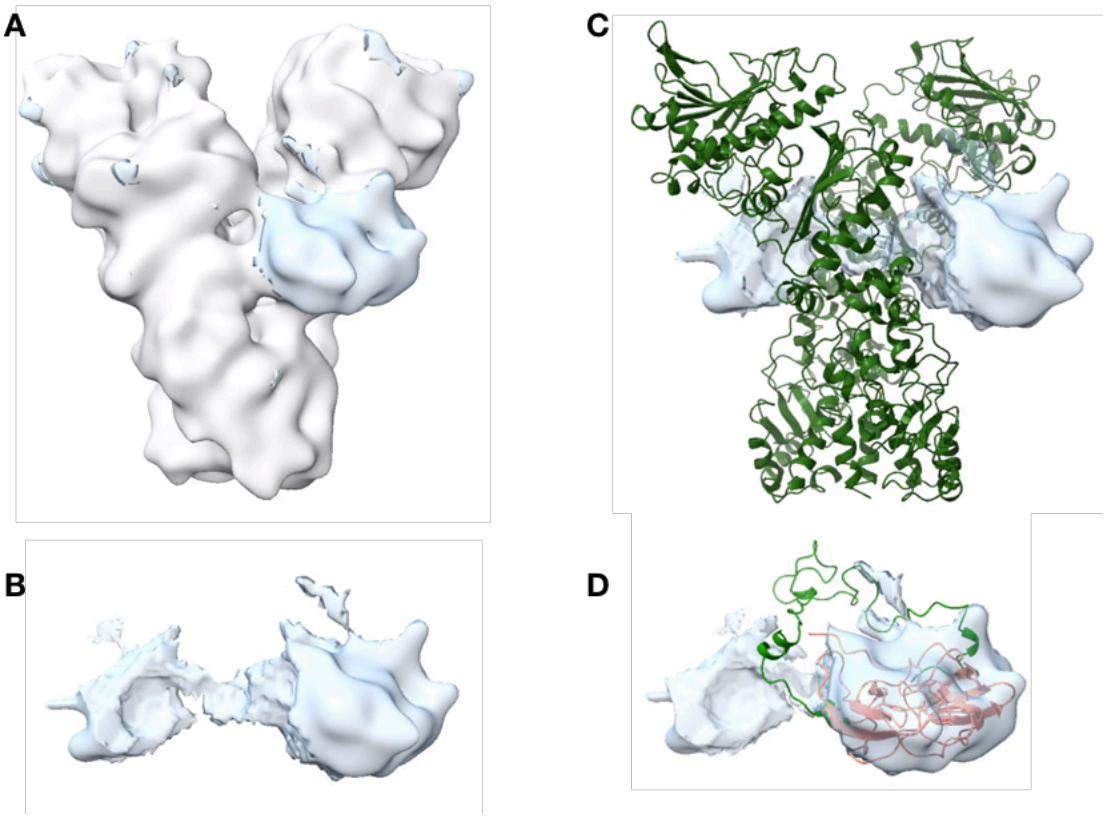

Figure 7. The density unaccounted by HtpG fits the globular domain of L2
A) Map zoned to 7Å of the HtpG model shows density for L2 in cyan. **B**) Density for L2 **C**) L2 density shows that it interacts with HtpG in a CD$ manner. **D**) The globular domain of L2 fits well into the density and positions the C-terminal tail towards the lumen of HtpG.

The current model for HtpG:L2 shows that their interaction is very similar to that of CDK4 on ATP-bound Hsp90 (Figure 8A and 8B), indicating that this mode of interaction is conserved across Hsp90 homologs, clients and nucleotide states.

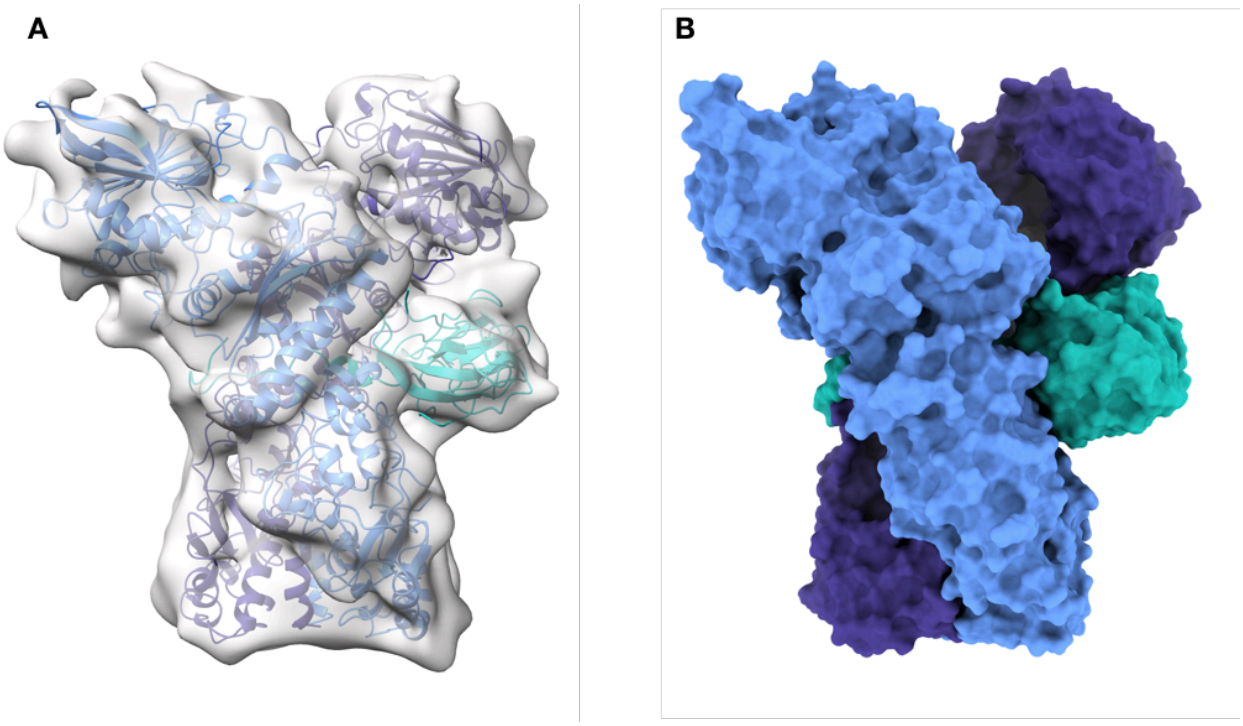

Figure 8. Current model of the apo-HtpG:L2 complex
A) Model of HtpG:L2 fit into the cryoEM map and relaxed in Rosetta. HtpG in shades of blue and L2 in green. **B**) Surface rendering of the HtpG:L2 model showing HtpG clamping around L2.

The observed L2 interactions with HtpG also match the regions of HtpG that had been previously mapped to interact with clients, in particular with the model client Δ131Δ and the ribosomal protein L2 (Street et al., 2014, Genest et al., 2013) at the interface of the C-terminal and middle domains. (Figure 9).

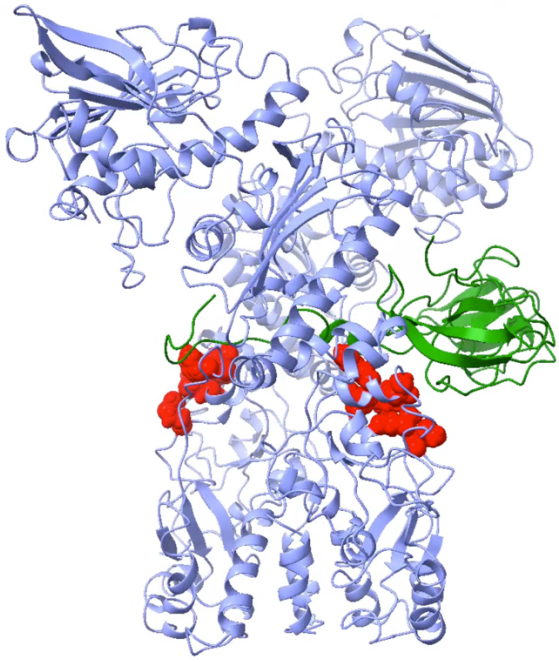

Figure 9. L2 interacts with HtpG at previously mapped regions
L2 (green) interacts with the regions (depicted as red surface) of HtpG (in blue) that had been previously mapped to interact with Δ131Δ and L2.

In the current model, L2 appears to make additional interactions with HtpG different from those observed with Cdk4 or mapped with Δ131Δ. The main one is between the globular domain of L2 and the N-terminal domain of the HtpG protomer it contacts the most (Figure 8B). This interaction could stabilize the N-terminal domain of HtpG through an interaction with the lid region of Hsp90 that would have an impact on ATP binding and rotation of the N-terminal domain, regulating closure and hydrolysis of HtpG. A structure at higher resolution is needed to shed light on the molecular details of this interaction.

Discussion and future directions

The current cryoEM map of apo-HtpG:L2, though at low resolution, already shows several key aspects of the interaction between the chaperone and the client. Despite being

different Hsp90 homologs, different client proteins, and in a different nucleotide state, HtpG engages L2 in a remarkably similar fashion to how hHsp90 engages CDK4: two domains on either side of Hsp90 connected by density through the lumen of the chaperone.

At this resolution, the region of L2 that goes through the two HtpG protomers cannot be resolved with enough detail to discern its secondary structure but, given that HtpG is not fully closed and the size of the luminal density, there is enough space in it to accommodate either an unfolded peptide or a helix of L2, as is the case with Δ131Δ. Based on the proposed fit of L2 into the cryoEM map and using the structure of L2 as it exists in the ribosome, the region of L2 that crosses the lumen of Hsp90 consists of a helix turn followed by an unstructured loop (Figure 10).

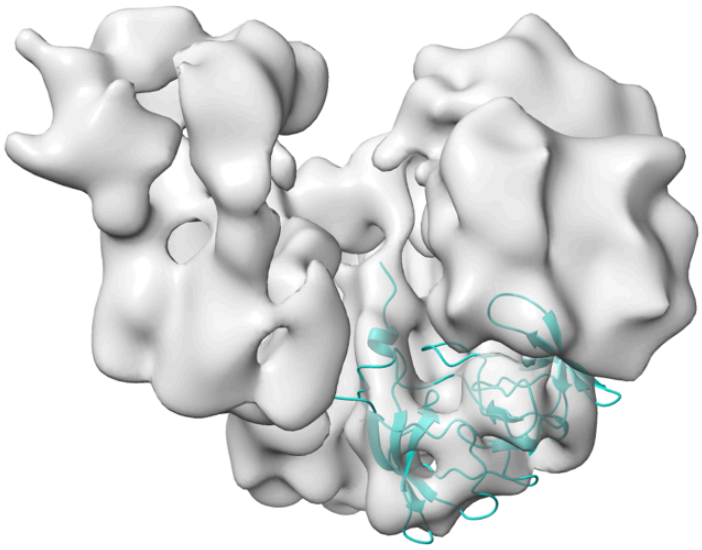

Figure 10. Model of the region of L2 through the lumen of HtpG
Based on the fit from a ribosomal structure of L2 (green), its C-terminal tail points directly into the tubular density through lumen of HtpG which, at this resolution, can accommodate either an unfolded peptide (as is the case with CDK4 and hHSP90) or a helix.

As this complex contains apo HtpG, which is not closed, one can imagine a model where a helical region of the client binds in the open state and, upon closure of Hsp90, this helix is either slightly unfolded to compensate for the smaller space in that region of the chaperone in the closed state, or shifted along the lumen of Hsp90 so that a different region of the client, likely devoid of secondary structure, is now going through the chaperone. To elucidate this, and more broadly the effects of Hsp90 closure on the client, I'm currently also working on collecting data for a closed HtpG:L2 complex incubated with AMPPNP.

To fully understand the molecular details of the observed interaction, a higher resolution map is needed. Despite collecting large datasets with upwards of 2 million particles, the resolution of the map has not improved. Based on my experience with graphene oxide grids as well as on that of others at UCSF for whom proteins seem to be partially unfolded when on GO, it's possible that GO acts as an air-water interface and the resolution I can obtain for this complex on that surface is intrinsically limited by it.

Amino grids, made with a GO layer functionalized with NH_2 groups provide an alternative surface with different properties that could also be amenable to imaging this complex, and are also manufactured in-house by Agard lab member Feng Wang. I have now switched to these grids and from a small dataset I have a recent, though not fully yet refined, map of the complex at 7Å (Figure 11). I am now in the process of collecting a larger dataset using these grids.

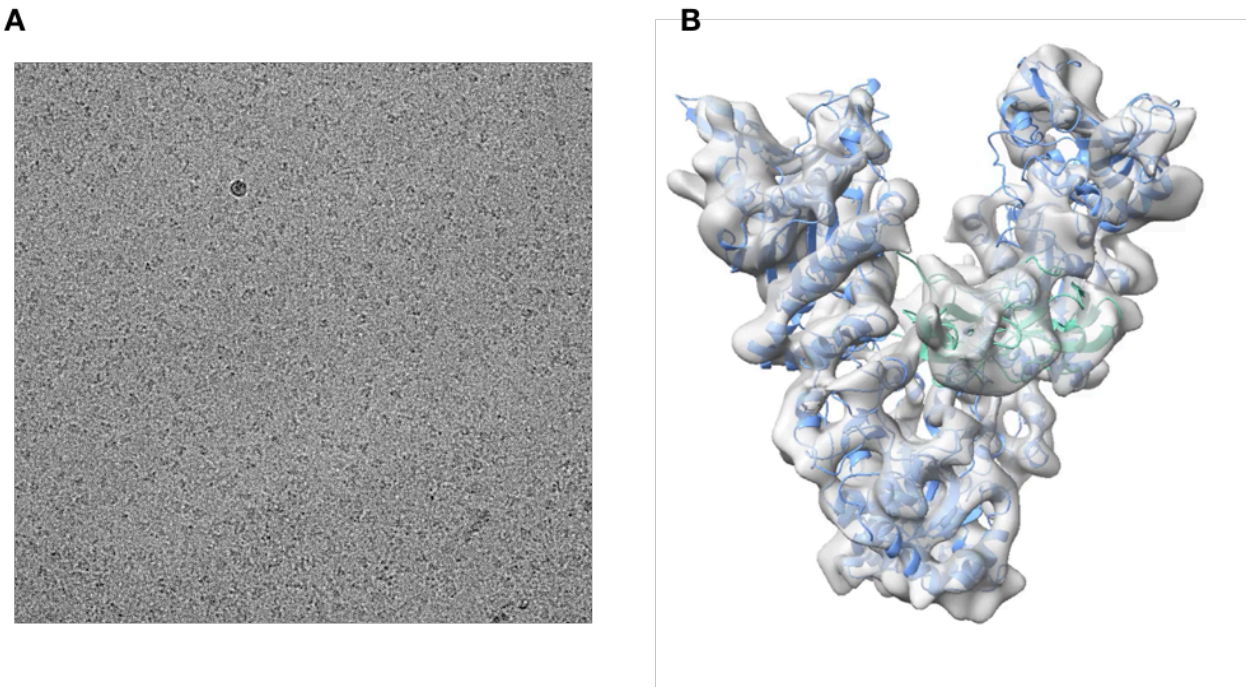

Figure 11. apo-HtpG:L2 on GO-NH2 grids
A) Representative micrograph of 250nM HtpG:L2 on GO-NH_2 grids. **B)** 7Å map from a small dataset collected on GO-NH_2 grids.

This structure provides evidence supporting that the different conformational states of Hsp90 are conserved across homologs but differentially regulated, and supports a conserved mechanism of interaction between Hsp90 and different classes of clients where Hsp90 clamps between domains stabilizing structural and likely short-lived transitions in the client. This structure together with a structure of the closed complex will provide much needed comparative data for different nucleotide states of an Hsp90:client complex to better understand the molecular mechanism of Hsp90 function.

Methods

Protein expression and purification

A pET151DTOPO vector containing 6His-TEV-HtpG was transformed into BL21(DE3) cells. A single colony was used to grow 70mL of culture overnight. Cultures were scaled up by adding 10mL of overnight culture to 1L of TB media supplemented with 1x Kanamycin for a total of 6L. Cultures were grown at 37C to OD_{600}=0.8, induced with 1mM IPTG at 16C overnight and lysed in 40mM HEPES pH 7.5, 500mM KCl, 1 Roche protease inhibitor. Lysate was spun down at 3500G and the supernatant incubated in nickel resin for 20 minutes, washed with 2CV of 40mM HEPES pH 7.5, 500mM KCl, washed with 2CV of 40mM HEPES pH 7.5, 100mM KCl, and finally eluted with 40mM HEPES pH 7.5, 100mM NaCl and 300mM Imidazole-HCl pH 7.5. The elution was run on a MonoQ ion exchange column connected to an akta and run with a 10% - 100% buffer B gradient (Buffer A: 40mM HEPES pH 7.5, 100mM KCl, buffer B: 40mM HEPES pH 7.5, 1M KCl). The main peak was then further purified on an S200 SEC column (40mM HEPES pH 7.5, 100mM KCl) with the major peak pooled, concentrated to around 100µM, flash-frozen in LN2 and stored at -80C.

L2 construct lacking the N-terminal tail (first 61 residues) was previously purified by Daniel Elnatan as previously described (Motojima-Miyazaki et al, 2010).

CryoEM grid preparation and data acquisition

Graphene oxide grids were prepared in-house by Feng Wang as previously described (Palovcak et al., 2018) using 300-mesh Au-quantifoil grids. Bare GO grids were prepared with Vitrobot Mark III (FEI Company), using 20°C and 100% humidity. 3.5uL of sample at

concentration of 250nM were applied to non-glow Au-Quantifoil 1.2/1.3 thick carbon grids, single blotted for 6 seconds using 0 force and plunge frozen in liquid ethane cooled by liquid nitrogen. GO-NH_2 grids were prepared similarly but with 4 second blots and 0 force.

Images for bare GO grids were taken at UCSF on FEI Arctica electron microscope operating at 200kV with a nominal magnification of 36,000x. Images were recorded by Gatan K2 Summit detector (Gatan Company) with super resolution mode (0.745Å/pix). Defocus varied from 1.5µm to 3µm. Each image was fractionated to 50 frames (0.2 seconds/frame, total exposure of 10 seconds) for a total dose of 58e/$Å^2$.

Images for GO-NH_2 grids were taken at UCSF on FEI Arctica electron microscope operating at 200kV with a nominal magnification of 36,000x. Images were recorded by Gatan K3 Summit detector (Gatan Company) with super resolution mode (0.575Å/pix). Defocus varied from 1.5µm to 3.5µm. Each image was fractionated to 120 frames (0.02 seconds/frame, total exposure of 2.4 seconds) for a total dose of 60e/$Å^2$.

CryoEM data processing

Movie motion correction was done using Motioncor2 (Zheng et al., 2017). CTF estimation was done using Gctf (Zhang, 2016). Image curation, 2D classification, ab-initio modelling, 3D classification and refinements were performed on CryoSPARC 2.4.2 (Punjani, Rubinstein, Fleet, & Brubaker, 2017).

References

Dollins, D. E., Warren, J. J., Immormino, R. M., & Gewirth, D. T. (2007). Structures of GRP94-nucleotide complexes reveal mechanistic differences between the hsp90 chaperones. *Molecular Cell*, *28*(1), 41–56. http://doi.org/10.1016/j.molcel.2007.08.024

Genest, O., Reidy, M., Street, T. O., Hoskins, J. R., Camberg, J. L., Agard, D. A., et al. (2013). Uncovering a Region of Heat Shock Protein 90 Important for Client Binding in E. coli and Chaperone Function in Yeast. *Molecular Cell*, *49*(3), 464–473. http://doi.org/10.1016/j.molcel.2012.11.017

Krukenberg, K. A., Southworth, D. R., Street, T. O., & Agard, D. A. (2009). pH-dependent conformational changes in bacterial Hsp90 reveal a Grp94-like conformation at pH 6 that is highly active in suppression of citrate synthase aggregation. *Journal of Molecular Biology*, *390*(2), 278–291. http://doi.org/10.1016/j.jmb.2009.04.080

Motojima-Miyazaki, Y., Yoshida, M., & Motojima, F. (2010). Ribosomal protein L2 associates with E. coli HtpG and activates its ATPase activity., *400*(2), 241–245. http://doi.org/10.1016/j.bbrc.2010.08.047

Palovcak, E., Wang, F., Zheng, S. Q., Yu, Z., Li, S., Betegon, M., et al. (2018). A simple and robust procedure for preparing graphene-oxide cryo-EM grids. *Journal of Structural Biology*, *204*(1), 80–84. http://doi.org/10.1016/j.jsb.2018.07.007

Punjani, A., Rubinstein, J. L., Fleet, D. J., & Brubaker, M. A. (2017). cryoSPARC: algorithms for rapid unsupervised cryo-EM structure determination. *Nature Methods*, *14*(3), 290–296. http://doi.org/10.1038/nmeth.4169

Shiau, A. K., Harris, S. F., Southworth, D. R., & Agard, D. A. (2006). Structural Analysis of E. coli hsp90 reveals dramatic nucleotide-dependent conformational rearrangements., *127*(2), 329–340. http://doi.org/10.1016/j.cell.2006.09.027

Street, T. O., Zeng, X., Pellarin, R., Bonomi, M., Sali, A., Kelly, M. J. S., et al. (2014). Elucidating the Mechanism of Substrate Recognition by the Bacterial Hsp90 Molecular Chaperone. *Sciencedirect.com*. http://doi.org/10.1016/j.jmb.2014.04.001

Sung, N., Lee, J., Kim, J.-H., Chang, C., Joachimiak, A., Lee, S., & Tsai, F. T. F. (2016). Mitochondrial Hsp90 is a ligand-activated molecular chaperone coupling ATP binding to dimer closure through a coiled-coil intermediate. *Proceedings of the National Academy of Sciences*, *113*(11), 201516167–2957. http://doi.org/10.1073/pnas.1516167113

Verba, K. A., Wang, R. Y.-R., Arakawa, A., Liu, Y., Shirouzu, M., Yokoyama, S., & Agard, D. A. (2016). Atomic structure of Hsp90-Cdc37-Cdk4 reveals that Hsp90 traps and stabilizes an unfolded kinase. *Science (New York, N.Y.)*, *352*(6293), 1542–1547. http://doi.org/10.1126/science.aaf5023

Yosef, I., Goren, M. G., Kiro, R., Edgar, R., & Qimron, U. (2011). High-temperature protein G is essential for activity of the Escherichia coli clustered regularly interspaced short palindromic repeats (CRISPR)/Cas system. *Proceedings of the National Academy of Sciences*, *108*(50), 20136–20141. http://doi.org/10.1073/pnas.1113519108

Zhang, K. (2016). Gctf: Real-time CTF determination and correction. *Journal of Structural Biology*, *193*(1), 1–12. http://doi.org/10.1016/j.jsb.2015.11.003

Zheng, S. Q., Palovcak, E., Armache, J.-P., Verba, K. A., Cheng, Y., & Agard, D. A. (2017). MotionCor2: anisotropic correction of beam-induced motion for improved cryo-electron microscopy. *Nature Methods*, *14*(4), 331–332. http://doi.org/10.1038/nmeth.4193

Publishing Agreement

It is the policy of the University to encourage the distribution of all theses, dissertations, and manuscripts. Copies of all UCSF theses, dissertations, and manuscripts will be routed to the library via the Graduate Division. The library will make all theses, dissertations, and manuscripts accessible to the public and will preserve these to the best of their abilities, in perpetuity.

Please sign the following statement:

I hereby grant permission to the Graduate Division of the University of California, San Francisco to release copies of my thesis, dissertation, or manuscript to the Campus Library to provide access and preservation, in whole or in part, in perpetuity.

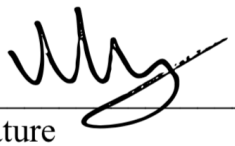

Author Signature

03/25/19

Date